SCUOLA DI DOTTORATO

UNIVERSITÀ DEGLI STUDI DI MILANO-BICOCCA

Department of Biotechnology and Biosciences

PhD program Translational and Molecular Medicine - DIMET

Cycle XXXII°

Mitochondria as the *core* of neuroinflammation and neurodegeneration in models of neuronal and astrocytic dysfunction

Surname: Martorana Name: Francesca

Registration number: 823663

Tutor: Prof. Francesca Granucci

Co-tutor: Dr. Anna Maria Colangelo

ACADEMIC YEAR 2018/19

Se camminassimo solo nelle giornate di sole

non raggiungeremmo mai

la nostra destinazione

P. Coelho

Table of contents

CHAPTER 1

INTRODUCTION

Neurodegenerative diseases are characterized by dysfunction and loss of specific neuronal populations in response to age-related modifications of brain parenchyma, as well as due to toxic or traumatic events. Neuronal degeneration is contributed by a complex crosstalk among various molecular and biochemical events that include accumulation of intracellular and extracellular aggregates of misfolded proteins, decreased availability of neurotrophic factors, metabolic and oxidative stress leading to mitochondrial dysfunction. In addition, more recently neuroinflammatory processes have been shown to be the hallmark of most neuropathological conditions, including Alzheimer's and Parkinson's disease (PD). Indeed, chronic neuroinflammation has been suggested to affect neuronal homeostasis by compromising neuroglial communication and synaptic function.

1. Neuron-glia interaction in neuroinflammation

Glial cells are the most prominent population of cells of the brain. They were discovered by the German pathologist Virchow in 1846, who coined the term "glia" to designate a class of cells

surrounding neuron of the Central Nervous System (CNS), apparently serving the nervous system as a kind of “glue” (the meaning of the greek word *glia*) [1]. At the beginning of the 20th century, glial cells were identified as an heterogenous population. In particular, Ramon y Cajal and Rio Hortega identified microglia and oligodendrocytes by using metallic impregnation of tissue samples [2,3]. Starting from them, microglia and oligodendrocytes have progressively acquired more importance among the cells of the CNS, thanks to their roles in exerting immune functions (microglia) and in myelinating axons of projecting neurons (oligodendrocytes). Importantly, a third type of glial cells, originally defined macroglia but known with the name of astrocytes, constitute the most abundant group of cells with a glial phenotype in the brain. Not too long ago, it was believed that astrocytes were inactive elements just providing a scaffold function in the CNS. Now, it is known that astrocytes play important roles in neuronal function and homeostasis. They supply energy metabolites to neurons [4], regulate the blood flow and the blood-brain barrier [5], control the levels of extracellular ions, neurotransmitter and fluids [6–8], and modulate synaptic activity [9]. Astrocytes are strategically positioned between neurons and blood vessels, with their fine processes surrounding the neuronal synapses at one side and intimately interacting with the walls of blood vessels at the other. As a consequence, it is not surprising that astrocytes have been suggested to play an important role in the pathogenesis of a variety of CNS disorders [10], including neurodegenerative

diseases such as Alzheimer's (AD) and Parkinson's diseases (PD) [11,12]. In this evolving scenario, it is important to understand the contribution of astrocytes to the initial phases of neurodegeneration.

1.1 Astrocytes: housekeeper of the Brain

Among neuroglial cells, astrocytes are the most heterogenous cell type that differ at the morphological, developmental, molecular and functional level [13]. Astrocytes can be classified in several different classes (Fig.1). In particular, the vast majority of astrocytes belong to the protoplasmic phenotype, which is characterized by irregular morphology and very dense branched processes and populate the grey matter. The other group is represented by fibrillary (or fibrous) astrocytes characterized by simpler morphology with thinner processes in comparison with protoplasmic astrocytes. This second type is frequently observed in the white matter. Besides these two main categories, further morphological analyses allowed the identification of additional subset of astroglial cells distributed in varying proportions across different CNS regions [14]. These include tanycytes; the retinal Müller cells and the cerebellar Bergmann glia; radial astrocytes; velate astrocytes; interlaminar astrocytes; perivascular and marginal astrocytes; and ependymocytes. The classification of the different astrocytic subtypes has been based on the expression of specific markers that allowed to visualize the cells by immunochemical labeling. In particular, a widely used marker for identifying and labelling astrocytes is the glial fibrillar acidic

protein (GFAP). In addition to GFAP, astrocytes in the CNS express a series of marker which helps for their identification: S100β (calcium-binding protein), glutamine synthetase (GS), the astrocytic glutamate transporters GLAST/EAAT1 and GLT-1/EAAT2 [14].

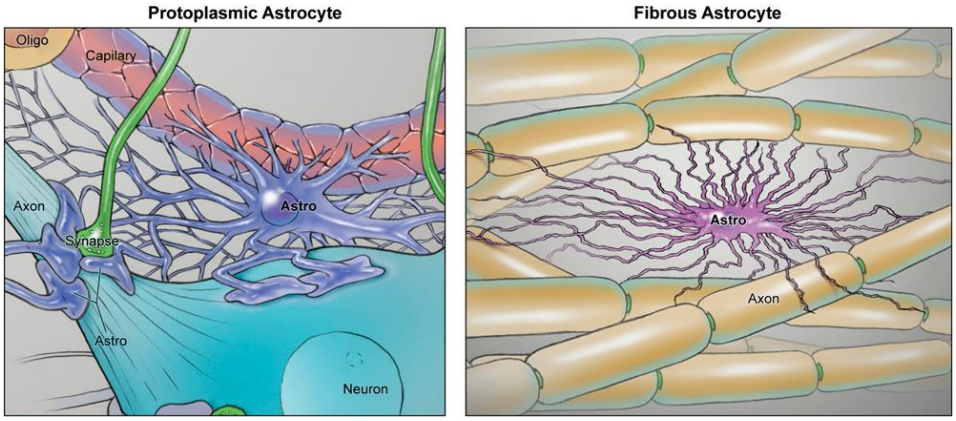

Fig.1. Schematic representation of protoplasmic and fibrous astrocytes. (*Molofsky A.V. et al., Genes and Development, 2012*)

Among the different astroglial subpopulations, the best characterized cells, in terms of morphology and organization, are the protoplasmic astrocytes. This type of astrocytes displays a complex branching of their processes. Single-cell microinjection of a fluorescent dye has revealed that they cover discrete territories with little or minimal overlap with adjacent astrocytes [15]. Probably, this organization is ideal for maximizing the control exerted by astrocytes over the thousands of synapses that are located within these small territories. Several studies of electron microscopy on ultra-thin sections of tissues have

revealed an intimate connection between these astrocytic processes and single synapses [16]. The knowledge of this interaction has given rise to the concept of “tripartite synapse” (fig.2) [17,18].

This latter hypothesis postulates active reciprocal communication between astroglial and neuronal components of the synapse and highlightes astroglial contribution into synaptic transmission mediated by vesicular release of neurotransmitters from glial compartments. “Gliotransmitters” are released by astrocytes and can modulate neuronal excitability and release of neurotransmitters [9,19]. Gliotransmitters comprise mediators such as ATP, glutamate, D-serine, trophic factors and others [20]. The question to be answered is how exactly the secretion of gliotransmitters by astrocytes is triggered, and what is their physiological role. Astrocytes are equipped with a full set of membrane receptors which allow them to signal following synaptic release of classical neurotransmitters (glutamate or γ-amino butyric acid, GABA), purinergic mediators [9] and molecules associated with the inflammatory reaction [21]. Interestingly, astrocytes integrates the signalling pathways initiated by these molecules by using Ca^{2+} waves, causing sustained modulatory actions on neighbouring neurons [22]. Hence, it is obvious that astrocytes dysfunction may lead to neuronal impairment.

Several lines of evidence indicate that astrocytes undergo a variety of changes in the CNS in response to different types of injury or disease. The main reaction is known as “reactive

astrocytosis". Typical hallmarks of this activation include hypertrophy, hyperplasia, and the accumulation of cytoplasmic fibrillary material, particularly GFAP in the activated cells [23].

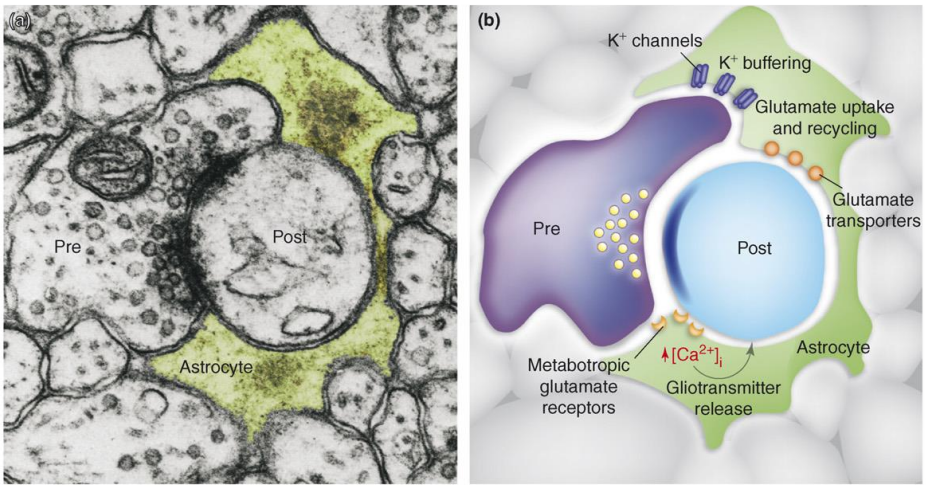

Fig.2. Schematic representation of tripartite synapse (*Halassa M.M et al., Trends in Molecular Medicine, 2007*)

1.2 The inflammatory state of the brain

Inflammation is a key biological process in response to injury, infection and trauma suffered by cells or tissues. Inflammatory-like response in the CNS is usually referred as neuroinflammation. Pathologies, infections, or injuries of the CNS are accompanied by an inflammatory process, which occurs locally in the brain parenchyma. Indeed, toxic (e.g. misfolded proteins, neurotoxins) or traumatic stimuli activate microglia, the so-called "sentinels" of the brain, which move to the site of injury to protect neurons. This is achieved by their phagocytic activity (to clear out toxic molecules) and production of growth factors

and cytokines, which activate astrocytes. Reactive astrocytes undergo morphological and functional changes (e.g. metabolism, production of neurotrophic factors) aiming to counteract the initial damage. While acute neuroinflammatory responses may be neuroprotective, since they contribute to repair the damaged tissue and minimize further injury, chronic neuroinflammation is a long-standing and often self-perpetuating neuroinflammatory response that persists long after an initial injury or insult [24]. Neuroinflammation and increased inflammatory cytokines, are associated with pathogenesis of many neurodegenerative disorders including PD, AD, Amyotrophic lateral sclerosis (ALS) and Huntington disease (HD), all characterized by gradual loss of neurons in specific brain areas and consequent loss of brain functions (e.g. cognition, memory, or movement).

Evidence indicates that oxidative stress is implicated in neurodegenerative disorders and ischemia. At physiological levels, reactive oxygen species (ROS) play an important role in many biological processes, such as cell growth and signalling, synthesis of biological molecules, immune response and metabolism [25]. However, excessive accumulation of ROS can oxidize proteins, nucleic acids and lipids, thereby participating in aging and neurodegenerative diseases [26]. The brain is vulnerable to oxidative damage because it has an elevated oxygen consumption. This high O_2 uptake is due to the wide amounts of adenosine triphosphate (ATP) needed for its normal activity to maintain neuronal intracellular ion homeostasis. Neuronal membranes are rich of phospholipids containing

polyunsaturated fatty acid esters that are sensitive to ROS, causing an extensive membrane damage. Indeed, ROS are able to disrupt receptor activity, ionic homeostasis, and neurotransmission of adrenergic, dopaminergic, serotonergic and GABAergic systems [27–29]. Moreover, ROS impair mitochondria integrity, reduce ATP production and increase mitochondria-derived ROS [30]. Thus, making the brain susceptible to oxidative insults.

Several studies have shown that chronic oxidative and inflammatory stress lead to activation of microglia and astrocytes which induce release of inflammatory factors [31,32]. Reactive astrogliosis is commonly regarded as a sign of neuroinflammatory reaction that occurs in brain parenchyma. In fact, microglial cells are considered the cellular component of the resident innate immune system in the CNS and represent key effectors of the neuroinflammatory response [33]. During injury or disease, astrocytes recognize molecules known as “danger signals” [34] by expression of specific class of membrane receptor, called pattern-recognition receptors (PRR). Four different types of PRR have been identified: Toll-like receptors (TLRs), C-type lectin receptors, cytoplasmic proteins [35,36]. Among them, TLRs are widely expressed in glial cells, and various members of these family are largely characterized [37]. Evidence suggests a critical role of TLR2 and TLR4 in the aetiology of chronic inflammatory and neurodegenerative diseases [38].

The major downstream signalling pathways activated upon ligation with PRR are the I-kappa-B (IkB) and Mitogen-Activated Protein Kinase (MAPK). In turn, these kinases modulate several transcription factors belonging to the families of Nuclear Factor kB (NF-kB), the Activator Protein 1 (AP-1) and the Interferon Regulatory Factors (IRFs), which control a wide range of genes depending on cell type [39]. Many of these genes encode for inflammatory cytokines such as Tumor Necrosis Factor α (TNFα), Interleukin-1β (IL-1β) and Interleukin-6 (IL-6), chemokines, antimicrobial proteins (e.g. iNOS).

Released cytokines cause astrocytic activation. Whether reactive gliosis exacerbates tissue damage or exerts beneficial functions in response to heterogenous stimuli, remains to be understood [40]. In some cases, the activation of glial cells has been associated to pathological neuroinflammatory responses and neurodegenerative events. However, in other cases, activated astrocytes appear to exert beneficial effects in the CNS by producing several mediators of neuroprotection, growth and differentiation, anti-inflammatory cytokines, chemokines, and angiogenic factors [41]. Furthermore, a wide range of growth factors are reported to be up regulated by astroglia during brain injuries. Among these, there are Nerve Growth Factor (NGF), Brain-Derived Neurotrophic Factor (BDNF), Neurotrophin-3 (NT3), Ciliary Neurotrophic Factor (CNTF), Vascular Endothelial Growth Factor (VEGF), Basic Fibroblast Growth Factor (bFGF), Insulin Growth Factor 1 (IGF1) and Glial Cell-Line Derived Neurotrophic Factor (GDNF) [42–45]. Ultimately, it can be

postulated that inflammation in CNS diseases is an ambivalent process that may have both protective and destructive effects. The way through which the nervous tissue controls the balance between these two mechanisms represents a critical question currently unsolved.

2. Mitochondria

Mitochondria are cellular organelles of proteobacterial origin and are known as the “powerhouse” of the cell because they are the major site of ATP production for cell survival and many other vital functions. Multiple mechanisms are based on proper mitochondrial function, ranging from oxidative phosphorylation (to produce ATP) to a number of mechanisms to maintain cellular homeostasis, such as those associated to redox signalling and their role in modulating metabolism [46,47]. Moreover, they buffer the intracellular cytosolic Ca^{2+}, thus contributing to regulate Ca^{2+} signalling and protect cells from excessive Ca^{2+} influx [46,48].

Mitochondria are very dynamic organelles that continuously undergo fission and fusion processes, which are necessary for cell survival and adaptation to the changing conditions needed for cell growth, division, and distribution of mitochondria during differentiation [49]. The maintenance of a dynamic mitochondrial network is functional to the metabolic state of the cell. For example, in the axon of neurons

mitochondria show a high degree of fission and fusion processes so they can reach functional points in which energy production is particularly necessary, such as the synapses. As a consequence, alterations in mitochondrial dynamics are likely to participate in the progression of axonal, and thus neuronal, neurodegeneration in several diseases [46,50,51].

2.1 Events of mitochondrial dynamics

The morphology of mitochondria is ensured by the activity of proteins mediating mitochondrial fusion and fission (fig.3) [52]. Mitochondrial fusion in mammals is mediated by the fusion proteins mitofusin 1 (Mfn1) and Mfn2 and optic atrophy 1 (OPA1). Fusion is important for mitochondrion-mitochondrion interactions, and it promotes the exchange of metabolites and mitochondrial DNA. Mfn1 and Mfn2 are dynamin-related GTPases that are responsible for fusion of outer mitochondrial membranes. OPA1 is also a dynamin-related GTPase, which is responsible for fusion of inner mitochondrial membranes.

Mitochondrial fission in mammals is mediated by dynamin-related protein 1 (Drp1), which is also a large GTPase. Fission mainly contributes to mitochondrial renewal and redistribution [53]. Mitochondrial fission and fusion are important quality control mechanisms to preserve mitochondria and regulate their turnover.

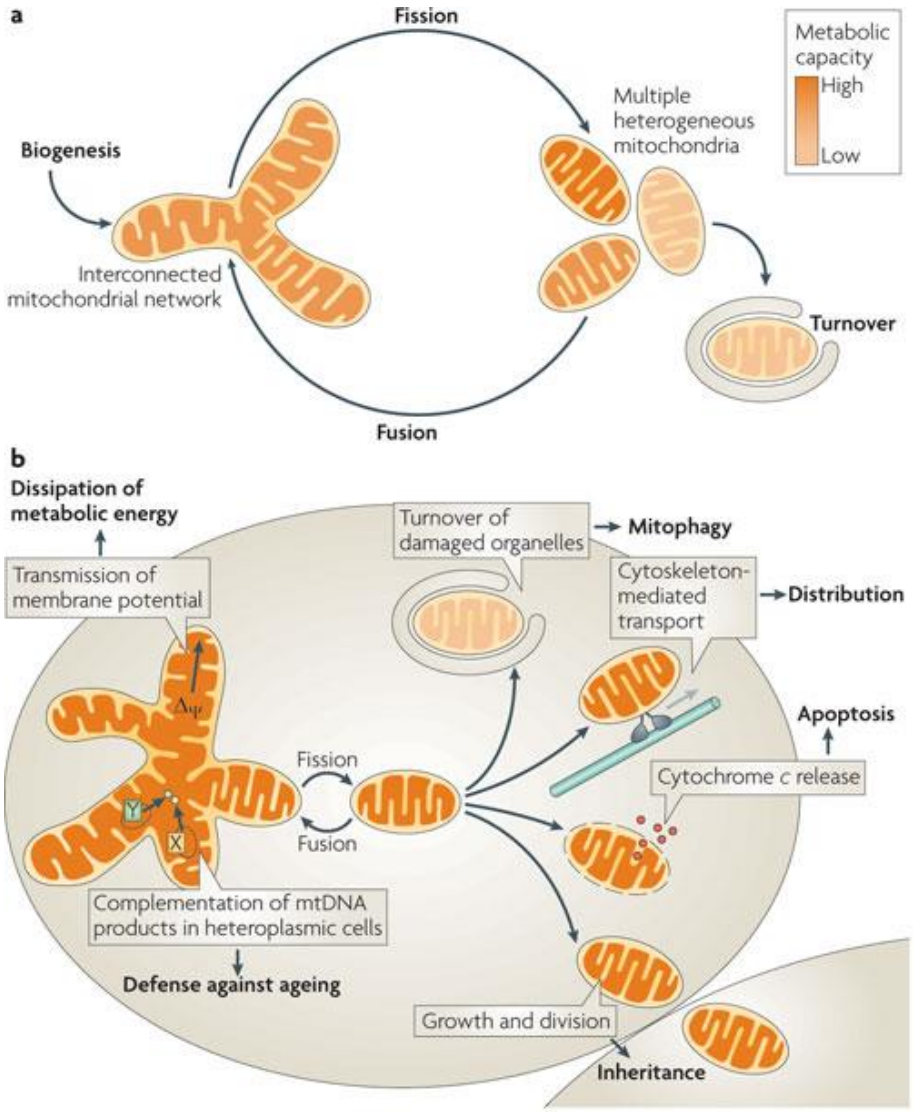

Fig.3. Schematic representation of fission-fusion processes (*Westermann B., Nature Reviews Molecular Cell Biology, 2010*)

Mitochondrial biogenesis and mitophagy regulate cellular adaptation in response to mitochondrial malfunction. Thus, these mechanisms are highly regulated and influence both

mitochondrial and cellular homeostasis. The importance of coordination between these two processes is underlined by evidence indicating that increased mitochondrial content is a common denominator of several pathologic conditions [54,55].

The regulation of mitochondrial biogenesis is obtained by the activation of several transcription factors, in response to diverse stimuli, such as nutrient availability, hormones and growth factors. Among these transcription factors, nuclear respiratory factors (NRF1 and NRF2), estrogen-related receptors (ERR-α, ERR-β, ERR-γ) and the peroxisome proliferator-activated receptor gamma co-activator 1-alpha (PGC-1α) are major modulators in the context of mitochondrial proliferation [56]. Mitophagy is a major mechanism for mitochondrial quality control. Dysfunctional mitochondria are recognized by the autophagic machinery, resulting in their engulfment by autophagosomes and trafficking to the lysosome for degradation. There are multiple mitophagy pathways, including one mediated by Pink1 and Parkin, molecules involved in familial forms of PD [57].

Dysfunctional mitochondria are supposed to play a cardinal role in the pathogenesis of various neurological disorders such as multiple sclerosis, AD, PD and stroke. Both mitochondrial dysfunction and neuroinflammatory processes lead to increased production of ROS that are detrimental for neurons. Signs of neuroinflammation, mitochondrial impairment and neurodegeneration are all present in the brain of patients suffering from previously mentioned neurological diseases. A

more accurate characterization of the mechanisms underlying the cross-talk between these events could allow the development of neuroprotective pharmacological strategies and limit the progression of these disabling neurological disorders.

3. Cross talk between autophagy and mitochondrial function

Autophagy is a cellular process that acts as a survival mechanism in starving cells but, at the same time, extensive autophagy is commonly observed in dying cells, leading to its classification as an alternative form of programmed cell death [58]. Autophagy is characterized by the formation of autophagosomes, a double-membrane vesicle, that sequesters organelles or portions of cytosol and fuse with lysosomes [59]. In the recent years, it become clear that cells also use autophagy as physiological process for recycling damaged molecules and organelles [60]. Different types of autophagy have been identified, among these mitophagy represents a specific subtype of autophagy. This mechanism is important for the mitochondria quality control that removes damaged mitochondria [61]. In the last years, emerging evidence indicates that the process of autophagy may play an essential role in acute and chronic inflammation and the impairment of autophagic machinery in neurons contributes to neurodegeneration [62,63]. This hypothesis is based on the observation that inhibition of

autophagy results in the accumulation of dysfunctional mitochondria which has a harmful impact on the bioenergetic status of the cell [62].

Autophagy (mitophagy) might be relevant to neuronal function, because neurons are more prone to accumulate ROS and dysfunctional mitochondria due to their oxidative metabolism. Mitochondrial alterations might be also triggered by metabolic alterations linked to neuronal differentiation (during neurogenesis) or neuroinflammatory processes (ROS production by activated microglia).

Taken together, this information suggests a scenario in which autophagy, inflammation and cell death are interconnected each other and mitochondria are at the core of this interplay.

3.1 Autophagy

Autophagy is an evolutionary conserved eukaryotic process that eliminates intracellular components through lysosomal degradation for recycling, to generate macromolecular building blocks and energy under stress conditions, to remove damaged organelles, to adapt to changing nutrient conditions and to maintain cellular homeostasis. Depending on the mode used to degrade the substrate into the lysosomal lumen, autophagy can be classified in macroautophagy, microautophagy and chaperone-mediated autophagy (fig.4).

Macroautophagy, often referred as autophagy, occurs when the material is sequestered into double-membrane vesicles called

autophagosome [64,65]. Based on the material to be degraded within the autophagosome, a subset of classification have been developed:

a) Mitophagy: sequestration and selective degradation of mitochondria
b) Pexophagy: sequestration and selective degradation of peroxisomes
c) Reticulophagy: sequestration and selective degradation of ER
d) Ribophagy: sequestration and selective degradation of ribosomes
e) Xenophagy: selective degradation of microbes (bacteria, fungi, or virus)
f) Aggrephagy: selective degradation of protein aggregates
g) Crinophagy: direct fusion of secretory vesicles with lysosomes.

In microautophagy, lysosomes do not fuse with autophagic vesicles, but directly surround the cytoplasmic cargos via invagination of the lysosomal membrane, followed by vesicle scission and degradation of the content in the lysosomes [66]. Microautophagy functions as “housekeeping” mechanism for the degradation of cytosolic materials. Moreover, microautophagy plays an important role in early mammalian development. Indeed, it is used to deliver endosomes to lysosomes in the visceral endoderm of mouse embryos [67].

In Chaperone-mediated autophagy (CMA) only single proteins are delivered to lysosomes for degradation [68]. Recent studies

have demonstrated the ability of CMA to participate in the regulation of multiple cellular functions suggesting that CMA failures with age may aggravate diseases such as age-associated neurodegeneration and cancer [69].

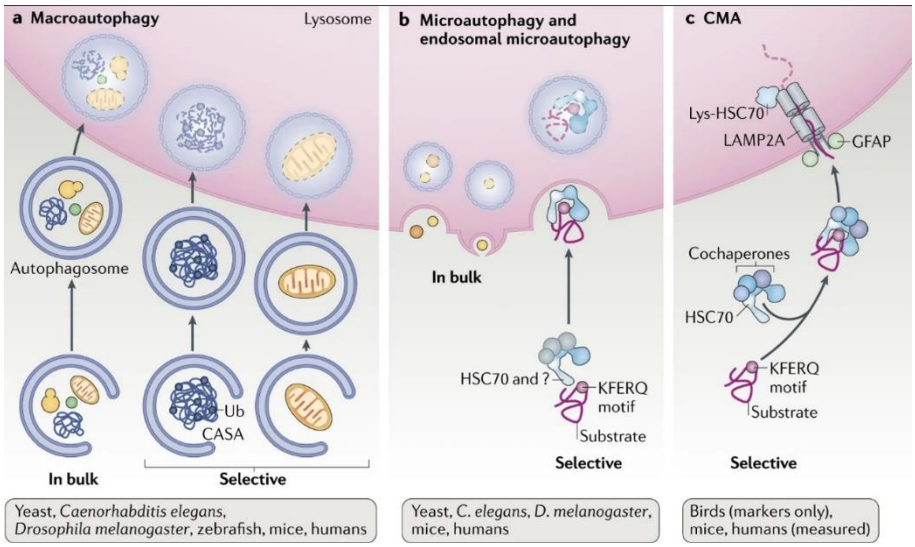

Fig. 4. Schematic autophagic pathways. (*Kaushik S. and Cuervo A.M. Nature Reviews Molecular Cell Biology 2018*)

3.1.1 The autophagic process

Activation of autophagy involves the so-called core autophagy machinery that includes multiple conservative Autophagy-Related Genes (Atg). The process is induced by decoupling of a complex named the pre-initiation complex from the suppressive regulation of the target of rapamycin (TOR) Complex 1. Inhibition of TOR leads to the activation of ULK complex that, by recruiting other Atg proteins, forms a complex

with the Focal Adhesion Kinase FIP200 [70]. This complex allows to the activation of the class III phosphatidylinositol 3-kinase (PI3K) complex, comprising Beclin-1 and vacuolar protein sorting 34 (VPS34), which catalyses the assembly of phagophore originating from various sources [71]. Two ubiquitin-like conjugation systems allow the formation of the autophagosome. One is the Atg5-Atg12-Atg16L1 system that promotes the stabilization/elongation of the developing of autophagosome and, simultaneously, the activation of the second system. This second system involves Atg4, Atg7, Atg3 and the microtubule-associated protein 1 light chain 3 factors (LC3s) [72]. The last step of autophagy include the fusion of the autophagosome with a lysosome, a process mediated by the endosomal protein Rab7 and the lysosomal protein Lamp-2 [73], and the degradation of the internalized cargo by lysosomal proteases.

3.1.2 Autophagy in neurodegeneration

A growing body of evidence suggests the existence of a correlation between alteration of the autophagic machinery and the onset of several diseases such as cancer, infection, heart disease, ageing and neurodegeneration (Fig.5). It has been found an accumulation of autophagic vacuoles in dystrophic neurites in the brains of AD patients which suggests a block of the autophagic flux [74]. Moreover, mutations in Parkin or PINK-1 are associated with autosomal recessive forms of PD and have been shown to impact the functionality of mitochondria [75,76].

In fact, it has been suggested that the autophagic quality control of mitochondria may be, at least in part, responsible for the disease [77].

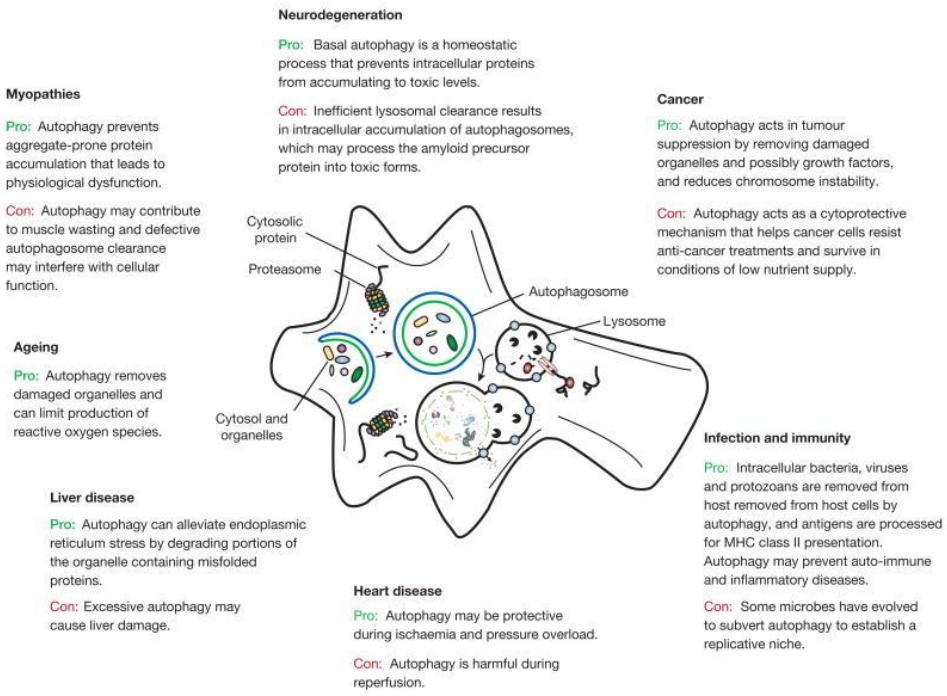

Fig.5. Autophagy in human disease (*Mizushima N. et al., Nature 2008*)

SCOPE OF THE THESIS

During the three-years PhD project, the purpose of the study has been to investigate alterations of neuroglial network linked to neuroinflammation and how they affect neuronal function, by focusing in particular on the role of mitochondrial dynamics, and morphology and activity at neuronal and astrocytic levels. Specifically, our studies included:

Chapter 2: evaluation of the anti-gliosis and neuroprotective properties of natural antioxidants in *in-vitro* models of neuroinflammation.

Chapter 3: identification of a specific mechanism of mitochondrial remodeling during NGF-differentiation, which play a key role in both neurogenesis and nerve regeneration.

References

[1] Wang DD, Bordey A. The astrocyte odyssey. Prog Neurobiol 2008;86:342–67. https://doi.org/10.1016/j.pneurobio.2008.09.015.

[2] GLOBUS JH. THE CAJAL AND HORTEGA GLIA STAINING METHODS: A NEW STEP IN THE PREPARATION OF FORMALDEHYDE-FIXED MATERIAL. Arch Neurol Psychiatry 1927;18:263–71. https://doi.org/10.1001/archneurpsyc.1927.02210020107006.

[3] Tremblay M-È, Lecours C, Samson L, Sánchez-Zafra V, Sierra A. From the Cajal alumni Achúcarro and Río-Hortega to the rediscovery of never-resting microglia. Front Neuroanat 2015;9. https://doi.org/10.3389/fnana.2015.00045.

[4] Bélanger M, Allaman I, Magistretti PJ. Brain energy metabolism: focus on astrocyte-neuron metabolic cooperation. Cell Metab 2011;14:724–38. https://doi.org/10.1016/j.cmet.2011.08.016.

[5] Quaegebeur A, Lange C, Carmeliet P. The neurovascular link in health and disease: molecular mechanisms and therapeutic implications. Neuron 2011;71:406–24. https://doi.org/10.1016/j.neuron.2011.07.013.

[6] Danbolt NC. Glutamate uptake. Prog Neurobiol 2001;65:1–105.

[7] Kofuji P, Newman EA. Potassium buffering in the central nervous system. Neuroscience 2004;129:1045–56. https://doi.org/10.1016/j.neuroscience.2004.06.008.

[8] Simard M, Nedergaard M. The neurobiology of glia in the context of water and ion homeostasis. Neuroscience 2004;129:877–96. https://doi.org/10.1016/j.neuroscience.2004.09.053.

[9] Volterra A, Meldolesi J. Astrocytes, from brain glue to communication elements: the revolution continues. Nat Rev Neurosci 2005;6:626–40. https://doi.org/10.1038/nrn1722.

[10] Barres BA. The mystery and magic of glia: a perspective on their roles in health and disease. Neuron 2008;60:430–40. https://doi.org/10.1016/j.neuron.2008.10.013.

[11] Sofroniew MV, Vinters HV. Astrocytes: biology and pathology. Acta Neuropathol (Berl) 2010;119:7–35. https://doi.org/10.1007/s00401-009-0619-8.

[12] Verkhratsky A, Parpura V, Pekna M, Pekny M, Sofroniew M. Glia in the pathogenesis of neurodegenerative diseases. Biochem Soc Trans 2014;42:1291–301. https://doi.org/10.1042/BST20140107.

[13] Verkhratsky A, Nedergaard M. Physiology of Astroglia. Physiol Rev 2018;98:239–389. https://doi.org/10.1152/physrev.00042.2016.

[14] Reichenbach A, Wolburg H. Astrocytes and Ependymal Glia. Neuroglia, New York: Oxford University Press; 2004. https://doi.org/10.1093/acprof:oso/9780195152227.003.0002.

[15] Bushong EA, Martone ME, Jones YZ, Ellisman MH. Protoplasmic astrocytes in CA1 stratum radiatum occupy separate anatomical domains. J Neurosci Off J Soc Neurosci 2002;22:183–92.

[16] Halassa MM, Fellin T, Haydon PG. The tripartite synapse: roles for gliotransmission in health and disease. Trends Mol Med 2007;13:54–63. https://doi.org/10.1016/j.molmed.2006.12.005.

[17] Araque A, Parpura V, Sanzgiri RP, Haydon PG. Tripartite synapses: glia, the unacknowledged partner. Trends Neurosci 1999;22:208–15. https://doi.org/10.1016/s0166-2236(98)01349-6.

[18] Hasan U, Singh SK. The Astrocyte-Neuron Interface: An Overview on Molecular and Cellular Dynamics Controlling Formation and Maintenance of the Tripartite Synapse. Methods Mol Biol Clifton NJ 2019;1938:3–18. https://doi.org/10.1007/978-1-4939-9068-9_1.

[19] Hamilton NB, Attwell D. Do astrocytes really exocytose neurotransmitters? Nat Rev Neurosci 2010;11:227–38. https://doi.org/10.1038/nrn2803.

[20] Petrelli F, Bezzi P. Novel insights into gliotransmitters. Curr Opin Pharmacol 2016;26:138–45. https://doi.org/10.1016/j.coph.2015.11.010.

[21] Glass CK, Saijo K, Winner B, Marchetto MC, Gage FH. Mechanisms underlying inflammation in neurodegeneration. Cell 2010;140:918–34. https://doi.org/10.1016/j.cell.2010.02.016.

[22] Araque A, Carmignoto G, Haydon PG. Dynamic signaling between astrocytes and neurons. Annu Rev Physiol 2001;63:795–813. https://doi.org/10.1146/annurev.physiol.63.1.795.

[23] Eddleston M, Mucke L. Molecular profile of reactive astrocytes--implications for their role in neurologic disease. Neuroscience 1993;54:15–36. https://doi.org/10.1016/0306-4522(93)90380-x.

[24] Frank-Cannon TC, Alto LT, McAlpine FE, Tansey MG. Does neuroinflammation fan the flame in neurodegenerative diseases? Mol Neurodegener 2009;4:47. https://doi.org/10.1186/1750-1326-4-47.

[25] Holmström KM, Finkel T. Cellular mechanisms and physiological consequences of redox-dependent signalling. Nat Rev Mol Cell Biol 2014;15:411–21. https://doi.org/10.1038/nrm3801.

[26] Uttara B, Singh AV, Zamboni P, Mahajan RT. Oxidative Stress and Neurodegenerative Diseases: A Review of Upstream and Downstream Antioxidant Therapeutic Options. Curr Neuropharmacol 2009;7:65–74. https://doi.org/10.2174/157015909787602823.

[27] Kvaltínová Z, Lukovic L, Stolc S. Effect of incomplete ischemia and reperfusion of the rat brain on the density and affinity of alpha-adrenergic binding sites in the cerebral cortex. Prevention of changes by stobadine and vitamin E. Neuropharmacology 1993;32:785–91. https://doi.org/10.1016/0028-3908(93)90187-8.

[28] Joseph JA, Denisova N, Fisher D, Shukitt-Hale B, Bickford P, Prior R, et al. Membrane and receptor modifications of oxidative stress vulnerability in aging. Nutritional considerations. Ann N Y Acad Sci 1998;854:268–76. https://doi.org/10.1111/j.1749-6632.1998.tb09908.x.

[29] Sah R, Galeffi F, Ahrens R, Jordan G, Schwartz-Bloom RD. Modulation of the GABA(A)-gated chloride channel by reactive oxygen species. J Neurochem 2002;80:383–91. https://doi.org/10.1046/j.0022-3042.2001.00706.x.

[30] Lin MT, Beal MF. Mitochondrial dysfunction and oxidative stress in neurodegenerative diseases. Nature 2006;443:787–95. https://doi.org/10.1038/nature05292.

[31] Leszek J, Barreto GE, Gąsiorowski K, Koutsouraki E, Ávila-Rodrigues M, Aliev G. Inflammatory Mechanisms and Oxidative Stress as Key Factors Responsible for Progression of Neurodegeneration: Role of Brain Innate Immune System. CNS Neurol Disord Drug Targets 2016;15:329–36.

[32] Niranjan R. The role of inflammatory and oxidative stress mechanisms in the pathogenesis of Parkinson's disease: focus on astrocytes. Mol Neurobiol 2014;49:28–38. https://doi.org/10.1007/s12035-013-8483-x.

[33] Ransohoff RM, Schafer D, Vincent A, Blachère NE, Bar-Or A. Neuroinflammation: Ways in Which the Immune System Affects the Brain. Neurother J Am Soc Exp Neurother 2015;12:896–909. https://doi.org/10.1007/s13311-015-0385-3.

[34] Zhang Q, Kang R, Zeh HJ, Lotze MT, Tang D. DAMPs and autophagy: cellular adaptation to injury and unscheduled cell death. Autophagy 2013;9:451–8. https://doi.org/10.4161/auto.23691.

[35] Takeuchi O, Akira S. Pattern recognition receptors and inflammation. Cell 2010;140:805–20. https://doi.org/10.1016/j.cell.2010.01.022.

[36] Gong T, Liu L, Jiang W, Zhou R. DAMP-sensing receptors in sterile inflammation and inflammatory diseases. Nat Rev Immunol 2019. https://doi.org/10.1038/s41577-019-0215-7.

[37] Farina C, Aloisi F, Meinl E. Astrocytes are active players in cerebral innate immunity. Trends Immunol 2007;28:138–45. https://doi.org/10.1016/j.it.2007.01.005.

[38] Arroyo DS, Soria JA, Gaviglio EA, Rodriguez-Galan MC, Iribarren P. Toll-like receptors are key players in neurodegeneration. Int Immunopharmacol 2011;11:1415–21. https://doi.org/10.1016/j.intimp.2011.05.006.

[39] Smale ST. Selective transcription in response to an inflammatory stimulus. Cell 2010;140:833–44. https://doi.org/10.1016/j.cell.2010.01.037.

[40] Burda JE, Sofroniew MV. Seducing astrocytes to the dark side. Cell Res 2017;27:726–7. https://doi.org/10.1038/cr.2017.37.

[41] Liberto CM, Albrecht PJ, Herx LM, Yong VW, Levison SW. Pro-regenerative properties of cytokine-activated astrocytes. J Neurochem 2004;89:1092–100. https://doi.org/10.1111/j.1471-4159.2004.02420.x.

[42] Garcia-Estrada J, Garcia-Segura LM, Torres-Aleman I. Expression of insulin-like growth factor I by astrocytes in response to injury. Brain Res 1992;592:343–7. https://doi.org/10.1016/0006-8993(92)91695-b.

[43] Messersmith DJ, Murtie JC, Le TQ, Frost EE, Armstrong RC. Fibroblast growth factor 2 (FGF2) and FGF receptor expression in an experimental demyelinating disease with extensive remyelination. J Neurosci Res 2000;62:241–56. https://doi.org/10.1002/1097-4547(20001015)62:2<241::AID-JNR9>3.0.CO;2-D.

[44] Chen L-W, Zhang J-P, Kwok-Yan Shum D, Chan Y-S. Localization of nerve growth factor, neurotrophin-3, and glial cell line-derived neurotrophic factor in nestin-expressing reactive astrocytes in the caudate-putamen of 1-methyl-4-phenyl-1,2,3,6-tetrahydropyridine-treated C57/Bl mice. J Comp Neurol 2006;497:898–909. https://doi.org/10.1002/cne.21014.

[45] Hohlfeld R, Kerschensteiner M, Meinl E. Dual role of inflammation in CNS disease. Neurology 2007;68:S58-63; discussion S91-96. https://doi.org/10.1212/01.wnl.0000275234.43506.9b.

[46] Knott AB, Perkins G, Schwarzenbacher R, Bossy-Wetzel E. Mitochondrial fragmentation in neurodegeneration. Nat Rev Neurosci 2008;9:505–18. https://doi.org/10.1038/nrn2417.

[47] Yen W-L, Klionsky DJ. How to live long and prosper: autophagy, mitochondria, and aging. Physiol Bethesda Md 2008;23:248–62. https://doi.org/10.1152/physiol.00013.2008.

[48] Singaravelu K, Nelson C, Bakowski D, de Brito OM, Ng S-W, Di Capite J, et al. Mitofusin 2 regulates STIM1 migration from the Ca2+ store to the plasma membrane in cells with depolarized mitochondria. J Biol Chem 2011;286:12189–201. https://doi.org/10.1074/jbc.M110.174029.

[49] van der Bliek AM, Shen Q, Kawajiri S. Mechanisms of mitochondrial fission and fusion. Cold Spring Harb Perspect Biol 2013;5. https://doi.org/10.1101/cshperspect.a011072.

[50] Bossy-Wetzel E, Barsoum MJ, Godzik A, Schwarzenbacher R, Lipton SA. Mitochondrial fission in apoptosis, neurodegeneration and aging. Curr Opin Cell Biol 2003;15:706–16. https://doi.org/10.1016/j.ceb.2003.10.015.

[51] Di Filippo M, Chiasserini D, Tozzi A, Picconi B, Calabresi P. Mitochondria and the link between neuroinflammation and neurodegeneration. J Alzheimers Dis JAD 2010;20 Suppl 2:S369-379. https://doi.org/10.3233/JAD-2010-100543.

[52] Scott I, Youle RJ. Mitochondrial fission and fusion. Essays Biochem 2010;47:85–98. https://doi.org/10.1042/bse0470085.

[53] Ni H-M, Williams JA, Ding W-X. Mitochondrial dynamics and mitochondrial quality control. Redox Biol 2015;4:6–13. https://doi.org/10.1016/j.redox.2014.11.006.

[54] Vafai SB, Mootha VK. Mitochondrial disorders as windows into an ancient organelle. Nature 2012;491:374–83. https://doi.org/10.1038/nature11707.

[55] Malpass K. Neurodegenerative disease: defective mitochondrial dynamics in the hot seat-a therapeutic target common to many neurological disorders? Nat Rev Neurol 2013;9:417. https://doi.org/10.1038/nrneurol.2013.138.

[56] Ploumi C, Daskalaki I, Tavernarakis N. Mitochondrial biogenesis and clearance: a balancing act. FEBS J 2017;284:183–95. https://doi.org/10.1111/febs.13820.

[57] Chu CT. Mechanisms of selective autophagy and mitophagy: Implications for neurodegenerative diseases. Neurobiol Dis 2019;122:23–34. https://doi.org/10.1016/j.nbd.2018.07.015.

[58] Debnath J, Baehrecke EH, Kroemer G. Does autophagy contribute to cell death? Autophagy 2005;1:66–74. https://doi.org/10.4161/auto.1.2.1738.

[59] He C, Klionsky DJ. Regulation mechanisms and signaling pathways of autophagy. Annu Rev Genet 2009;43:67–93. https://doi.org/10.1146/annurev-genet-102808-114910.

[60] Yang Z, Klionsky DJ. An overview of the molecular mechanism of autophagy. Curr Top Microbiol Immunol 2009;335:1–32. https://doi.org/10.1007/978-3-642-00302-8_1.

[61] Ashrafi G, Schwarz TL. The pathways of mitophagy for quality control and clearance of mitochondria. Cell Death Differ 2013;20:31–42. https://doi.org/10.1038/cdd.2012.81.

[62] Hara T, Nakamura K, Matsui M, Yamamoto A, Nakahara Y, Suzuki-Migishima R, et al. Suppression of basal autophagy in neural cells causes neurodegenerative disease in mice. Nature 2006;441:885–9. https://doi.org/10.1038/nature04724.

[63] Mizushima N, Hara T. Intracellular quality control by autophagy: how does autophagy prevent neurodegeneration? Autophagy 2006;2:302–4. https://doi.org/10.4161/auto.2945.

[64] Baba M, Takeshige K, Baba N, Ohsumi Y. Ultrastructural analysis of the autophagic process in yeast: detection of autophagosomes and their characterization. J Cell Biol 1994;124:903–13. https://doi.org/10.1083/jcb.124.6.903.

[65] Feng Y, He D, Yao Z, Klionsky DJ. The machinery of macroautophagy. Cell Res 2014;24:24–41. https://doi.org/10.1038/cr.2013.168.

[66] Mijaljica D, Prescott M, Devenish RJ. Microautophagy in mammalian cells: revisiting a 40-year-old conundrum. Autophagy 2011;7:673–82. https://doi.org/10.4161/auto.7.7.14733.

[67] Wada Y, Sun-Wada G-H, Kawamura N. Microautophagy in the visceral endoderm is essential for mouse early development. Autophagy 2013;9:252–4. https://doi.org/10.4161/auto.22585.

[68] Agarraberes FA, Dice JF. A molecular chaperone complex at the lysosomal membrane is required for protein translocation. J Cell Sci 2001;114:2491–9.

[69] Kaushik S, Cuervo AM. The coming of age of chaperone-mediated autophagy. Nat Rev Mol Cell Biol 2018;19:365–81. https://doi.org/10.1038/s41580-018-0001-6.

[70] Hara T, Mizushima N. Role of ULK-FIP200 complex in mammalian autophagy: FIP200, a counterpart of yeast Atg17? Autophagy 2009;5:85–7. https://doi.org/10.4161/auto.5.1.7180.

[71] Lamb CA, Yoshimori T, Tooze SA. The autophagosome: origins unknown, biogenesis complex. Nat Rev Mol Cell Biol 2013;14:759–74. https://doi.org/10.1038/nrm3696.

[72] Itakura E, Mizushima N. Characterization of autophagosome formation site by a hierarchical analysis of mammalian Atg proteins. Autophagy 2010;6:764–76. https://doi.org/10.4161/auto.6.6.12709.

[73] Romano PS, Gutierrez MG, Berón W, Rabinovitch M, Colombo MI. The autophagic pathway is actively modulated by phase II Coxiella burnetii to efficiently replicate in the host cell. Cell Microbiol 2007;9:891–909. https://doi.org/10.1111/j.1462-5822.2006.00838.x.

[74] Nixon RA. Endosome function and dysfunction in Alzheimer's disease and other neurodegenerative diseases. Neurobiol Aging 2005;26:373–82. https://doi.org/10.1016/j.neurobiolaging.2004.09.018.

[75] Exner N, Treske B, Paquet D, Holmström K, Schiesling C, Gispert S, et al. Loss-of-function of human PINK1 results in mitochondrial pathology and can be rescued by parkin. J Neurosci Off J Soc Neurosci 2007;27:12413–8. https://doi.org/10.1523/JNEUROSCI.0719-07.2007.

[76] Lutz AK, Exner N, Fett ME, Schlehe JS, Kloos K, Lämmermann K, et al. Loss of parkin or PINK1 function increases Drp1-dependent mitochondrial fragmentation. J Biol Chem 2009;284:22938–51. https://doi.org/10.1074/jbc.M109.035774.

[77] Truban D, Hou X, Caulfield TR, Fiesel FC, Springer W. PINK1, Parkin, and Mitochondrial Quality Control: What can we Learn about Parkinson's Disease Pathobiology? J Park Dis 2017;7:13–29. https://doi.org/10.3233/JPD-160989.

CHAPTER 2

Differential Modulation of NF-κB in Neurons and Astrocytes Underlies Neuroprotection and Antigliosis Activity of Natural Antioxidant Molecules

Francesca Martorana,[1,2] Maria Foti,[3] Assunta Virtuoso,[4] Daniela Gaglio,[2] Federica Aprea,[1,2] Tiziana Latronico,[5] Rocco Rossano,[6] Paolo Riccio,[6] Michele Papa,[2,4] Lilia Alberghina,[2,7] and Anna Maria Colangelo [1,2,7]

1 Laboratory of Neuroscience "R. Levi-Montalcini," Department of Biotechnology and Bioscience, University of Milano-Bicocca, Milano, Italy.

2 SYSBIO Centre of Systems Biology ISBE.ITALY, University of Milano-Bicocca, Milano, Italy.

3 School of Medicine, University of Milano-Bicocca, Monza, Italy.

4 Laboratory of Morphology of Neuronal Network, Department of Public Medicine, University of Campania "Luigi Vanvitelli", Napoli, Italy.

5 Department of Biosciences, Biotechnologies and Biopharmaceutics, University of Bari, Italy.

6 Department of Sciences, University of Basilicata, Potenza, Italy.

7 NeuroMI, Milan Center for Neuroscience, University of Milano-Bicocca, Milano, Italy

Oxidative Medicine and Cellular Longevity

Volume 2019, Article ID 8056904, 16 pages

Published 14 August 2019

doi.org/10.1155/2019/8056904

ABSTRACT

Neuroinflammation, a hallmark of chronic neurodegenerative disorders, is characterized by sustained glial activation and the generation of an inflammatory loop, through the release of cytokines and other neurotoxic mediators that cause oxidative stress and limit functional repair of brain parenchyma. Dietary antioxidants may protect against neurodegenerative diseases by counteracting chronic neuroinflammation and reducing oxidative stress. Here, we describe the effects of a number of natural antioxidants (polyphenols, carotenoids, and thiolic molecules) in rescuing astrocytic function and neuronal viability following glial activation by reducing astrocyte proliferation and restoring astrocytic and neuronal survival and basal levels of reactive oxygen species (ROS). All antioxidant molecules are also effective under conditions of oxidative stress and glutamate toxicity, two maladaptive components of neuroinflammatory processes. Moreover, it is remarkable that their antioxidant and anti-inflammatory activity occurs through differential modulation of NF-κB binding activity in neurons and astrocytes. In fact, we show that inflammatory stimuli promote a significant induction of NF-κB binding activity in astrocytes and its concomitant reduction in neurons. These changes are prevented in astrocytes and neurons pretreated with the antioxidant molecules, suggesting that NF-κB plays a key role in the modulation of survival and anti-inflammatory responses. Finally, we newly demonstrate that effective antigliosis and neuroprotective activity is achieved with

a defined cocktail of four natural antioxidants at very low concentrations, suggesting a promising strategy to reduce inflammatory and oxidative damage in neurodegenerative diseases with limited side effects.

1. Introduction

Neuroinflammation and increased oxidative stress are common hallmarks of chronic neurodegenerative disorders including Alzheimer's (AD) and Parkinson's (PD) diseases, Amyotrophic Lateral Sclerosis (ALS), and Multiple Sclerosis (MS) [1–6]. Neuroinflammatory processes involve the activation of glial cells (astrocytes and microglia) and the release of growth factors and inflammatory mediators (such as cytokines) aiming at counteracting the toxic events and promoting neuronal repair. Nevertheless, chronic astrocytic activation (reactive gliosis) may hold deleterious consequences that limit functional repair of brain parenchyma [4, 6, 7]. Reactive gliosis is characterized by proliferation and loss of proper astrocytic function, including a decrease of glial (GLAST/GLT1) and vesicular (vGLUT) glutamate transporters, which compromises synaptic function and leads to excitotoxicity [8–10]. Moreover, activated microglia produce reactive oxygen species (ROS) which further increase brain oxidative stress [5, 11, 12].

Compelling evidence has greatly enhanced the interest for the role of some dietary molecules in the prevention of many diseases, including neurodegenerative and neuroinflammatory disorders. Most dietary supplements (i.e., polyphenols, carotenoids, and thiolic compounds) are potent antioxidants. Their antioxidant and anti-inflammatory activities have been reported in cellular and animal models of neurodegeneration involving oxidative stress, such as Aβ toxicity models of AD, neurotoxin (6-OHDA or MPTP) models of PD, MS, traumatic

brain injury, and ischemia [13–16]. Moreover, several reports have shown that antioxidants activate pathways and transcription factors (such as NF-κB, Nrf2/Keap1/ARE, and PPAR/PGC-1α) that regulate metabolism and inflammatory responses [13–16]. Among transcription factors, NF-κB is induced in response to several stimuli in neurons and astrocytes. In neurons, NF-κB is activated by stress stimuli and regulates the transcription of survival genes, including growth factors, such as Nerve Growth Factor (Colangelo AM, unpublished), Bcl-2, IAP, and Mn-SOD [17]. In astrocytes, NF-κB participates in complex inflammatory loops regulating production and release of proinflammatory cytokines, such as Interleukin-1β, Tumor Necrosis Factor α (TNFα), and inducible NO synthase (iNOS) [17–19].

Natural antioxidants include polyphenols (flavonoids and nonflavonoids), as well as carotenoids and thiolic compounds. The main flavonoid molecules include quercetin (QRC) and catechins (green tea extract (GTE)), while key nonflavonoid molecules are resveratrol (RSV), curcumin (CRC), and hydroxytyrosol (Oliplus (OLP)) [20, 21]. Polyphenols are known for their effects against microbial agents, as well as for counteracting the effect of diets rich in saturated and trans-fatty acids by downregulating production of molecules related to inflammation, oxidative stress, and angiogenesis. Their known neuroprotective activity [22–27] has been reported to be dose-dependent [28], due to their hormesis effects at high concentrations [28, 29].

Other natural antioxidants are carotenoids (such as lycopene (LYC)) [30, 31] and thiolic compounds including α-lipoic acid (ALA), glutathione, and N-acetyl cysteine (NAC), known for their anti-inflammatory activity [32, 33]. For instance, ALA has been proved to act as an effective immunomodulator in the Experimental Autoimmune Encephalomyelitis (EAE) model of MS [34].

Because of their metabolic effects and their low bioavailability, the intake of polyphenols is recommended to occur as a mixture of different flavonoids and nonflavonoids [35, 36]. Combinations of polyphenols and other antioxidant compounds at low doses may increase bioavailability of dietary molecules and avoid their potential toxicity, while providing neuroprotection against oxidative stress and inflammatory processes, thus representing a promising approach in inflammation-based neurological disorders.

Here, we used primary cultures of neurons and astrocytes to assess the antigliosis and neuroprotective properties of several natural antioxidants. Our data revealed that all tested antioxidants (i) decrease gliosis by reducing astrocytic proliferation and (ii) protect cortical neurons exposed to conditioned medium (CM) from reactive astrocytes, as well as under conditions of glutamate oxidative stress toxicity; (iii) all antioxidants act through differential modulation of NF-κB in neurons and astrocytes. Finally, (iv) we newly demonstrate that effective antigliosis and neuroprotective activity can be achieved by defined cocktails of dietary antioxidants at low doses, as a

new strategy to reduce inflammatory and oxidative damage in neurodegenerative disorders with limited side effects.

2. Materials and Methods

2.1. Drugs and Reagents. Resveratrol (RSV), quercetin (QRC), curcumin (CRC), lycopene (LYC), alpha-lipoic acid (ALA), Oliplus (OLP, a mixture including hydroxytyrosol), green tea extract (GTE), and N-acetyl cysteine (NAC) were from Nutraceutica srl (Monterenzio, Bologna, Italy). 2′,7′- Dichlorodihydrofluorescein diacetate was purchased from Thermo Fisher Scientific. The TranSignal Protein/DNA Array I and EMSA Gel Shift Kit were purchased by Panomics Inc. (Fremont, CA, USA).

2.2. Primary Cortical Neurons and Astrocyte Cultures. Cortical neurons were prepared from neonatal (P1-P2) C57BL/6 mice (Harlan Laboratories, Italy) following a previously described protocol [37]. In brief, cortices were dissected, washed in dissociation medium, and digested by trypsin (0.15%) in the presence of deoxyribonuclease (DNase, 1 mg/ml; Sigma). Following mechanical dissociation, cells (1×10^6/ml) were plated onto poly-D-lysine- (1 mg/ml) coated dishes. Neurons were cultured in Neurobasal medium (Thermo Fisher Scientific) supplemented with B27 (Thermo Fisher Scientific), bFGF 10 ng/ml (Thermo Fisher Scientific), glutamine, and antibiotics (Euroclone) at 37° C in 5% CO^2. Cultures were used after 8 days in vitro (DIV).

Primary astrocytes were prepared according to a previously described protocol [10]. Cortices were dissected in Hank's Balanced Salt Solution containing HEPES/Na pH 7.4 (10 mM) and dissociated in trypsin (2.5 mg/ml) and DNase (1 mg/ml). Astrocytes were cultured in 75cm^2 flasks in Dulbecco's modified Eagle's medium (DMEM, Euroclone) containing 10% fetal bovine serum (FBS) and antibiotics. Flasks were then shaken at 200 rpm to remove type 2 astrocytes, oligodendrocytes, and microglia. For experiments, cells were plated onto poly-D-lysine-coated dishes and exposed to Tumor Necrosis Factor α (TNFα) (10 ng/ml) or lipopolysaccharide (LPS, 1 μg/ml).

2.3. Astrocyte Proliferation. Cortical astrocytes were plated onto poly-D-lysine-coated 35 mm dishes (5000 cells/well). Cells were synchronized in serum-free medium for 24 h, followed by incubation in growth media containing TNFα (10 ng/ml) or LPS (1 μg/ml) in the presence/absence of the indicated antioxidant molecules at the following concentrations: RSV 10 μM, QRC 10 μM, CRC 10 μM, LYC 10 μM, ALA 10 μM, OLP 100 μg/ml, GTE 12.5 μg/ml, and NAC 300 μM. Cells were detached by trypsin (0.25%) at defined time points (1, 2, 3, 4, 5, 6, 7, 9, 12, and 14 days). Viable cells were counted by trypan blue exclusion and expressed as percent of control.

2.4. BrdU-ELISA Cell Proliferation Assay. BrdU incorporation was assessed as described in [10] by using the BrdU Cell Proliferation Assay (Chemicon). Cells were plated onto poly-D-

lysine-coated 96-multiwell plates (2000 cells/well). After synchronization in serum-free medium, cells were incubated in growth media containing TNFα (10 ng/ml) or LPS (1 μg/ml) in the presence/absence of the indicated antioxidant molecules. Proliferating cells were labeled by adding BrdU (10 μM) to the wells during the last 24 h of treatments. Plates were then processed according to the manufacturer's instructions. BrdU incorporation was measured by using a microplate reader (Bio-Rad) at 450 nm and expressed as percent of control.

2.5. Cell Viability. Cell viability was assessed by using the MTT assay as described in [38]. Cortical neurons or astrocytes (5000 cells/well) were cultured on poly-D-lysine-coated 96-multiwell plates. Tetrazolium salts (0.5 mg/ml) were added to the culture medium during the last 4 h of treatments, followed by addition of MTT solubilization buffer (100 μl) for 1 h. Absorbance was measured by using a microplate reader at 570 nm (700 nm reference wavelength). MTT conversion levels were reported as a percent of control.

2.6. Determination of ROS. ROS production was measured according to a previously described protocol [38] by incubating cells with the ROS-sensitive fluorescent probe 2′,7′-dichlorodihydrofluorescein diacetate (DCFH2-DA, Thermo Fisher Scientific). Cells (10^5 /well) were grown onto poly-D-lysine-coated 6-multiwell plates and loaded with DCFH2-DA (10 μM) for 30 min before the end of treatments. Cells were

immediately washed with PBS and collected in 0.25% trypsin. Fluorescence measurements were performed by FACS (FACScan, Becton-Dickinson) using the Cell Quest software (BD Bioscience). Geo-mean values of 10000 cells in the gated regions were used for data analysis by WinMDI software and expressed as percent of control.

2.7. Quantitative RT-PCR. For quantitative RT-PCR, cells (1×10^6/well) were treated with LPS (1 μg/ml) and the indicated antioxidants for 3-6 h. Total RNA extraction was performed in a TRIzol Reagent (Invitrogen), followed by purification on a Qiagen RNeasy column (Mini kit, Qiagen) and DNase digestion by RNase-free DNase Set, Qiagen. Total RNA was quantified by using a NanoDrop ND-1000 Spectrophotometer, Thermo Scientific. Reverse transcription was performed on 1 μg of total RNA by using random primers and the High-Capacity cDNA Reverse Transcription Kit (Applied Biosystems). Quantitative RT-PCR (qRT-PCR) was carried out on 10 ng of total cDNA using primer sets for selected genes and the Power SYBR Green PCR Master Mix (Applied Biosystems) on a 7500 fast real-time PCR (Applied Biosystems). All samples were assessed in duplicate. Raw data (Ct (threshold cycle)) obtained from Applied Biosystems software were used to calculate the relative mRNA levels (GAPDH as housekeeping gene) by the $2^{-\Delta\Delta Ct}$ method ($\Delta Ct = Ct_{target} - GAPDH$, $\Delta\Delta Ct = \Delta Ct_{stimulated} - \Delta Ct_{not\ treated}$).

2.8. Protein/DNA Arrays. Transcription factors were identified by using the TranSignal Protein/DNA Array I (Panomics Inc.), according to manufacturer instructions. Briefly, neurons (4×10^6) were plated in 60 mm dishes. After treatments, nuclear extracts were prepared as previously described [39]. Nuclear proteins (15 µg) were incubated with the TranSignal Probe Mix containing biotin-labeled DNA binding oligonucleotides. Protein/DNA complexes were separated from free probes using spin columns (Panomics Inc.) and hybridized to an array membrane spotted with the consensus-binding sequences of 56 different transcription factors, followed by reaction with streptavidin-HRP conjugate. Signals were detected by chemiluminescence reaction and exposure to X-ray film. Bands were quantified by densitometry using NIH-ImageJ software.

2.9. Electrophoretic Mobility Shift Assay (EMSA). Binding of NF-κB in nuclear extracts was assessed by the electrophoretic mobility shift assay (EMSA) using biotin-labeled double-stranded NF-κB (5′-CCAGTGGAATTCCCCAG-3′) oligonucleotides (EMSA Gel Shift Kit, Panomics Inc.). Binding reactions were carried out for 30 min at 15° C in a 25 µl mixture containing 6 µg of nuclear protein, 10 mM Tris, 50 mM KCl, 1 mM dithiothreitol, 5 mM MgCl2, 0.06% bromophenol blue, 0.25 µg of BSA, 2 µg poly(dI-dC), and 2 pmol of oligonucleotide probe (10 ng biotin-labeled NF-κB(p65) probe). Binding specificity was confirmed by competition with a 200-fold excess of unlabeled NF-κB oligonucleotides. Nuclear extracts from HeLa cells were also

used as a positive CTR (EMSA Gel Shift Kit, Panomics). Protein-DNA complexes were separated through 6% nondenaturing polyacrylamide gel electrophoresis (PAGE, 120 V in 0.5% Trisborate-EDTA), transferred to positively charged nylon membranes (Pall Biodyne B® membrane, Pall Corporation, East Hills, NY) at 300 mA for 30 min, and UV cross-linked for 3 min. After blocking, bands were visualized by streptavidin-horseradish peroxidase (HRP) reaction, followed by the enhanced chemiluminescence detection system (ECL, Amersham) and exposure to Kodak X-OMAT Autoradiography Film. Bands were quantified by densitometry using NIH-ImageJ software.

2.10. Western Blot Analysis. Total protein extraction and Western blotting were performed following a previously described protocol [10]. After treatments, cells were immediately washed and scraped in ice-cold PBS and lysed in lysis buffer (20 mM Tris pH 8.0, 137 mM NaCl, 1% NonidetP40, 10% glycerol, and 1 mM DTT) containing Protease and Phosphatase Inhibitor Cocktail (PhosSTOP, Roche). Following 20 min incubation on ice, cellular debris were pelleted by centrifugation at 14000 g for 10 min at 4° C. Protein concentration was determined by the Bio-Rad protein assay (Bio-Rad).

Cell lysates (20-25 μg total protein) in loading buffer (50 mM Tris pH 6.8, 2% SDS, 100 mM DTT, 10% glycerol, and 0.1% bromophenol blue) were separated on 10% SDS-PAGE gels and transferred to nitrocellulose (Schleicher & Schuell). After blocking with 5% nonfat milk in TBST buffer (10 mM Tris pH 7.5, 150 mM

NaCl, and 0.2% Tween-20), blots were probed overnight at 4° C with the mouse vGLUT antibody (1 : 5000; Synaptic System) in TBST, followed by exposure to HRP-conjugated donkey anti-mouse IgG (1 : 10000; Amersham Biotech). Protein bands were detected by enhanced chemiluminescence (ECL, Amersham Biosciences) and quantified by densitometry using NIHImageJ software. β-Actin was used to normalize for differences between samples.

2.11. Statistical Analysis. Data are shown as the mean ± SEM. Statistical analysis was carried out by using GraphPad Prism for Windows 6.0 (GraphPad Software, San Diego, CA, USA). Intergroup variance was determined by ANOVA and Dunnett's multiple comparison test. Values of $p < 0.05$, <0.01, or <0.001 were taken as statistically significant.

3. Results

3.1. Effect of Antioxidant Molecules on Astrocyte Proliferation. Glial activation by inflammatory cytokines causes increased astrocytic proliferation [10] and formation of a glial scar that may limit neuronal repair [7, 9]. To assess the effect of antioxidant molecules on glial proliferation, we used cortical astrocytes activated by TNFα (10 ng/ml) or LPS (1 μg/ml). Figure 1 shows that the number of astrocytes dramatically increases (2-5-fold) during a 14-day time course (to simulate prolonged chronic glial activation) both in TNFα-treated astrocytes (Figures 1(a) and 1(d)) and, to a lesser extent, in LPS-treated cultures (Figures 1(b)

and 1(c)). Both TNFα- and LPS-induced proliferations are prevented by cotreatment with RSV (10 μM) by 4 or 7 days, respectively (Figure 1(a)).

LPS-induced astrocytic growth during a 7-day time course is also reduced by either QRC (10 μM), ALA (10 μM), or CRC (10 μM) (Figure 1(b)), as well as by LYC (10 μM), OLP (100 μg/ml), NAC (300 μM), or GTE (12.5 μg/ml) (Figure 1(c)). Selection of antioxidant concentrations was based on their dose-dependent effect on astrocytic and neuronal survival, which were similar to the doses found to be effective on neuronal PC12 cells [28].

We previously reported that effective neuroprotection was achieved with defined cocktails of antioxidants [28]. Interestingly, we found that both TNFα- and LPS-induced proliferations are reduced in astrocytes cultured with a defined cocktail of selected antioxidant molecules at lower concentrations (pool = RSV 5 μM, QRC 5 μM, OLP 7 μg/ml, and NAC 60 μM) (Figure 1(d)). No effect was seen with the single antioxidants at the low doses used in the cocktail (Figure 1(e)).

Reduction of the cell number can be due to either decreased proliferation or decreased cell survival. The effect of antioxidants on astrocytic growth was further examined in the presence of BrdU for 24 h. We found that astrocyte treatment with LPS for 7 days promotes a 60% increase of BrdU incorporation ($p \leq 0.01$) that is fully prevented by cotreatment with either RSV (10 μM), QRC (10 μM), ALA (10 μM), CRC (10 μM), LYC (10 μM), GTE (12.5 μg/ml), or NAC (300 μM) or partially reduced by OLP (100 μg/ml) (Figure 1(f)). Reduction of BrdU incorporation is also

observed in astrocytes treated with LPS in the presence of the defined pool (Figure 1(f)). These data confirmed that the decrease of cell growth elicited by these molecules is due to inhibition of astrocytic proliferation and not the consequence of decreased survival.

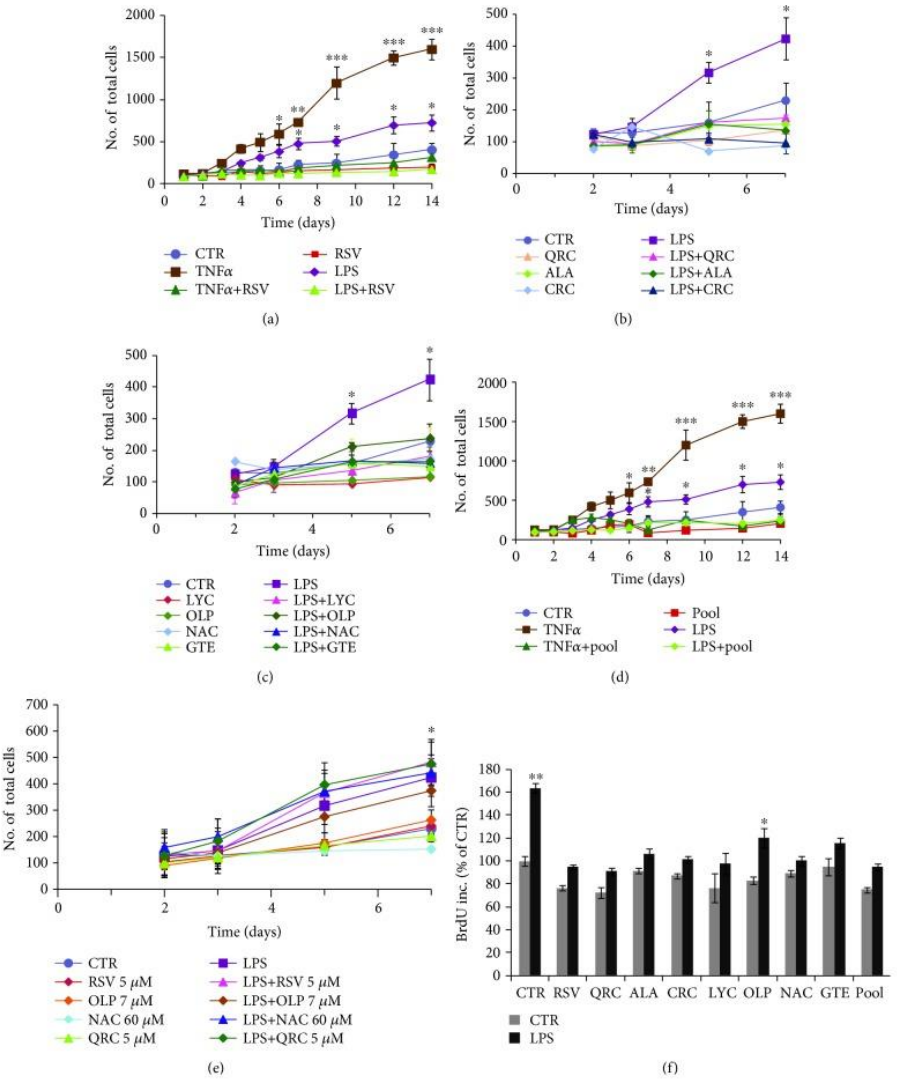

Figure 1: Reduction of astrocyte proliferation by antioxidant molecules. (a) Cell counts by trypan blue exclusion in astrocytes treated with TNFα (10 ng/ml) or LPS (1 μg/ml) and the effect of cotreatment with RSV (10 μM). (b, c) Cell numbers in astrocytes treated with LPS (1 μg/ml) and the effect of cotreatment with QRC (10 μM), ALA (10 μM), or CRC (10 μM) (b) and LYC (10 μM), OLP (100 μg/ml), NAC (300 μM), or GTE (12.5 μg/ml) (c). (d) Effect of the pool on TNFα- or LPS-induced proliferation of astrocytes. Data in (a–d) are the mean ± SEM of five independent experiments. (e) Effect of antioxidants at low doses used in the pool. (f) BrdU incorporation in cortical astrocytes stimulated with LPS (1 μg/ml) for 7 days and the antiproliferative effect of the indicated antioxidants and the pool. Data, expressed as percent

of CTR, are the mean ± SEM of three independent experiments, each performed in duplicate. $^{*}p \leq 0.05$, $^{**}p \leq 0.01$, and $^{***}p \leq 0.001$ versus CTR (ANOVA and Dunnett's multiple comparison test).

3.2. Antioxidants Improve Astrocytic Viability during Inflammatory Stimuli and Oxidative Stress. Neuroinflammation is characterized by increased ROS production by activated microglia [11, 12]. Therefore, we examined whether antioxidants sustain astrocytic survival under oxidative stress, a condition linked to neuroinflammation. Indeed, we found that astrocyte viability is slightly decreased by TNFα (24%) or LPS (20%) for 24 h but is improved during cotreatment with RSV, LYC, or OLP or significantly enhanced by QRC, ALA, CRC, NAC, or GTE ($p \leq 0.05$, 0.01, or 0.001), as compared to CTR or TNFα/LPS-treated samples (Figure 2(a)). The effect on survival was associated to a decrease of ROS levels. Time course studies showed that astrocytic ROS levels are not greatly changed by treatment with TNFα (10 ng/ml) or LPS (1 μg/ml) for 6-12-24-48-72 h (data not shown); a modest but significant induction of intracellular ROS content is found in cultures treated with TNFα (23%) or LPS (29%) for 6 or 12 h, respectively (Figure 2(b)). Both basal and TNFα/LPS-induced ROS are significantly decreased by treatment with RSV, QRC, ALA, CRC, OLP, NAC, or GTE (Figure 2(b)). No effect was seen with LYC, but an interference with the ROS-sensitive dye is possible, as evident in Figure 2(d). All antioxidants are also able to deplete both basal and H_2O_2-induced intracellular ROS (Figure 2(d)) and partially or fully

prevent the 80% reduction of survival induced by H2O2 (200 μM) treatment for 12 h (Figure 2(c)). In all these conditions (both TNFα/LPS- and H_2O_2-treated astrocytes), ROS levels and cell viability are efficiently preserved by the antioxidant cocktail (Figures 2(a)–2(d)), suggesting that supplementation of low-dose antioxidant cocktail can protect astrocytes against mechanisms triggered by neuroinflammation and oxidative stress. Alteration of astrocytic function following glial activation has been shown to reduce levels of vGLUT [10]. In agreement with previous studies, we found that both TNFα (10 ng/ml) and LPS (1 μg/ml) treatments for 24 h significantly decrease vGLUT levels, which are partially restored by cotreatment with RSV (Figures 2(e) and 2(f)), suggesting that RSV is able to rescue proper astrocytic function.

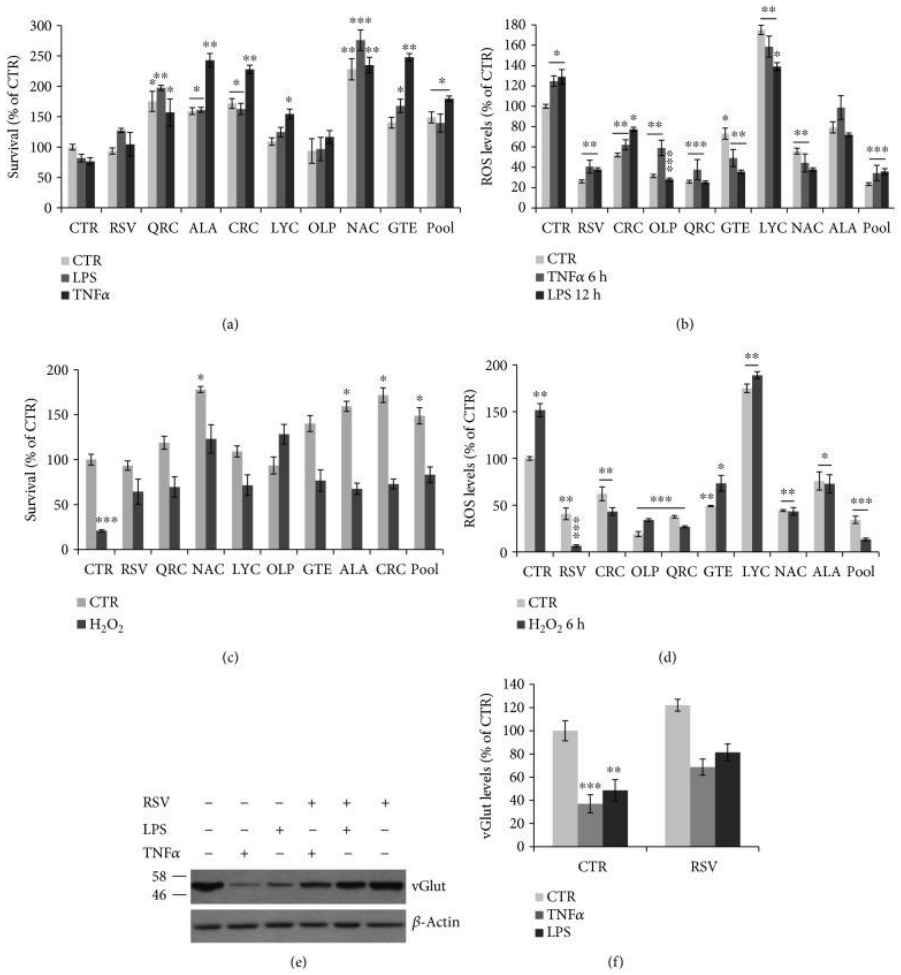

Figure 2: Effect of antioxidants on ROS levels and astrocyte viability. (a) Survival by the MTT assay of cortical astrocytes stimulated with TNFα (10 ng/ml) or LPS (1 μg/ml) for 24 h and the effect of RSV (10 μM), QRC (10 μM), ALA (10 μM), CRC (10 μM), LYC (10 μM), OLP (100 μg/ml), GTE (12.5 μg/ml), NAC (300 μM), or pool. (b) Quantitation of astrocytic ROS levels by FACS analysis of DCH2F-DA fluorescence following stimulation with TNFα (10 ng/ml) for 6 h, or LPS (1 μg/ml) for 12 h, and effect of the indicated antioxidants and pool. (c) MTT assay on astrocytes exposed to H_2O_2 (200 μM) for 24 h in the presence or absence of the indicated antioxidants and pool. (d) ROS levels in astrocytes treated with H_2O_2 (200 μM) for 6 h in the presence or absence of the indicated antioxidants and pool. All data are expressed as percent of CTR. MTT data are the mean ± SEM of three independent experiments, each performed with 4-6 samples for each treatment. ROS data

are the mean ± SEM of three independent experiments, each performed in duplicate. (e, f) Western blot analysis and quantitation of vGLUT levels in astrocytes treated for 24 h with TNFα (10 ng/ml) or LPS (1 μg/ml) and the effect of RSV cotreatment. Data, expressed as percent of CTR, are the mean ± SEM of three independent experiments. $^{*}p \leq 0.05$, $^{**}p \leq 0.01$, and $^{***}p \leq 0.001$ versus CTR (ANOVA and Dunnett's multiple comparison test).

3.3. Effect of Antioxidant Molecules on Neuroprotection against Reactive Gliosis-Induced Toxicity. Cytokines and chemokines released by activated glial cells during chronic neuroinflammation can compromise neuronal function [7, 9]. To assess glia-mediated neurotoxicity, cortical neurons were exposed for 24 h to conditioned medium (CM-LPS) prepared from astrocytes cultured in the presence of LPS (1 μg/ml) for 48 h. Data in Figure 3(a) show that CM-LPS causes a 40% decrease of neuronal viability, as compared to cortical neurons treated with CM from untreated astroglial cells (CM-CTR). Loss of neuronal survival is fully prevented or significantly enhanced in cortical neurons cotreated with either RSV (10 μM), QRC (10 μM), ALA (10 μM), CRC (10 μM), LYC (10 μM), OLP (100 μg/ml), GTE (12.5 μM), or NAC (300 μM) before addition of CM-LPS (Figure 3(a)). The effect of antioxidants on neuronal survival was also evident after treatment of neurons with CM-TNFα (data not shown) and associated with decreased intracellular ROS content. In fact, ROS production shows a 50-80% rise in neurons exposed for 6 or 24 h to CM-LPS or CM-TNFα from astrocytes (CM-A), or microglia (CM-M), or mixed astroglial cells (CM-AM), as compared to CM-CTR (Figure 3(b)), suggesting that neuronal

oxidative stress can be ascribed to both activated astrocytes and microglia. ROS production induced by CM-LPS for 6 h is restored to basal levels by RSV, QRC, ALA, CRC, GTE, or NAC or slightly lowered by LYC or OLP (Figure 3(c)). It is remarkable that neuroprotection against CM-LPS-mediated toxicity is also achieved with the cocktail (antioxidant pool) (Figures 3(a) and 3(c)).

Glutamate excitotoxicity is known to be part of the oxidative stress response following glial activation [7, 9]. Therefore, we examined the effect of antioxidant molecules in neuroprotection against oxidative stress and glutamate toxicity. As shown in Figure 3(d), treatment for 12 h with H_2O_2 (200 μM) or Glut (200 μM) causes a 30% and 45% decrease of neuronal viability, respectively. Time course studies showed that both stimuli also cause a 3-6-fold increase of ROS levels (Figure 3(e)). Both survival and ROS content are restored in neurons cotreated with RSV, QRC, ALA, OLP, GTE, or NAC, as well as by the antioxidant cocktail (Figures 3(d) and 3(f)). These data indicate that the low-dose cocktail of antioxidants is effective in neuroprotection against these two components of neuroinflammation.

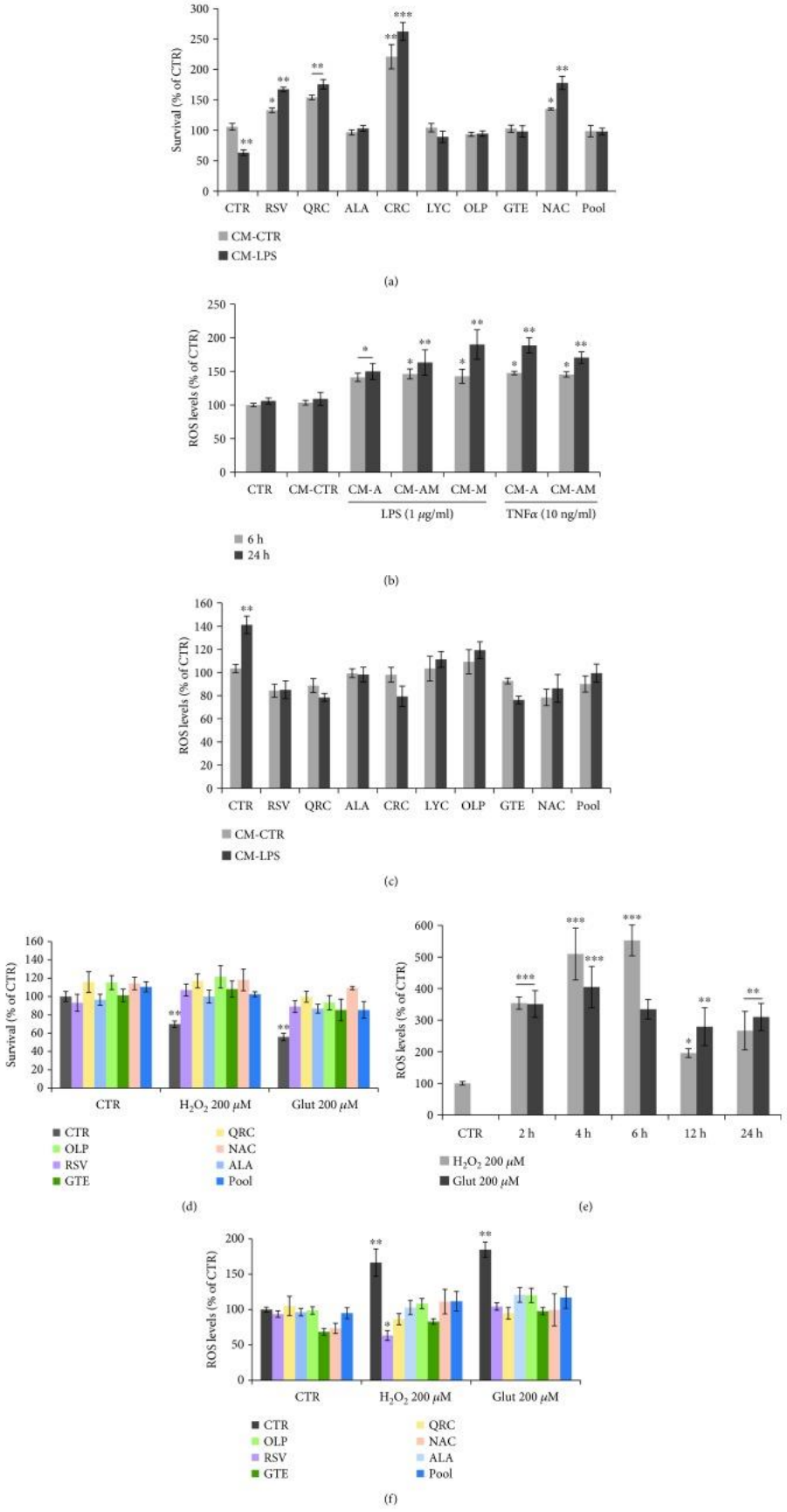
Survival (% of CTR)
CTR RSV QRC ALA CRC LYC OLP GTE NAC Pool
CM-CTR
CM-LPS
(a)
ROS levels (% of CTR)
CTR CM-CTR CM-A CM-AM CM-M CM-A CM-AM
LPS (1 μg/ml)
TNFα (10 ng/ml)
6 h
24 h
(b)
ROS levels (% of CTR)
CTR RSV QRC ALA CRC LYC OLP GTE NAC Pool
CM-CTR
CM-LPS
(c)
Survival (% of CTR)
CTR
H2O2 200 μM
Glut 200 μM
CTR
OLP
RSV
GTE
QRC
NAC
ALA
Pool
(d)
ROS levels (% of CTR)
CTR 2 h 4 h 6 h 12 h 24 h
H2O2 200 μM
Glut 200 μM
(e)
ROS levels (% of CTR)
CTR
H2O2 200 μM
Glut 200 μM
CTR
OLP
RSV
GTE
QRC
NAC
ALA
Pool
(f)

Figure 3: Effect of antioxidant molecules on neuronal ROS levels and survival. (a) MTT assay of cortical neurons exposed for 24 h to CM-LPS from LPS-stimulated astrocytes. Where indicated, neurons were preincubated ON with RSV (10 μM), QRC (10 μM), ALA (10 μM), CRC (10 μM), LYC (10 μM), OLP (100 μg/ml), GTE (12.5 μg/ml), NAC (300 μM), or pool-R. (b) Quantitation of neuronal ROS levels by FACS analysis of DCH2F-DA fluorescence following exposure to CM from LPS- or TNFα-stimulated astrocytes for 6 or 24 h. (c) Neuronal ROS levels following a 6 h treatment with CM-LPS. Where indicated, neurons were preincubated with the indicated antioxidants or the pool. (d) Survival of cortical neurons following 12 h treatment with H_2O_2 (200 μM) or Glut (200 μM), in the presence/absence of the indicated antioxidants or the lower concentration pool. (e) Time course of neuronal ROS production during incubation with H_2O_2 (200 μM) or Glut (200 μM). (f) Neuronal ROS levels following treatment with H_2O_2 (200 μM) or Glut (200 μM). Where indicated, neurons were preincubated with the indicated antioxidants or the pool. Data are expressed as percent of CTR. MTT data are the mean ± SEM of three independent experiments, each performed with 4-6 samples for each treatment. ROS data are the mean ± SEM of three experiments in duplicate. $^{*}p \leq 0\ 05$, $^{**}p \leq 0\ 01$, and $^{***}p \leq 0\ 001$ versus CTR (ANOVA and Dunnett's multiple comparison test).

3.4. Differential Regulation of NF-κB in Neurons and Astrocytes under Conditions of Reactive Gliosis. Modulation of cell survival and function involves modulation of gene transcription. Among transcription factors, we focused on NF-κB whose binding activity is modulated by survival signaling molecules and inflammatory responses [17–19].

We first assessed the effect of LPS treatment on astrocytes by RT-PCR analysis of p65/RelA, the main component of NF-κB. We found that exposure of astrocytes to LPS (1 μg/ml) for 3 h causes a 3-fold induction of p65/RelA mRNA content that is strongly prevented in astrocytes pretreated for 30 min with RSV (10 μM), QRC (10 μM), or LYC (10 μM) before addition of LPS (Figure 4(c)). A slight reduction of p65/RelA mRNA levels by

RSV, but not by QRC or LYC, is also observed at 6 h (data not shown).

In addition, we investigated NF-κB activity by EMSA. We found that NF-κB binding activity is strongly induced in astrocytes treated with LPS (1 μg/ml) for 2 h (Figures 4(a) and 4(d)). The intensity of DNA-protein complexes is lowered in nuclear extracts isolated from astrocytes preincubated for 30 min with RSV (10 μM), QRC (10 μM), CRC (10 μM), ALA (10 μM), LYC (10 μM), or NAC (300 μM). LPS-induced NF-κB activity is not significantly affected by OLP (100 μg/ml) or GTE (12.5 μg/ml) (Figures 4(a) and 4(d)). The inhibitory activity of these molecules on NF-κB binding is also observed during treatments with TNFα (10 ng/ml) (Figures 4(b) and 4(d)). Because of the role of NF-κB in regulating proinflammatory genes (such as cytokines), our data suggest that antioxidant molecules might efficiently reduce deleterious effects of the glial inflammatory loop due to excess cytokine release.

NF-κB plays also an important role in neuronal survival. It was remarkable to observe an opposite trend of NF-κB binding activity in cortical neurons. EMSA of nuclear extracts revealed that CM-TNFα (Figures 5(a)–5(c) and 5(g)) or CM-LPS (Figures 5(d) and 5(g)) cause a significant reduction of NF-κB binding activity that is prevented by pretreatment for 30 min with RSV (10 μM) (Figures 5(a) and 5(g)), QRC (10 μM) or LYC (10 μM) (Figures 5(b) and 5(g)), and ALA (10 μM) or NAC (10 μg/ml) (Figures 5(c) and 5(g)). The binding was specific, as it was fully

competed by addition of excess unlabeled oligonucleotide (Figures 4(b) and 5(e)). The effect of RSV on NF-κB was further confirmed by Western blot analysis showing cytosolic p65 protein accumulation in neurons treated with CM-LPS (Figure 5(f)). It is remarkable that NF-κB binding activity is restored by the defined antioxidant pool both in cortical astrocytes (Figures 4(a), 4(b), and 4(d)) and in cortical neurons (Figures 5(a), 5(d), and 5(g)).

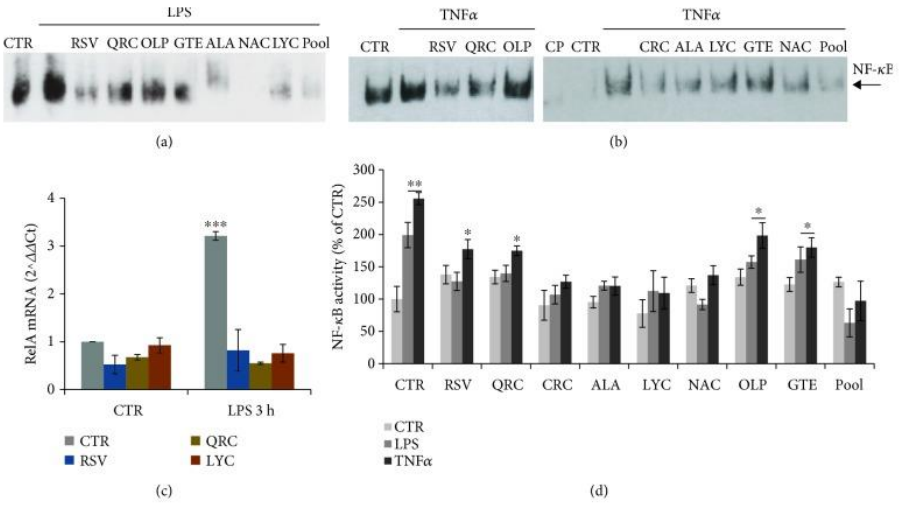

Figure 4: Effect of antioxidants on astrocytic NF-κB binding activity. (a, b) EMSA of nuclear extracts from astrocytes stimulated for 2 h with LPS (a) or TNFα (b) and the effect of RSV (10 μM), QRC (10 μM), OLP (100 μg/ml), GTE (12.5 μg/ml), CRC (10 μM), ALA (10 μM), LYC (10 μM), NAC (300 μM), or pool. CP = competition assay with excess unlabeled oligonucleotide. (c) qRT-PCR on total RNA prepared from astrocytes treated with LPS for 3 h. Where indicated, astrocytes were preincubated with RSV (10 μM), QRC (10 μM), or LYC (10 μM). Data, expressed as fold of induction (ΔΔCt), are the mean of two independent experiments. (d) Quantitative analysis of NF-κB binding activity by ImageJ software. Data, expressed as percent of CTR, are the mean ± SEM of three experiments. $^{*}p \leq 0.05$, $^{**}p \leq 0.01$, and $^{***}p \leq 0.001$ versus CTR (ANOVA and Dunnett's multiple comparison test).

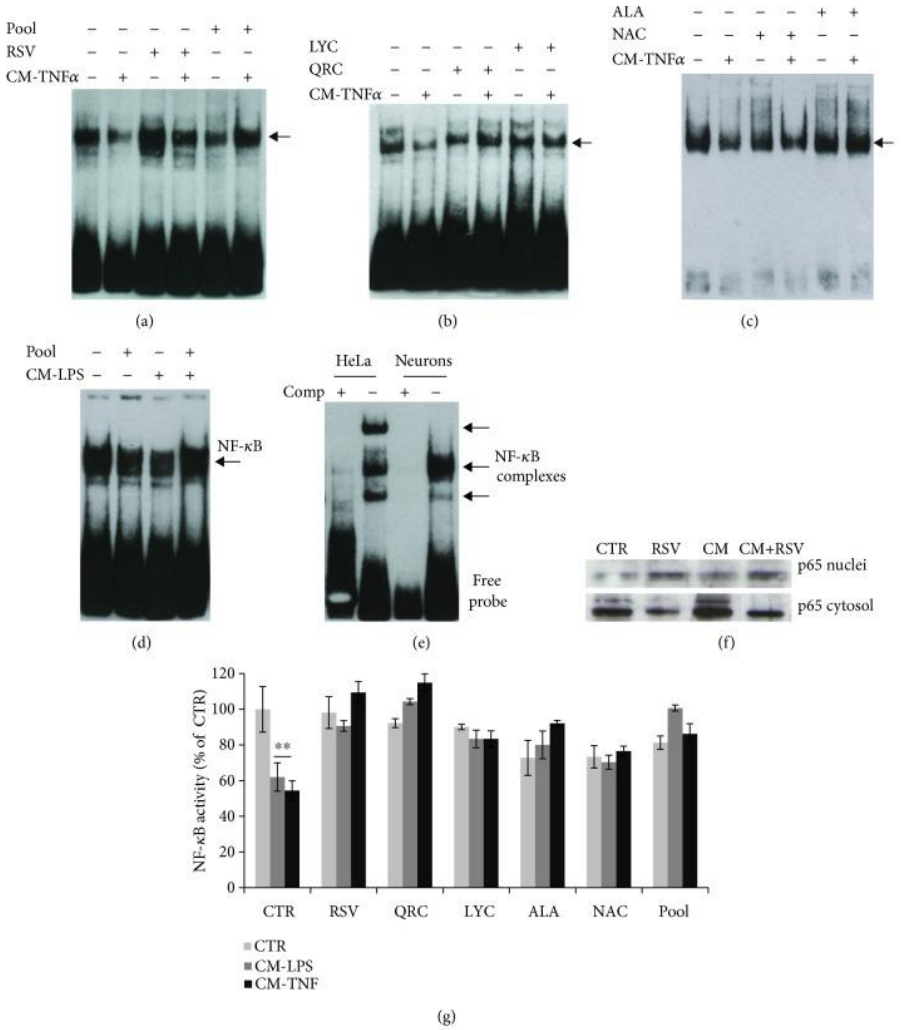

Figure 5: Effect of antioxidants on neuronal NF-κB binding activity. (a–d) EMSA of nuclear extracts prepared from cortical neurons treated for 2 h with CM from astrocytes stimulated with TNFα (a–c) or LPS (d). Where indicated, neurons were pretreated for 30 min with RSV (10 μM) (a), QRC (10 μM) or LYC (10 μM) (b), ALA (10 μM) or NAC (300 μM) (c), or the pool (a, d). (e) Competition assay with excess unlabeled oligonucleotide on nuclear extracts from neurons treated with TNFα or HeLa cells (positive CTR, EMSA NF-κB kit, Panomics). (f) Western blot analysis of p65 protein in cytosol or nuclear extracts from neurons treated with CM-LPS. (g) Quantitative analysis of NF-κB binding activity by ImageJ software. Data, expressed as percent of CTR, are the mean ± SEM of three experiments. $^{**}p \leq 0\ 01$ versus CTR (ANOVA and Dunnett's multiple comparison test).

3.5. Effect of Glial Activation and RSV on Neuronal Transcription Factors. To investigate the effect of glial activation on neuronal gene transcription, we analyzed DNA binding activity of various transcription factors by protein-DNA array. Consistent with the EMSA data, protein-DNA arrays revealed a decrease of the NF-κB signal in nuclear extracts prepared from neurons treated for 2 h with CM-LPS and a significant induction (about 2-fold) in RSV and in CM+RSV-treated neurons (Figures 6(a)–6(c)), thus confirming the role of decreased NF-κB binding activity in glia-mediated toxicity of neurons. In addition, quantitation of transcription factors showed that neuronal response to RSV involves a marked increase of binding activity for several transcription factors (CEBP, c-Myb, AP-1(2), AP-2(2), MEF-1/2, Myc/Max, SIE, Smad/SBE, Stat-6, TR, and HSE) (Figure 6(c)), suggesting that RSV has a crucial role in modulating neuronal gene expression. The role of these proteins in RSV-mediated action is currently under investigation.

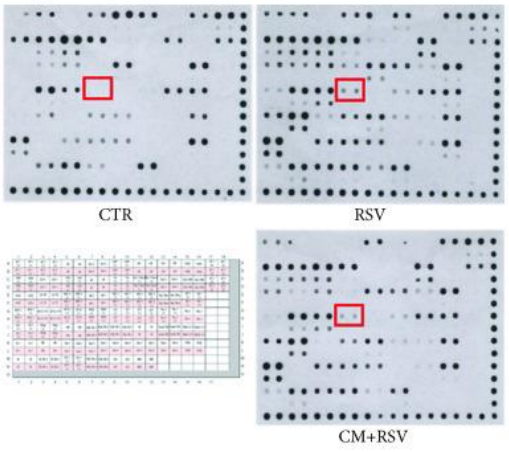

(a)

	1	2	3	4	5	6	7	8	9	10	11	12	13	14	15	16	17	18	19
A	1.068	1.073	0.813	1.069	0.207	0.198	1.017	1.062	1.744	1.735	0.180	1.266	0.179	0.194	1.414	1.438	1.767	1.675	
B	0.185	0.198	0.199	0.201	0.195	0.199	0.208	0.189	0.235	0.206	0.228	0.244	0.176	0.186	0.222	0.175	0.463	0.550	
C	1.407	1.444	1.482	1.487	1.756	1.792	1.498	1.510	0.208	0.193	0.240	0.245	1.103	1.051	0.186	0.173	1.035	0.981	
D	0.243	0.302	0.507	0.594	0.678	0.769	0.268	0.222	0.171	0.157	0.179	0.178	0.349	0.325	0.175	0.178	0.178	0.169	
E	0.195	0.210	0.653	0.691	0.772	0.832	0.423	0.330	1.233	1.201	0.236	0.263	0.172	0.185	1.413	1.370	CTR		
F	0.186	0.185	0.204	0.190	0.211	0.210	0.214	0.208	0.216	0.215	0.181	0.181	0.175	0.178	0.203	0.190			
G	0.394	0.394	1.559	1.594	1.274	1.229	0.465	0.353	0.196	0.193	0.539	0.577	1.102	1.056	1.226	1.176			
H	0.193	0.184	0.368	0.381	0.439	0.419	0.202	0.201	0.190	0.187	0.187	0.193	0.196	0.180	0.187	0.184			
I	0.743	0.660	0.932	1.055	0.307	0.326	0.947	0.804	0.782	0.766	0.233	0.237	0.214	0.190	0.962	0.935			
J	0.176	0.183	0.194	0.203	0.203	0.187	0.206	0.191	0.175	0.166	0.177	0.188	0.182	0.171	0.172	0.178			
K	1.160	1.178	0.203	0.192	0.933	0.923	0.939	0.823	0.872	0.873	0.169	0.206	0.169	0.175	1.422	1.447			
L	0.379	0.400	0.200	0.192	0.207	0.196	0.210	0.202	0.175	0.182	0.185	0.176	0.181	0.173	0.200	0.232			
M	0.554	0.520	1.050	1.012	1.420	1.474	0.813	0.787	0.188	0.186	1.424	1.463	0.172	0.176	0.171	0.184			
N	0.182	0.188	0.188	0.216	0.233	0.221	0.187	0.182	0.186	0.171	0.218	0.198	0.175	0.164	0.160	0.168			
O																			

	1	2	3	4	5	6	7	8	9	10	11	12	13	14	15	16	17	18	19
A	0.909	0.870	0.824	0.895	0.196	0.191	0.914	0.994	1.281	0.175	1.089	1.084	0.159	0.189	1.177	1.183	1.407	1.242	
B	0.171	0.223	0.218	0.210	0.202	0.180	0.182	0.169	0.393	0.256	0.513	0.463	0.181	0.184	0.265	0.233	0.653	0.666	
C	1.405	1.500	1.428	1.413	1.701	1.639	1.359	1.356	0.497	0.425	0.234	0.222	1.392	1.275	0.217	0.209	0.911	0.808	
D	0.586	0.805	0.993	1.049	0.929	0.965	0.462	0.411	0.183	0.166	0.167	0.174	0.940	0.950	0.173	0.188	0.194	0.173	
E	0.814	1.021	0.802	0.733	0.953	0.995	0.725	0.622	1.208	1.166	0.978	1.046	0.673	0.614	1.436	1.442	RSV		
F	0.164	0.182	0.200	0.198	0.200	0.201	0.219	0.200	0.703	0.682	0.205	0.202	0.192	0.178	0.410	0.407			
G	0.552	0.550	1.411	1.500	1.358	1.367	0.753	0.777	0.214	0.199	0.645	0.643	1.042	1.015	1.238	1.204			
H	0.235	0.214	0.516	0.561	0.869	0.827	0.206	0.188	0.181	0.165	0.170	0.177	0.164	0.162	0.492	0.382			
I	1.144	1.145	1.586	1.648	0.641	0.595	0.946	0.871	1.123	1.152	0.632	0.623	0.350	0.360	1.206	1.201			
J	0.206	0.242	1.104	1.116	0.203	0.191	0.205	0.180	0.523	0.510	0.165	0.181	0.157	0.167	0.267	0.235			
K	1.598	1.726	0.197	0.196	1.062	1.068	1.114	1.032	0.937	0.988	0.205	0.194	0.573	0.600	1.424	1.408			
L	1.229	1.321	0.224	0.203	0.295	0.247	0.239	0.249	0.187	0.187	0.166	0.174	0.174	0.177	0.590	0.465			
M	0.608	0.686	1.380	1.371	1.213	1.260	1.226	1.288	0.764	0.762	1.202	1.222	0.168	0.177	0.168	0.185			
N	0.176	0.193	0.536	0.744	0.265	0.280	0.350	0.339	0.202	0.194	0.403	0.408	0.178	0.195	0.187	0.175			
O																			

	1	2	3	4	5	6	7	8	9	10	11	12	13	14	15	16	17	18	19
A	0.749	0.875	0.630	0.177	0.193	0.194	0.198	0.191	0.727	0.806	0.182	0.209	0.176	0.168	1.179	1.297	1.832	1.620	
B	0.168	0.181	0.174	0.189	0.187	0.198	0.205	0.201	0.193	0.192	0.180	0.184	0.171	0.163	0.184	0.197	0.433	0.278	
C	1.733	1.698	1.554	1.452	1.986	1.882	1.431	1.488	0.196	0.198	0.189	0.197	1.580	1.548	0.197	0.192	1.151	1.054	
D	0.624	0.722	0.958	0.966	0.989	0.999	0.229	0.241	0.207	0.206	0.189	0.186	0.686	1.135	0.185	0.183	0.214	0.189	
E	0.913	0.952	0.558	0.411	0.843	0.961	0.278	0.309	1.180	1.128	0.955	1.081	0.836	0.753	1.699	1.695	CM+RSV		
F	0.166	0.177	0.196	0.184	0.192	0.207	0.213	0.211	0.214	0.196	0.211	0.186	0.193	0.185	0.374	0.245			
G	0.398	0.397	1.893	1.916	1.496	1.551	0.720	0.659	0.212	0.209	0.582	0.701	1.298	1.277	1.373	1.360			
H	0.178	0.168	0.780	0.676	0.891	0.917	0.200	0.204	0.206	0.191	0.187	0.201	0.192	0.176	0.212	0.203			
I	1.203	1.227	1.807	1.988	0.365	0.266	0.971	0.894	1.278	1.280	0.563	0.641	0.515	0.486	1.440	1.453			
J	0.171	0.179	1.079	1.048	0.205	0.218	0.208	0.213	0.410	0.395	0.200	0.195	0.206	0.183	0.215	0.209			
K	2.085	2.143	0.201	0.202	1.278	1.273	1.205	1.135	1.022	1.067	0.198	0.187	0.458	0.445	1.671	1.716			
L	1.591	1.631	0.196	0.209	0.207	0.210	0.247	0.230	0.208	0.201	0.199	0.199	0.214	0.184	0.390	0.381			
M	0.793	0.742	1.449	1.429	1.273	1.252	1.305	1.415	0.792	0.269	0.970	1.311	0.207	0.188	0.200	0.203			
N	0.175	0.185	0.536	0.751	0.244	0.241	0.239	0.217	0.208	0.216	0.210	0.279	0.200	0.186	0.199	0.192			
O																			

(b)

Figure 6: (continued)

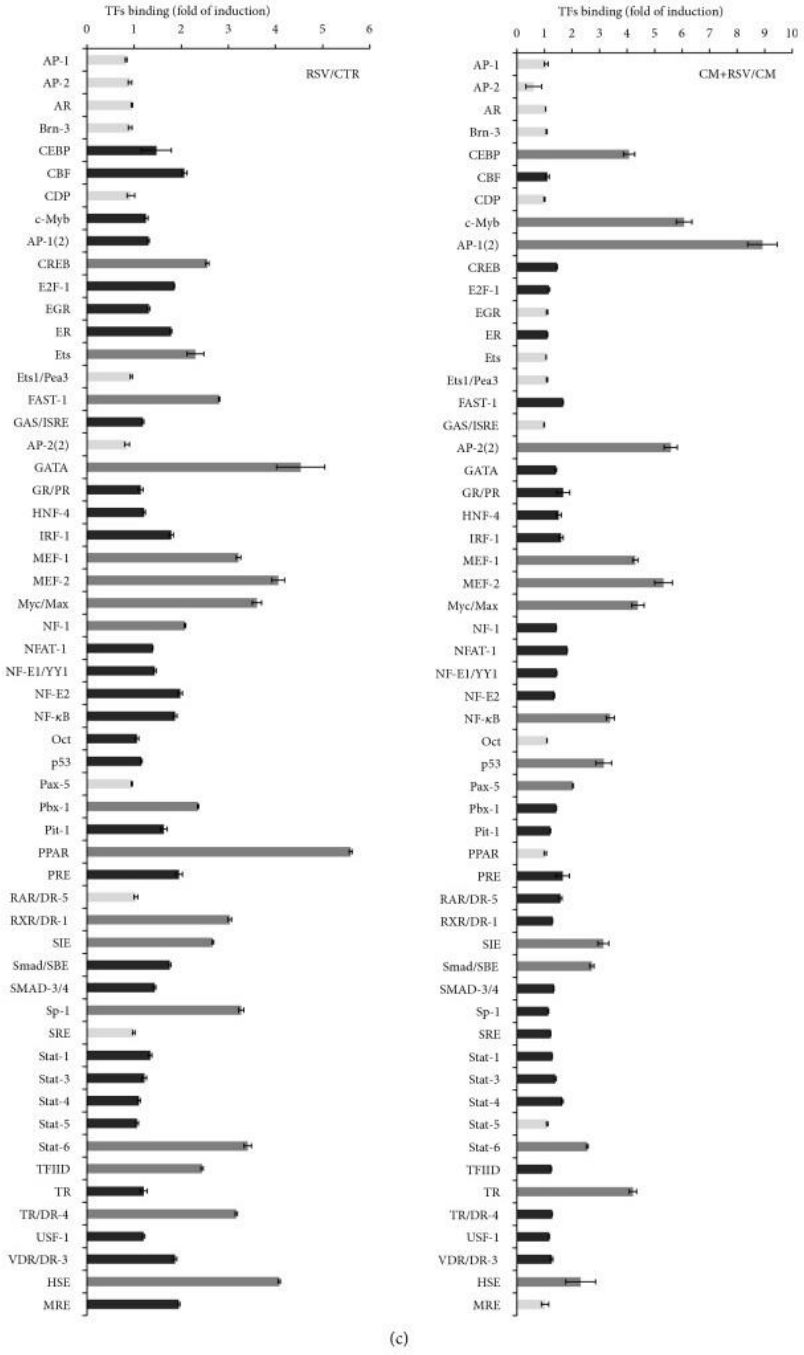

Figure 6: Modulation of neuronal transcription factor activity by glial activation and RSV. (a) Protein-DNA array of nuclear extracts prepared from cortical neurons treated for 2 h with CM (from LPS-stimulated astrocytes),

RSV (10 μM), or CM-LPS plus RSV. The grid for location of transcription factors (https://www.biocat.com/bc/pdf/MA1210_MA1215_Protein_DNA_Arrays). (b) Quantitation of transcription factors. (c) Bar graph for quantitative analysis of the ratio RSV/CTR and CM-LPS+RSV/CM-LPS. Light grey square = no change or reduction versus CTR; dark grey square = induction versus CTR (1 > 2-fold); grey square = induction versus CTR (>2-fold).

4. Discussion

Epidemiological studies indicate that diets based on vegetables, fruit, and fish consumption are healthy and protect from cancer and neurodegenerative diseases. Healthy dietary factors (i.e., polyphenols, carotenoids, and thiolic compounds) are known for their antioxidant activity. In addition, they have a marked anti-inflammatory action and influence cell metabolism by modulating the activity of enzymes, nuclear receptors, and transcription factors [35, 36].

Neuroinflammation and oxidative stress underlie neuronal and astrocytic dysfunction in neurodegenerative diseases [3, 11, 12]. In this study, we demonstrate that distinct classes of dietary antioxidants (RSV, QRC, ALA, CRC, LYC, OLP, NAC, and GTE) are able to (i) rescue neuronal viability (Figure 3) and (ii) astrocytic function (Figure 2) through mechanisms that involve (iii) reduction of astrocyte proliferation (Figure 1) and (iv) decrease of neuronal and astrocytic ROS production (Figures 2 and 3).

Our data are in agreement with a huge number of studies showing the beneficial antioxidant activity and neuroprotection of these molecules on neuronal and glial cells, both in vitro and

animal models of neurodegeneration, such as β-amyloid, or MPTP, or glutamate toxicity [22–28, 30–34]. In this regard, it is remarkable that RVS upregulates levels of the glutamate transporter vGLUT, in agreement with other studies showing that RSV improves astrocytic function by increasing glutamate uptake and glutamine synthetase activity [40–42]. Similar changes were found for ALA [43].

Antioxidants have been found to act through activation of a variety of signaling pathways. We focused on NF-κB, a multifunctional transcription factor regulating survival and proinflammatory genes in response to a variety of stress conditions that affect cellular homeostasis. A number of studies have shown that NF-κB is modulated by antioxidant molecules [27, 31, 44, 45]. Interestingly, we found that NF-κB binding activity changed in a cell-specific manner. Specifically, NF-κB binding activity increased in astrocytes treated with TNFα or LPS, sustaining current knowledge about the critical role of NF-κB in the glial inflammatory loop fostering cytokine production and neurotoxicity. In neurons, constitutive NF-κB activity is suggested to connect neuronal activity to cell survival pathways [46, 47]. Accordingly, we found that NF-κB binding activity was reduced by about 40-50% in neurons exposed to the"proinflammatory medium"(CM) from activated astrocytes. Remarkably, all tested molecules fully or partially restored basal conditions. These data are in line with our dynamic model of ROS management based on mathematical systems biology modeling, which shows the

complex molecular network connecting NF-κB to Nrf2/-Keap1/ARE in response to oxidative stress and how this pathway is regulated by a large number of stress sensors (DJ-1, Parkin, etc.) that act differently in different cellular contexts and perturbations to regulate mitochondrial function (Colangelo-Alberghina-Papa, unpublished). Finally, it was remarkable that the effect of antioxidants on astrocytic proliferation, neuronal survival, and intracellular ROS levels was efficiently achieved by treating cells with a defined cocktail of selected antioxidants at low concentrations (pool = RSV 5 μM, QRC 5 μM, OLP 7 μg/ml, and NAC 60 μM) (Figures 1–3). These data suggest that efficient neuronal and astrocytic functions are sustained by combinations of molecules belonging to distinct groups of dietary antioxidants (flavonoids, nonflavonoids, carotenoids, and thiolic compounds) at concentrations lower than those required for efficacy of each single molecule. These results are in line with our previous data of antioxidant efficacy within a strict range of concentrations in the low μM range. For instance, RSV displays neurotrophic properties on cortical neurons and neuronal PC12 [28] at very low concentrations (1-10 μM), while higher concentrations were toxic, in agreement with its well-known hormesis effect [28, 29].

Defined antioxidant cocktails were found to promote effective neuroprotection on NGF-deprived neuronal cells by depleting ROS levels and improving mitochondrial function [28].

In natural food, antioxidants are usually present in limited quantities and absorbed at even lower amounts. Moreover, it is well known that antioxidants have pleiotropic effects [35]. For

instance, some dietary antioxidants including polyphenols can downregulate the production of proinflammatory mediators, while other molecules can promote several biological functions in resting cells. Therefore, it is likely that administration of multiple dietary factors at low doses can mimic physiological conditions. Accordingly, the combined effects of two or more antioxidants have been reported [23, 28, 48–51]. However, synergistic protection by low-dose antioxidant cocktails has not been described so far in primary cultures of neurons and astrocytes. It was conceivable that the efficacy of our cocktail could be ascribed to the complementary biological activity of dietary antioxidants of the pool in modulating metabolism and mitochondrial function.

In conclusion, our study (i) provides evidence about the role of distinct dietary supplements in promoting neuronal and astrocytic function through cell-specific modulation of NF-κB and (ii) newly identifies a defined low-dose"physiological"antioxidant cocktail that reduces mechanisms of reactive gliosis and promotes neuroprotection.

Abbreviations

BrdU: Bromodeoxyuridine

DCH2F-DA: 2′ ,7′ -Dichlorodihydrofluorescein diacetate

EMSA: Electrophoretic mobility shift assay

NF-*κ*B: Nuclear factor kappa-light-chain-enhancer of activated B cells

ROS: Reactive oxygen species

ALA: Alpha-lipoic acid

CRC: Curcumin

GTE: Green tea extract

LYC: Lycopene

NAC: N-Acetyl cysteine

OLP: Oliplus

QRC: Quercetin

RSV: Resveratrol.

Data Availability

Data used to support the findings of this study are included within the article.

Conflicts of Interest

The authors declare that there is no conflict of interests regarding the publication of this paper.

Acknowledgments

This work was supported by grants from the Italian Ministry of Education, University and Research (MIUR) (PRIN2007 to AMC and MP; SYSBIO-Italian ROADMAP ESFRI Infrastructures to LA, MP, and AMC; SYSBIO-ISBE.ITALY; ALISEI-IVASCOMAR Italian National Cluster to AMC; and grant"Dipartimenti di Eccellenza-2017 to the University of Milano-Bicocca Department of Biotechnology and Biosciences") and by the EU H2020 CORBEL (Coordinated Research Infrastructures Building

Enduring Life-science Services) PID-2354 to AMC. PR acknowledges funding by the Fondazione Italiana Sclerosi Multipla (FISM) with grants 2010/R/35 and 2014/S/2.

References

[1] C. Mancuso, G. Scapagini, D. Currò et al., “Mitochondrial dysfunction, free radical generation and cellular stress response in neurodegenerative disorders,” Frontiers in Bioscience, vol. 12, no. 1, pp. 1107–1123, 2007.

[2] H. Lassmann, “Multiple sclerosis: Lessons from molecular neuropathology,” Experimental Neurology, vol. 262, Part A, pp. 2–7, 2014.

[3] R. Fischer and O. Maier, “Interrelation of oxidative stress and inflammation in neurodegenerative disease: role of TNF,”Oxidative Medicine and Cellular Longevity, vol. 2015, Article ID 610813, 18 pages, 2015.

[4] J. Leszek, G. E. Barreto, K. Gąsiorowski, E. Koutsouraki, M. Ávila-Rodrigues, and G. Aliev, “Inflammatory mechanisms and oxidative stress as key factors responsible for progression of neurodegeneration: role of brain innate immune system,”CNS & Neurological Disorders-Drug Targets, vol. 15, no. 3, pp. 329–336, 2016.

[5] B. Adamczyk and M. Adamczyk-Sowa, “New insights into the role of oxidative stress mechanisms in the pathophysiology and treatment of multiple sclerosis,” Oxidative Medicine and Cellular Longevity, vol. 2016, Article ID 1973834, 18 pages, 2016.

[6] J. J. Rodríguez-Arellano, V. Parpura, R. Zorec, and A. Verkhratsky, “Astrocytes in physiological aging and Alzheimer’s disease,” Neuroscience, vol. 323, pp. 170–182, 2016.

[7] A. M. Colangelo, L. Alberghina, and M. Papa, “Astrogliosis as a therapeutic target for neurodegenerative diseases,” Neuroscience Letters, vol. 565, pp. 59–64, 2014.

[8] V. Montana, E. B. Malarkey, C. Verderio, M. Matteoli, and V. Parpura, “Vesicular transmitter release from astrocytes,”Glia, vol. 54, no. 7, pp. 700–715, 2006, Review.

[9] M. V. Sofroniew, “Molecular dissection of reactive astrogliosis and glial scar formation,” Trends in Neurosciences, vol. 32, no. 12, pp. 638–647, 2009.

[10] G. Cirillo, A. M. Colangelo, M. Berbenni et al., “Purinergic modulation of spinal neuroglial maladaptive plasticity following peripheral nerve injury,” Molecular Neurobiology, vol. 52, no. 3, pp. 1440–1457, 2015.

[11] H. M. Gao, H. Zhou, and J. S. Hong, “NADPH oxidases: novel therapeutic targets for neurodegenerative diseases,” Trends in Pharmacological Sciences, vol. 33, no. 6, pp. 295–303, 2012.

[12] L. Qin, Y. Liu, J. S. Hong, and F. T. Crews, “NADPH oxidase and aging drive microglial activation, oxidative stress, and dopaminergic neurodegeneration following systemic LPS administration,” Glia, vol. 61, no. 6, pp. 855–868, 2013.

[13] C. Ramassamy, “Emerging role of polyphenolic compounds in the treatment of neurodegenerative diseases: a review of their intracellular targets,” European Journal of Pharmacology, vol. 545, no. 1, pp. 51–64, 2006.

[14] L. Gan and L. Mucke, “Paths of convergence: sirtuins in aging and neurodegeneration,” Neuron, vol. 58, no. 1, pp. 10–14, 2008.

[15] S. L. Albarracin, B. Stab, Z. Casas et al., “Effects of natural antioxidants in neurodegenerative disease,” Nutritional Neuroscience, vol. 15, no. 1, pp. 1–9, 2012.

[16] M. U. Rehman, A. F. Wali, A. Ahmad et al., “Neuroprotective strategies for neurological disorders by natural products: an update,” Current Neuropharmacology, vol. 17, no. 3, pp. 247–267, 2019.

[17] N. K. Jha, S. K. Jha, R. Kar, P. Nand, K. Swati, and V. K. Goswami, “Nuclear factor-kappa β as a therapeutic target for Alzheimer’s disease,” Journal of Neurochemistry, vol. 150, no. 2, pp. 113–137, 2019.

[18] Q. Li and I. M. Verma, “NF-κB regulation in the immune system,”Nature Reviews Immunology, vol. 2, no. 10, pp. 725–734, 2002.

[19] S. Pugazhenthi, Y. Zhang, R. Bouchard, and G. Mahaffey,“Induction of an inflammatory loop by interleukin-1β and tumor necrosis factor-α involves

NF-kB and STAT-1 in differentiated human neuroprogenitor cells," PLoS One, vol. 8, no. 7, article e69585, 2013.
[20] L. Bravo, "Polyphenols: chemistry, dietary sources, metabolism, and nutritional significance," Nutrition Reviews, vol. 56, no. 11, pp. 317–333, 1998.
[21] C. Manach, G. Williamson, C. Morand, A. Scalbert, and C. Rémésy, "Bioavailability and bioefficacy of polyphenols in humans. I. Review of 97 bioavailability studies," The American Journal of Clinical Nutrition, vol. 81, no. 1, pp. 230S–242S, 2005.
[22] J. M. Jazvinšćak, L. Vuković, J. Puhović, J. Erhardt, and N. Oršolić, "Neuroprotective effect of quercetin against hydrogen peroxide-induced oxidative injury in P19 neurons,"Journal of Molecular Neuroscience, vol. 47, no. 2, pp. 286–299, 2012.
[23] J. Bournival, P. Quessy, and M. G. Martinoli, "Protective effects of resveratrol and quercetin against MPP+ -induced oxidative stress act by modulating markers of apoptotic death in dopaminergic neurons," Cellular and Molecular Neurobiology, vol. 29, no. 8, pp. 1169–1180, 2009.
[24] R. D. Wight, C. A. Tull, M. W. Deel et al., "Resveratrol effects on astrocyte function: relevance to neurodegenerative diseases,"Biochemical and Biophysical Research Communications, vol. 426, no. 1, pp. 112–115, 2012.
[25] J. Lee, D. G. Jo, D. Park, H. Y. Chung, and M. P. Mattson, "Adaptive cellular stress pathways as therapeutic targets of dietary phytochemicals: focus on the nervous system," Pharmacological Reviews, vol. 66, no. 3, pp. 815–868, 2014, Review.
[26] M. Currò, A. Trovato-Salinaro, A. Gugliandolo et al., "Resveratrol protects against homocysteine-induced cell damage via cell stress response in neuroblastoma cells," Journal of Neuroscience Research, vol. 93, no. 1, pp. 149–156, 2015.
[27] B. Bellaver, L. D. Bobermin, D. G. Souza et al., "Signaling mechanisms underlying the glioprotective effects of resveratrol against mitochondrial dysfunction," Biochimica et Biophysica Acta (BBA) - Molecular Basis of Disease, vol. 1862, no. 9, pp. 1827–1838, 2016.
[28] F. Amara, M. Berbenni, M. Fragni et al., "Neuroprotection by cocktails of dietary antioxidants under conditions of nerve growth factor deprivation,"

Oxidative Medicine and Cellular Longevity, vol. 2015, Article ID 217258, 15 pages, 2015.

[29] E. J. Calabrese, M. P. Mattson, and V. Calabrese, “Resveratrol commonly displays hormesis: occurrence and biomedical significance,” Human & Experimental Toxicology, vol. 29, no. 12, pp. 980–1015, 2010.

[30] A. V. Rao and L. G. Rao, “Carotenoids and human health,”Pharmacological Research, vol. 55, no. 3, pp. 207–216, 2007.

[31] S. Hwang, J. W. Lim, and H. Kim, “Inhibitory effect of lycopene on amyloid-*β*-induced apoptosis in neuronal cells,”Nutrients, vol. 9, no. 8, p. 883, 2017.

[32] S. Salinthone, V. Yadav, R. V. Schillace, D. N. Bourdette, and D. W. Carr, “Lipoic acid attenuates inflammation via cAMP and protein kinase A signaling,” PLoS One, vol. 5, no. 9, 2010.

[33] R. Bavarsad Shahripour, M. R. Harrigan, and A. V. Alexandrov, “N-Acetylcysteine (NAC) in neurological disorders: mechanisms of action and therapeutic opportunities,”Brain and Behavior: A Cognitive Neuroscience Perspective, vol. 4, no. 2, pp. 108–122, 2014.

[34] S. E. Fiedler, V. Yadav, A. R. Kerns et al., “Lipoic acid stimulates cAMP production in healthy control and secondary progressive MS subjects,” Molecular Neurobiology, vol. 55, no. 7, pp. 6037–6049, 2018.

[35] P. Riccio, “The molecular basis of nutritional intervention in multiple sclerosis: a narrative review,” Complementary Therapies in Medicine, vol. 19, no. 4, pp. 228–237, 2011.

[36] P. Riccio, R. Rossano, and G. M. Liuzzi, “May diet and dietary supplements improve the wellness of multiple sclerosis patients? A molecular approach,” Autoimmune Diseases, vol. 2010, Article ID 249842, 12 pages, 2010.

[37] G. Sala, D. Marinig, C. Riva et al., “Rotenone down-regulates HSPA8/hsc70 chaperone protein in vitro: a new possible toxic mechanism contributing to Parkinson’s disease,” Neurotoxicology, vol. 54, pp. 161–169, 2016.

[38] F. Martorana, D. Gaglio, M. R. Bianco et al., “Differentiation by nerve growth factor (NGF) involves mechanisms of crosstalk between energy

homeostasis and mitochondrial remodeling,"Cell Death & Disease, vol. 9, no. 3, article 391, 2018.

[39] A. M. Colangelo, P. F. Johnson, and I. Mocchetti, "*β*-Adrenergic receptor-induced activation of nerve growth factor gene transcription in rat cerebral cortex involves CCAA T/enhancer-binding protein *δ*," Proceedings of the National Academy of Sciences of the United States of America, vol. 95, no. 18, pp. 10920–10925, 1998.

[40] A. Q. dos Santos, P. Nardin, C. Funchal et al., "Resveratrol increases glutamate uptake and glutamine synthetase activity in C6 glioma cells," Archives of Biochemistry and Biophysics, vol. 453, no. 2, pp. 161–167, 2006.

[41] L. M. de Almeida, C. C. Piñeiro, M. C. Leite et al., "Resveratrol increases glutamate uptake, glutathione content, and S100B secretion in cortical astrocyte cultures," Cellular and Molecular Neurobiology, vol. 27, no. 5, pp. 661–668, 2007.

[42] H. Zhou, Q. Chen, D. L. Kong, J. Guo, Q. Wang, and S. Y. Yu, "Effect of resveratrol on gliotransmitter levels and p38 activities in cultured astrocytes,"Neurochemical Research, vol. 36, no. 1, pp. 17–26, 2011, Epub 2010 Sep 15.

[43] J. Kleinkauf-Rocha, L. D. Bobermin, M. Machado Pde, C. A. Gonçalves, C. Gottfried, and A. Quincozes-Santos, "Lipoic acid increases glutamate uptake, glutamine synthetase activity and glutathione content in C6 astrocyte cell line," International Journal of Developmental Neuroscience, vol. 31, no. 3, pp. 165–170, 2013.

[44] K. Pahan, F. G. Sheikh, A. M. Namboodiri, and I. Singh, "N-Acetyl cysteine inhibits induction of no production by endotoxin or cytokine stimulated rat peritoneal macrophages, C6 glial cells and astrocytes," Free Radical Biology and Medicine, vol. 24, no. 1, pp. 39–48, 1998.

[45] J. Chen, Y. Zhou, S. Mueller-Steiner et al., "SIRT1 protects against microglia-dependent amyloid-*β* toxicity through inhibiting NF-*κ*B signaling," Journal of Biological Chemistry, vol. 280, no. 48, pp. 40364–40374, 2005.

[46] A. L. Bhakar, L. L. Tannis, C. Zeindler et al., "Constitutive nuclear factor-*κ*B activity is required for central neuron survival," The Journal of Neuroscience, vol. 22, no. 19, pp. 8466–8475, 2002.

[47] J. A. Gustin, O. N. Ozes, H. Akca et al., “Cell type-specific expression of the IκB kinases determines the significance of phosphatidylinositol 3-kinase/Akt signaling to NF-κB activation,”Journal of Biological Chemistry, vol. 279, no. 3, pp. 1615–1620, 2004.

[48] A. Conte, S. Pellegrini, and D. Tagliazucchi, “Synergistic protection of PC12 cells from β-amyloid toxicity by resveratrol and catechin,” Brain Research Bulletin, vol. 62, no. 1, pp. 29–38, 2003.

[49] S. Grasso, V. Bramanti, D. Tomassoni et al., “Effect of lipoic acid and α-glyceryl-phosphoryl-choline on astroglial cell proliferation and differentiation in primary culture,” Journal of Neuroscience Research, vol. 92, no. 1, pp. 86–94, 2014.

[50] G. Aliev, J. Liu, J. C. Shenk et al., “Neuronal mitochondrial amelioration by feeding acetyl-L-carnitine and lipoic acid to aged rats,” Journal of Cellular and Molecular Medicine, vol. 13, no. 2, pp. 320–333, 2009.

[51] L. L. Zamin, E. C. Filippi-Chiela, P. Dillenburg-Pilla, F. Horn, C. Salbego, and G. Lenz, “Resveratrol and quercetin cooperate to induce senescence-like growth arrest in C6 rat glioma cells,”Cancer Science, vol. 100, no. 9, pp. 1655–1662, 2009.

CHAPTER 3

Differentiation by nerve growth factor (NGF) involves mechanisms of crosstalk between energy homeostasis and mitochondrial remodeling

Francesca Martorana,[1,2] Daniela Gaglio,[#2,3] Maria Rosaria Bianco,[#4] Federica Aprea,[1,2] Assunta Virtuoso,[4] Marcella Bonanomi,[2] Lilia Alberghina,[1,2,5] Michele Papa,[2,4] and Anna Maria Colangelo[1,2,5]

1 Laboratory of Neuroscience "R. Levi-Montalcini", Department of Biotechnology and Biosciences, University of Milano-Bicocca, 20126 Milano, Italy

2 SYSBIO.IT, Centre of Systems Biology, University of Milano-Bicocca, Milano, Italy

3 Institute of Molecular Bioimaging and Physiology, National Research Council (IBFM-CNR), Segrate, MI, Italy

4 Laboratory of Morphology of Neuronal Network, Department of Public Medicine, University of Campania "Luigi Vanvitelli", Napoli, Italy

5 NeuroMI Milan Center for Neuroscience, University of Milano-Bicocca, Milano, Italy

 # Contributed equally.

Cell Death and Disease

2018 Mar; 9(3): 391

10.1038/s41419-018-0429-9

ABSTRACT

Neuronal differentiation involves extensive modification of biochemical and morphological properties to meet novel functional requirements. Reorganization of the mitochondrial network to match the higher energy demand plays a pivotal role in this process. Mechanisms of neuronal differentiation in response to nerve growth factor (NGF) have been largely characterized in terms of signaling, however, little is known about its impact on mitochondrial remodeling and metabolic function. In this work, we show that NGF-induced differentiation requires the activation of autophagy mediated by Atg9b and Ambra1, as it is disrupted by their genetic knockdown and by autophagy blockers. NGF differentiation involves the induction of P-AMPK and P-CaMK, and is prevented by their pharmacological inhibition. These molecular events correlate with modifications of energy and redox homeostasis, as determined by ATP and NADPH changes, higher oxygen consumption (OCR) and ROS production. Our data indicate that autophagy aims to clear out exhausted mitochondria, as determined by enhanced localization of p62 and Lysotracker-red to mitochondria. In addition, we newly demonstrate that NGF differentiation is accompanied by increased mitochondrial remodeling involving higher levels of fission (P-Drp1) and fusion proteins (Opa1 and Mfn2), as well as induction of Sirt3 and the transcription factors mtTFA and PPARγ, which regulate mitochondria biogenesis and metabolism

to sustain increased mitochondrial mass, potential, and bioenergetics. Overall, our data indicate a new NGF-dependent mechanism involving mitophagy and extensive mitochondrial remodeling, which plays a key role in both neurogenesis and nerve regeneration.

Introduction

Cell differentiation is a complex process that requires modifications of biochemical and morphological properties to meet novel specialized functions. Neuronal differentiation, in particular, involves extensive remodeling of mitochondria and their distribution along newly formed neurite processes[1,2] .

Nerve growth factor (NGF) is crucial for differentiation and maintenance of specific neuronal populations[3,4] through activation of the tyrosine kinase TrkA and the p75 receptors, and their well-characterized signaling[5]. Specifically, axonal growth also involves localized increase of intracellular Ca^{2+} (refs. [6,7]), trafficking of mitochondria to the axonal branches[2,8] and increased mitochondrial membrane potential[9,10], suggesting the relevance of mitochondria in sustaining growth cone activity in response to NGF.

Mitochondria play a crucial role during neurogenesis and in post-mitotic neurons by supplying the energy requested for growth cone activity, axonal growth, and synaptic function[11]. Several studies found that neuronal differentiation is accompanied by metabolic reprogramming to meet the increased energy demand. This is achieved by fostering glucose and glutamine metabolism[12,13], as well as the oxidative phosphorylation[14,15], thus leading to higher generation of ROS and the need to increase mitochondrial biogenesis[12] and quality control by mitophagy[13].

Increasing evidence accumulated about the role of autophagy in differentiation and development[16]. Autophagy was

found to regulate the differentiation of neural stem cells[17], neuroblastoma[18], retinal ganglion cells[13], and myoblasts[19,20]. During autophagy, damaged proteins and/ or organelles are sequestered within autophagosomes through a complex process regulated by autophagyrelated (Atg) proteins. Autophagosomes fuse with lysosomes for degradation of their content, and the breakdown products are recycled as building blocks to maintain metabolic homeostasis under stress conditions[21,22]. In addition to Atg proteins, autophagy during neurogenesis was found to be regulated by Ambra1 (activating molecule in Beclin-1-regulated autophagy), whose deficiency caused neural tube defect[23,24].

Autophagy during differentiation of myoblasts and neuroblastoma resulted to be induced by AMP-activated kinase (AMPK)[18,19], a sensor of energy metabolism that activates autophagy through inhibition of mammalian TOR (mTOR)[22,25]. Phospho(Thr172)-AMPK can be induced by a rise in cellular AMP:ATP ratio and by reactive oxygen species (ROS)[22,25], as well as by Ca^{2+}-calmodulin-dependent protein kinase (CaMKK)[26,27]. In myoblasts and retinal ganglion cells, autophagy involved the selective removal of mitochondria[13,20].

Mitochondrial dynamics is crucial during axonal growth. Mitochondrial biogenesis[12] and cycles of fission–fusion regulate mitochondrial transition between elongated and fragmented mitochondria for translocation to neurites or removal by mitophagy[28,29]. Fragmentation is controlled by dynamin-related protein-1 (Drp1) through PKA or CaMKI phosphorylation, whereas optic atrophy-1 (Opa1) and mitofusin-1/2 (Mfn1-2)

regulate mitochondrial fusion from the inner and outer mitochondrial membrane, respectively[28–31].

In this study, we demonstrate that NGF-induced differentiation involves modulation of Atg9-Ambra1- dependent mitophagy through activation of P-AMPK and P-CaMK triggered by altered energy homeostasis and mobilization of intracellular Ca^{2+}. In addition, we newly show that mitophagy is accompanied by mechanisms of mitochondrial remodeling, both fission–fusion and biogenesis, which sustain increased mitochondrial mass and potential, and boost mitochondrial bioenergetics.

Results

Upregulation of autophagy during NGF-induced differentiation

To investigate mechanisms involved in NGF-induced differentiation, we employed PC12-615 cells overexpressing TrkA receptors[32], which differentiate more rapidly and in response to lower NGF concentrations[32] (Fig. 1a, b), compared to PC12wt (Supplementary Fig. S1A–C)[32,33]. To evaluate whether NGF differentiation induces autophagy, we measured LC3-II content[34]. Time-course studies showed that LC3-II levels do not change at short time-points, but start to increase in PC12-615 exposed to NGF (10 ng/ml) for 12 h (Fig. 1c) and remain twofold higher than CTR for 24–120 h, thus showing a trend that correlates with their initial neurite extension and the post-mitotic state (Fig. 1c and Supplementary Fig. S1D, G). These data were

confirmed by using the Cyto-ID® Autophagy detection kit. Both fluorimetric analysis (Fig. 1d) and fluorescence microscopy (Fig. 1e, f) show enhanced fluorescence at 24 h, but not at 4 h. NGF-mediated increase of LC3-II is similar to Rapamycin (Rap) and is partially prevented by 3-methyladenine (3-MA) and by wortmannin (WT) (Supplementary Fig. S1E, F, H, I).

LC3-II increase may represent either enhanced autophagosome synthesis or blockage of autophagosome degradation[34]. To rule out a block of the autophagosome turnover, we measured LC3-II levels in PC12 cells treated with NGF in the presence of Bafilomycin A1 (Baf). Baf-treated cells show a twofold increase of LC3-II that is further enhanced during co-treatment with NGF for 6–12 h (Fig. 2a, b). The same extracts show a significant reduction of p62/SQSTM1, an adaptor protein that facilitates autophagic degradation of poly-ubiquitinated proteins (Fig. 2a, c), thus supporting the role of NGF in fostering the autophagic flux. A similar trend was found at 24–48 h (Supplementary Fig. S2A–C). The apparent discrepancy between lack of LC3-II accumulation and reduced p62 protein levels at 6 h might reflect a higher degradation rate at this time (Supplementary Fig. S2D), as supported by the upregulation of the lysosomal cysteine protease cathepsin S (Ctss) (Supplementary Fig. S3A).

Finally, the role of NGF in modulating autophagy was confirmed by examining the autophagic flux in PC12 cells expressing a GFP-RFP-LC3 tandem fluorescent protein[34]. Untreated PC12 cells display some diffused fluorescence with a

few yellow-green dots. Fluorescence intensity is increased following NGF treatment for 6–48 h (Fig. 2d, e), as determined by orange-red fluorescent vesicles mostly located at growth cones (Fig. 2e, arrows). Induction of autophagosome formation by NGF or by Rap is partially prevented by 3-MA, while their maturation is blocked by Baf and by colchicine (CLC), a microtubuledepolymerizing agent that inhibits transport (and fusion) of autophagosomes to lysosomes (Fig. 2e and Supplementary Fig. S2E).

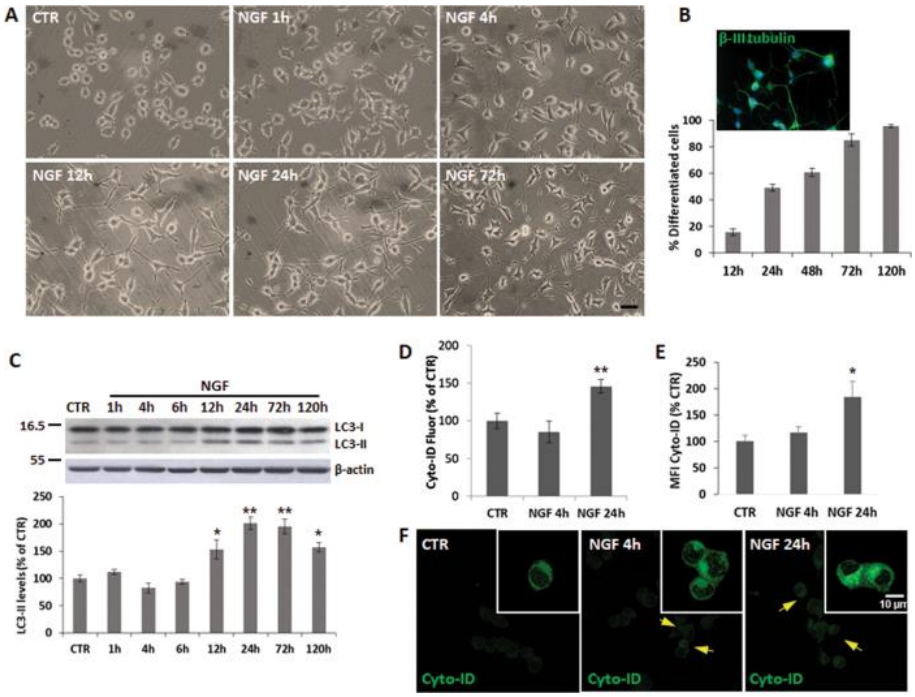

Fig. 1 NGF-differentiated PC12 cells show increased autophagy. **a** Representative images of PC12-615 exposed to NGF (10 ng/ml) for 1–4–12–24–72 h. Scale bar = 25 μm. **b** Neuronal PC12 differentiation is measured as percent of cells with neurite processes whose length is at least twice the diameter of cell body. A representative image of β-III tubulin staining is shown in the inset. Data are the mean ± SEM of at least three separate experiments, each performed in duplicate. **c** Densitometric analysis of LC3-II normalized by the β-actin content in PC12-615 cells exposed to NGF (10 ng/ml) for the indicated times. A representative immunoblot of LC3 is shown above. Data, expressed as percent of CTR, are the mean ± SEM of three independent experiments with duplicate samples. **d** Analysis of autophagy by fluorimetry using Cyto-ID® Autophagy detection kit in PC12- 615 treated with NGF for 4 or 24 h. Data are the mean ± SEM of two separate experiments, each with three independent samples. **e** Analysis of CytoID® autophagy by fluorescence microscopy in PC12-615 treated with NGF for 4 or 24 h. Data, expressed as percent of CTR, are the mean ± SEM of the mean fluorescence intensities (MFI) normalized by the total number of cells (about 100 cells) in ten random fields from three independent experiments in duplicate. **f** Representative images of Cyto-ID® fluorescence in PC12-615 treated with NGF for 4 or 24 h. Scale bar = 10 μm. $*p \leq 0.05$, $**p \leq 0.01$ vs. CTR (ANOVA and Dunnett's multiple comparisons test).

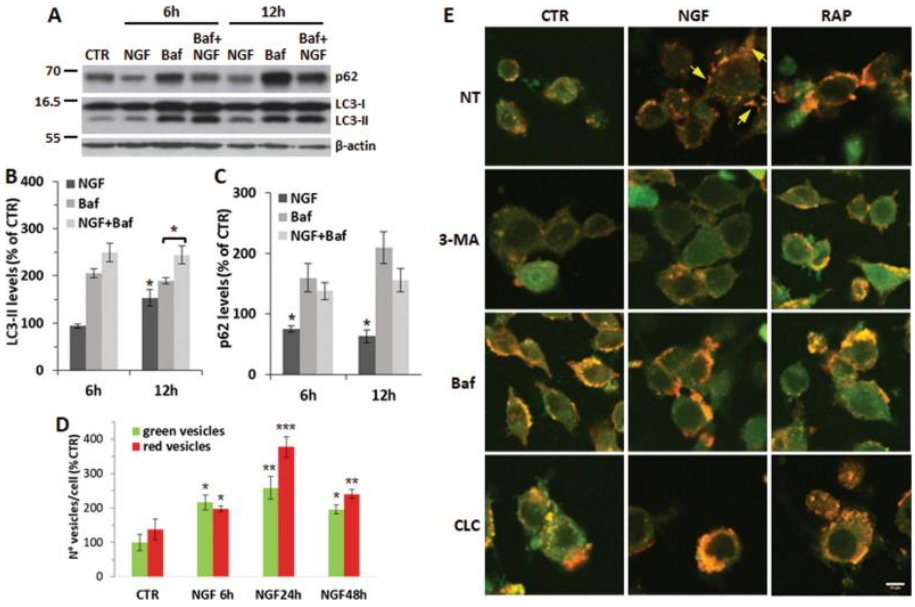

Fig. 2 Analysis of the autophagic flux in NGF-treated PC12 cells. **a** Representative immunoblots for LC3-II and p62 content in PC12-615 cells treated for 6 or 12 h with NGF (10 ng/ml) alone or in combination with Baf (100 nM). Values are normalized by the β-actin content. **b–c** Densitometric analysis of LC3-II (**b**) and p62 (**c**) normalized by β-actin. Data are the mean ± SEM of three independent experiments in duplicate. $*p \leq 0.05$ vs. CTR or Baf (*t*-test). **d** Quantitation of green and red vesicles in GFP-RFP-LC3-transfected cells by ImageJ software. Data, expressed as percent of CTR, are the mean ± SEM of the number of vesicles/cell (about 100 cells for each condition) in ten random fields from three separate experiments. $*p \leq 0.05$, $**p \leq 0.01$, $***p \leq 0.001$ vs. CTR (*t*-test). **e** Representative images of GFP-RFP-LC3 fluorescence in PC12 cells treated for 24 h with NGF (10 ng/ml) or Rap (200 nM) alone or in combination with 3-MA (10 mM), or Baf (100 nM) or CLC (1 μM). Scale bar = 10 μm

Inhibition of autophagy suppresses neuronal differentiation in response to NGF

To substantiate the activation of autophagy by NGF, we performed small-interfering RNA (siRNA) knockdown of autophagy-related genes. Reverse transcription PCR (RTPCR) analysis on NGF-treated cells shows upregulation of Atg9b and Atg12, together with Ambra1, which regulates autophagy during neuronal development[17,23] (Supplementary Fig. S3A). Their siRNA knockdown decreases protein levels (Supplementary Fig. S3B, D) and causes loss of NGF modulation of LC3-II (Fig. 3a and Supplementary Fig. S4A), as well as of beclin-1 (Supplementary Fig. S4B, D) and p62 (Supplementary Fig. S4C, E). Interestingly, siRNA knockdown studies established the relevance of autophagy in NGF-induced differentiation: both variants of si*Ambra1*, si*Atg9b* and si*Atg12* produce a 52–80% reduction of neurite outgrowth, compared to CTR and siRNA-*SCR* cells (Fig. 3b, c). It is noteworthy that siRNA-transfected cells show a rounded-up morphology and are more prone to cluster. Furthermore, upon NGF treatment most cells display enlarged growth cones, but do not differentiate properly (Fig. 3c). However, siRNA-transfected cells still showed enhanced GAP-43 levels in response to NGF (Supplementary Fig. S4F), suggesting that the block of autophagy does not interfere with NGF regulation of axonal components.

The impact of autophagy on NGF-mediated differentiation was confirmed by its pharmacological inhibition. Autophagy inhibition by 3-MA, or blockage of lysosomal activity (Baf or

NH_4Cl), or microtubule disruption (CLC or NOC) do not change the morphology of growing cells, but dramatically reduce their ability to differentiate in response to NGF (Fig. 4a, b). It is remarkable that NOC does not alter growth cone formation, but completely blocks neurite extension in response to NGF, while CLC causes extensive vacuolation (Fig. 4a, arrowheads), eventually leading to cell death (Fig. 5d). On the other hand, Rap (200 nM) does not affect NGF response (Fig. 4a, b), suggesting that autophagy is required for NGF-mediated differentiation, which occurs only after the appropriate NGF signaling.

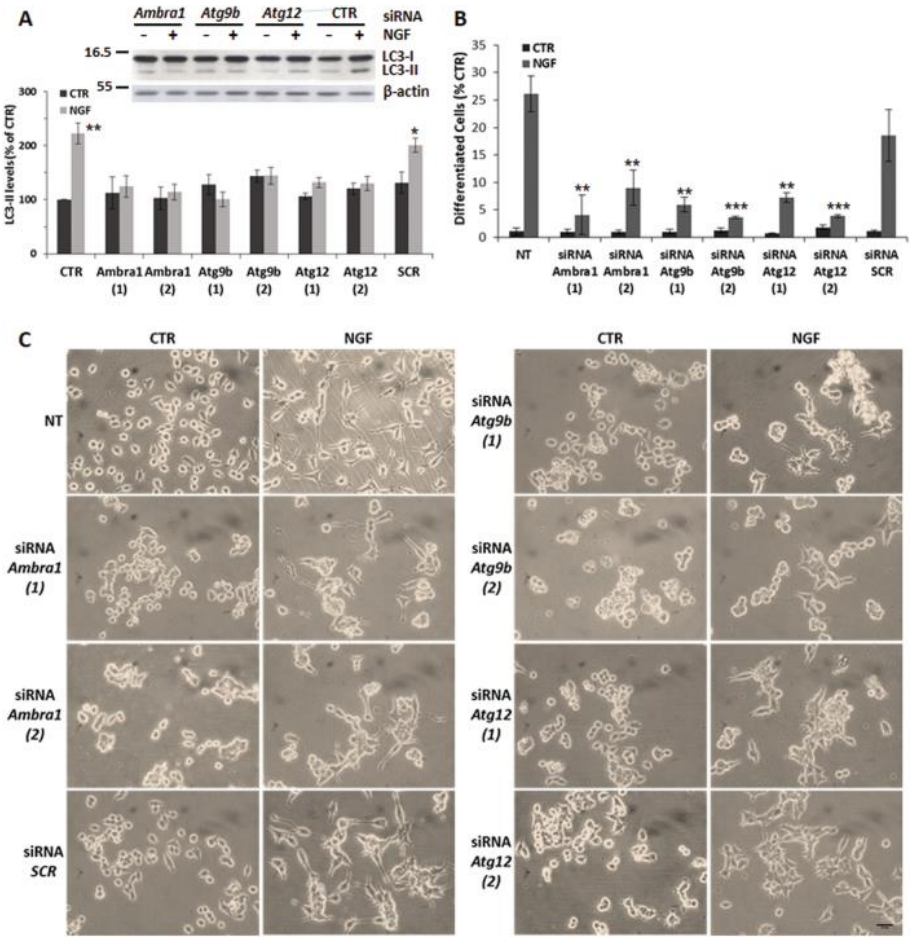

Fig. 3 Inhibition of NGF-mediated differentiation by autophagy siRNA knockout. **a** Densitometric analysis of LC3-II/β-actin ratio in PC12-615 cells transfected with siRNA for *Ambra*1, *Atg9b*, or *Atg12*, followed by NGF treatment for 24 h. A representative immunoblot of LC3-II is shown above. Data, expressed as percent of CTR, are the mean ± SEM of three independent experiments with duplicate samples. **b** Quantitation of NGF-induced differentiation in PC12-615 cells transfected with siRNA for *Ambra1*, *Atg9b* or *Atg12* (SCR as negative control). Data, expressed as percent of differentiated cells in ten random fields, are the mean ± SEM of three separate experiments. $*p \le 0.05$, $**p \le 0.01$, $***p \le 0.001$ vs. their respective CTR (**a**), or vs. NGF in non-transfected (NT) cells (**b**) (ANOVA and Dunnett's multiple comparisons test). **c** Representative images of NGF-induced differentiation in PC12-615 cells transfected with siRNA-*Ambra1*, siRNA-*Atg9b*, or siRNA-*Atg12* (siSCR as control) followed by exposure to NGF (10 ng/ ml) for 24 h. Scale bar = 25 μm

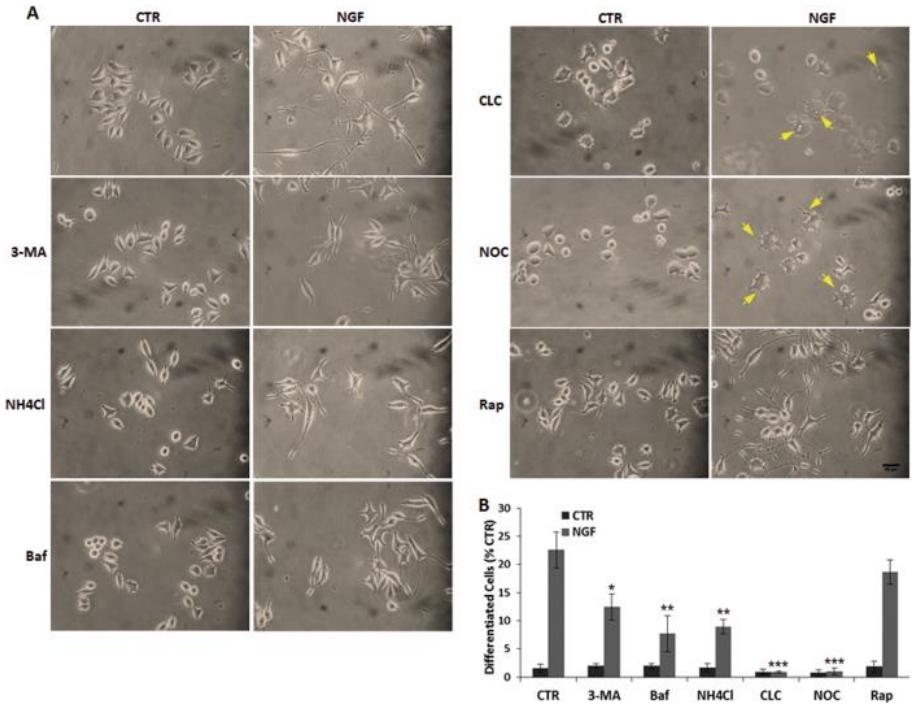

Fig. 4 Pharmacological inhibition of autophagy abolishes NGF-mediated differentiation. a Representative images of PC12-615 cells following treatment for 24 h with NGF (10 ng/ml) alone or in combination with 3-MA (10 mM), or Baf (100 nM), or NH_4Cl (12.5 mM), or CLC (1 μM), or NOC (1 μM), or Rap (200 nM). **b** Quantitation of NGF-induced differentiation in PC12-615 cells treated for 24 h with NGF alone or in combination with the autophagy blockers. Data, expressed as percent of differentiated cells in ten random fields, are the mean ± SEM of three separate experiments. $*p \leq 0.05$, $**p \leq 0.01$, $***p \leq 0.001$ vs. NGF (ANOVA and Dunnett's multiple comparisons test). Scale bar = 25 μm

Calcium and AMPK energy signaling underlie NGF-induced autophagy during differentiation

To investigate signaling pathways triggering autophagy during NGF-induced differentiation, we examined the activation of AMPK and mTOR, two kinases known to regulate autophagy[22]. Time-course studies revealed that NGF treatment for 1 h causes a 2.5–3-fold induction of P(Thr172)-AMPK, which remains higher than CTR up to 24 h (Fig. 6a). P-mTOR, instead, is slightly reduced between 12–24 h (Supplementary Fig. S5A), although an opposite trend of both kinases and p62 is observed with higher NGF concentrations (Supplementary Fig. S5B–E). P(Thr172)-AMPK can be induced by increased AMP/ATP ratio[22], as well as by N-CaMK-II in response to increased intracellular Ca^{2+} levels[26,27,35]. We found that CaMK is phosphorylated (P-Thr286) by 30 min of NGF treatment (Fig. 6b), in line with previous studies showing that NGF induces the mobilization of intracellular Ca^{2+} from the endoplasmic reticulum (ER) in a TrkA-dependent manner[6] .

To examine the impact of the Ca^{2+}-CaMKII and AMPK signaling on PC12 differentiation, we assessed the effect of their pharmacological inhibition. We found that both the AMPK inhibitor compound C (CC) and the selective $Ca^{2+/}$CaMKII inhibitor (STO609) dramatically prevent NGF-induced differentiation (Fig. 6c, d) and GAP-43 expression (Supplementary Fig. S6A). Both molecules inhibit autophagy[26,27], thus linking both kinases signaling to NGF-induced autophagy during differentiation. Neurite outgrowth is also dramatically

reduced by treating cells with NGF in combination with the cell-permeant Ca^{2+}-chelator Bapta-AM, or with the ER-Ca^{2+}-release inhibitor dantrolene (DA) or, to a lesser extent, with the ER-Ca^{2+}-ATPase inhibitor thapsigargin (TG) (Fig. 6c, d), thus confirming the relevance of ER-Ca^{2+} signaling in NGF-induced differentiation[6] . Lack of NGF differentiation during treatment with the pharmacological inhibitors is not due to cell death. Some apoptotic nuclei (1–12%) are found only in cells treated with the Ca^{2+} inhibitors alone, but not during co-treatment with NGF (Supplementary Fig. S6B, C), in agreement with previous findings of NGF-mediated neuroprotection against calcium ion-induced apoptotic cell death[36,37].

Interestingly, NGF also causes a slight increase of mitochondrial Ca^{2+} in a TrkA-dependent manner in PC12-615, but not in PC12nnr5 (Supplementary Fig. S7A–C). Mitochondrial Ca^{2+} is known to affect the activity of enzymes regulating ATP synthesis, including glycerol-3-phosphate dehydrogenase on the cytoplasmic side of the inner mitochondrial membrane, and pyruvate dehydrogenase, NAD-dependent isocitrate dehydrogenases and α-ketoglutarate dehydrogenase in the mitochondrial matrix[38]. However, the partial effect of Ca^{2+} and CaMKII inhibitors, as compared to CC, clearly suggests the intervention of mechanisms exclusively related to energy balance.

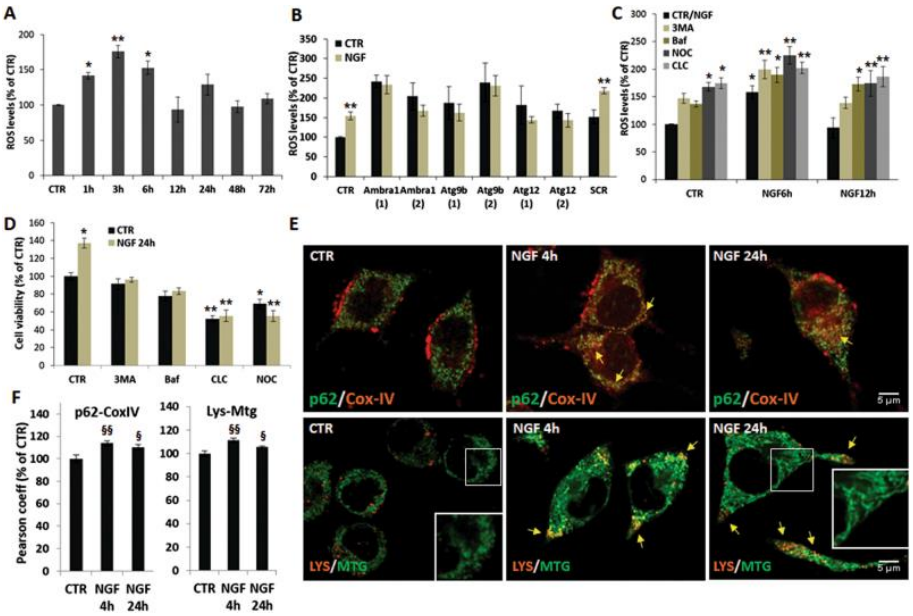

Fig. 5 NGF-mediated increase of ROS underlies the induction of mitophagy. **a** Time-course of ROS levels in PC12-615 cells treated with NGF (10 ng/ml) for the indicated times. **b** Effect of *Ambra-1*, *Atg9b*, or *Atg12* siRNA on ROS production after exposure to NGF for 6 h. **c** Effect of autophagy inhibitors on ROS content following NGF treatment for 6 or 12 h. Data in **a, b**, **c**, expressed as percent of CTR, are the mean ± SEM of three independent experiments with duplicate samples. **d** Effect of autophagy inhibitors on cell viability after NGF treatment for 24 h. Data, expressed as percent of CTR, are the mean ± SEM of two separate experiments, each with five samples. **e** Representative images of PC12-615 cells treated with NGF (10 ng/ml) for 4–24 h, followed by immunostaining for p62 (green)/CoxIV (red) or addition of LYS and MTG during the last 30 min of incubation. Scale bar = 5 µm. **f** Co-localization of p62/CoxIV or LYS/MTG measured by Pearson coefficient of correlation in about 100 cells for each condition in ten random fields. Data are the mean ± SEM of three independent experiments in duplicate. *$p \leq 0.05$, **$p \leq 0.01$ vs. their respective CTR (ANOVA and Dunnett's multiple comparisons test); § $p \leq 0.05$, $^{\S\S}p \leq 0.01$ vs. CTR (*t*-test)

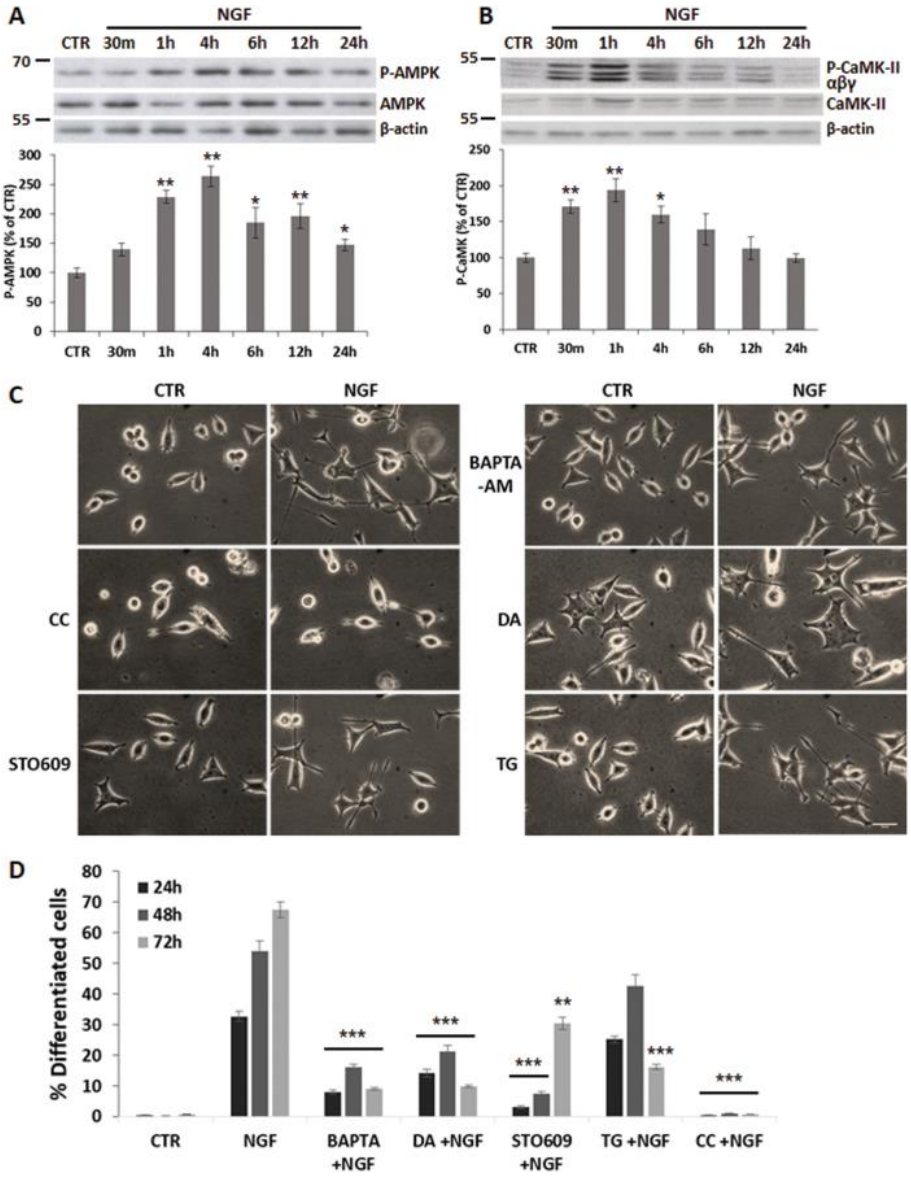

Fig. 6 AMPK and CaMK signaling in NGF-mediated differentiation. **a–b** Densitometric analysis and representative immunoblots of P(Thr172)- AMPK (**a**) and P(Thr286)-CaMK(α,β,γ) (**b**) during NGF treatment for the indicated times. Blots were probed for total AMPK and CaMK, respectively, as well for β-actin to normalize for protein content. Data, expressed as percent of CTR, are the mean ± SEM of three independent experiments in duplicate. **c** Representative images of PC12-615 treated for 24 h with NGF (10 ng/ml) alone or in combination with CC (10 μM), STO609 (25 μM), Bapta-AM (1 μM), DA (20 μM), or TG (100 nM). Scale bar = 25 μm. d Quantitation of NGF-induced differentiation in PC12-615 cells treated for 24–48–72 h with NGF

alone or in combination with kinases inhibitors or Ca^{2+} blockers. Data, expressed as percent of differentiated cells in ten random fields, are the mean ± SEM of three independent experiments in duplicate. $*p \leq 0.05$, $**p \leq 0.01$, $***p \leq 0.001$ vs. CTR (**a–b**) or vs. NGF (**d**) (ANOVA and Dunnett's multiple comparisons test)

Altered bioenergetics during NGF-induced differentiation

The increase of P-AMPK is indicative of altered energy homeostasis. Indeed, time-course studies revealed that intracellular ATP levels decrease by 20–35% after 1–2 h of NGF treatment (Fig. 7a) and are fully restored by 72 h, when cells are fully differentiated. To further evaluate the energy status, we measured NADPH/$NADP^+$ levels. NADPH, primarily produced in the pentose phosphate pathway, is used in anabolic reactions. We found that NGF causes a dramatic reduction of NADPH (34–50%) and NADPH/$NADP^+$ ratio (65%) after 1–3 h (Fig. 7b, c), followed by a net increase at 48–72 h. These data suggest that NGF either decreases ATP and NADPH synthesis, or increases their consumption.

These changes prompted us to assess whether NGFinduced differentiation affects the mitochondrial bioenergetics. Measurement of oxygen consumption rate (OCR) by the extracellular Flux Analyzer showed that NGF treatment for 24 h significantly increases the basal respiration compared to CTR (Fig. 7d–f). NGF-differentiated cells also show higher maximal respiration and spared respiratory capacity (Fig. 7d–f), which are indicative of a greater oxidative capacity, in line with previous findings that neuronal differentiation is associated with mitochondrial biogenesis and a functional reprogramming of

mitochondria metabolism[12]. Bioenergetic parameters are not significantly changed at 6 h. At this time, cells display enhanced, although not significant, ATP-linked respiration (Fig. 7f), suggesting that the drop of ATP is not due to decreased mitochondrial efficiency, but rather to its increased utilization. NGF-treated cells also exhibit higher proton-leak and non-mitochondrial respiration that might reflect increased NADPH oxidase activity and ROS production[39]. The higher ATP demand in NGF-differentiated cells was corroborated by a parallel increase of the glycolytic flux, as determined by the extracellular acidification rate (ECAR), in particular after addition of the respiratory chain inhibitors (Fig. 7e). All together, these data suggest that NGF increases mitochondrial function and that the temporary decrease of ATP and NADPH may reflect increased anabolic pathways during differentiation.

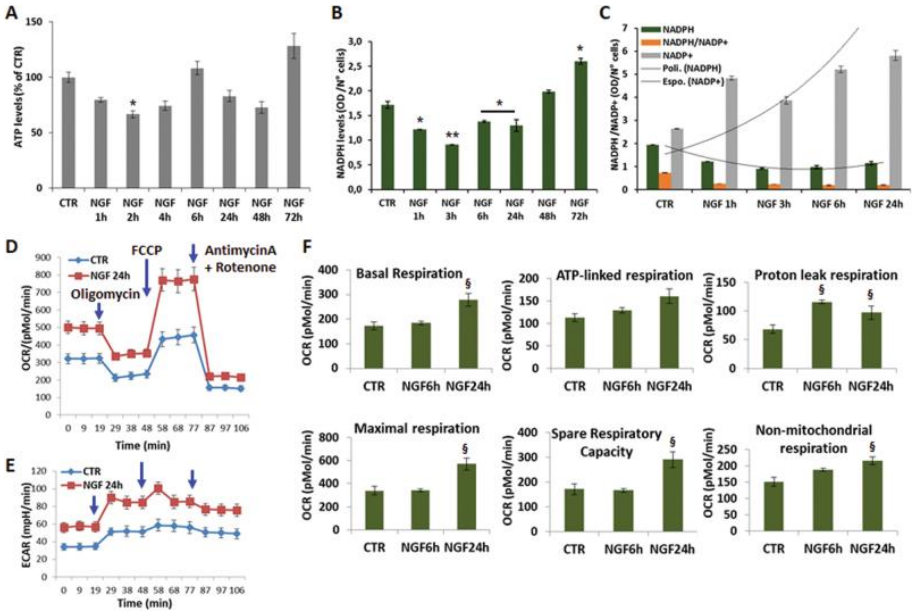

Fig. 7 Mitochondrial bioenergetics during NGF-induced differentiation. **a** ATP levels after treatment with NGF (10 ng/ml) for 1–72 h. Data, normalized by the protein content, are the mean ± SEM of three independent experiments in duplicate. **b** NADPH levels during NGF differentiation for 1–72 h. Data, normalized by the protein content, are the mean ± SEM of two separate experiments, each with three independent samples. **c** Modifications of NADPH, NADPH/NADP$^+$, and NADP$^+$ levels. **d–e** Representative OCR and ECAR profiles, respectively, after exposure to NGF (10 ng/ ml) for 24 h. Oligomycin A (1 μM), FCCP (0.8 μM), rotenone (0.5 μM) plus antimycin A (2 μM) were injected at the indicated times to determine the OCR linked to ATP turnover, maximal respiration and proton-leak, respectively. Data are the mean ± SEM of five–six samples, each normalized by the protein content. Similar profiles were obtained in three independent experiments. **f** Changes of bioenergetics parameters after exposure to NGF for 6 or 24 h. Data are the mean ± SEM of three separate experiments, each with five–six independent samples. *$p \leq 0.05$, **$p \leq 0.01$ vs. CTR (ANOVA and Dunnett's multiple comparisons test); § $p \leq 0.05$ vs. CTR (*t*-test)

Evidence of mitophagy during NGF-induced differentiation

Several studies suggest that neuronal differentiation involves increased ROS production and signaling, and is prevented by antioxidant molecules[12,40]. FACS analysis of DCFH-DA staining showed that exposure to NGF for 1–6 h causes a 1.5–2-fold increase of ROS, which return to basal levels at later time-points, when cells are differentiated (Fig. 5a and Supplementary Fig. S8A). ROS production in response to NGF is abolished by siRNA knockdown of Ambra1, Atg9b, or Atg12, but not by siRNA-SCR (Fig. 5b and Supplementary Fig. S8B), although basal ROS content in siRNA-transfected cells is higher than CTR. It is remarkable, however, that ROS levels are further enhanced by autophagy inhibitors and blockers, including 3-MA, Baf, CLC, and NOC (Fig. 5c and Supplementary Fig. S8C), as well as NH_4Cl and PL (data not shown). Nevertheless, NGF-mediated increase of ROS production minimally affects cell viability, which is severely compromised only in the presence of CLC or NOC (Fig. 5d). All together, these data suggest that NGFinduced ROS is not a deleterious event per se, in line with the concept that they might act as signaling molecules during differentiation[12,40]. Moreover, their further increase following genetic or pharmacologic blockade of autophagy suggests that NGF-induced autophagy might be functional to the removal of damaged mitochondria.

This hypothesis has been tested by confocal imaging studies showing a significant increase of p62 localization to mitochondria stained by CoxIV in PC12 cells challenged with

NGF for 4–24 h (Fig. 5e, f, arrows), in parallel with a net decrease of p62 fluorescence at 4 h (Supplementary Fig. S9A). These data were supported by the observation that NGF causes a significant increase of Lysotracker-red (LYS) staining at 4–24 h (Supplementary Fig. S9B) and its higher co-localization with Mitotracker-green (MTG), in particular at growth cones tips and along extending neurites (Fig. 5e, f, arrows), confirming that NGF-mediated increase of the autophagic flux (Figs. 1 and 2) involves its functional role in clearing damaged mitochondria.

NGF-induced differentiation involves modulation of mitochondrial function and dynamics

Alternation of fission/fusion cycles is crucial for mitochondria distribution along axonal branching during differentiation, as well as for their physiological turnover (mitophagy) and adaptation to metabolic perturbations[2,11]. To investigate the role of mitochondrial dynamics during NGF differentiation, we first assessed P-Drp-1, a pivotal protein in mitochondrial fragmentation. We found that NGF treatment stimulates an early induction of P-Drp-1 content (Fig. 8a), in line with a previous finding that NGF-induced axonal branching is reduced when mitochondrial fission is inhibited[2]. Moreover, we newly found that NGF causes a persistent upregulation of the mitochondrial fusion protein Opa1 (Fig. 8b), as well as of Mfn2 content at later times (24–48 h) (Fig. 8c), as confirmed by immunofluorescence staining (Fig. 8e and Supplementary Fig. S9C). It is remarkable that upregulation of fusion proteins is

associated with a larger number of mitochondria displaying an elongated tubular morphology (Fig. 5e, insets with enlarged image). These changes are paralleled by enhanced MTG staining in NGF-treated cells (Fig. 5e, and Supplementary Fig. S9B), suggesting that fission/fusion processes are accompanied by a net increase of mitochondrial mass and biogenesis.

To test this hypothesis, we examined molecular events linked to mitochondrial biogenesis and metabolism. Indeed, we found that exposure of PC12 to NGF induces a strong upregulation of Sirt3, a mitochondrial deacetylase known to regulate mitochondrial biogenesis and metabolism (Fig. 8d). Furthermore, NGF causes a dramatic increase of peroxisome proliferator-activated receptor-γ (PPARγ), a transcription factor that regulates glucose and lipid metabolism, as well as a slight but significant induction of the mitochondrial transcription factor mtTFA (Fig. 8d). Levels of Sirt3, PPARγ, and mtTFA also increase at 4 h, as well as the binding activity of PPARγ (data not shown). These data were supported by confocal microscopy studies showing that NGF increases ethydium bromide staining of peripheral mitochondria, in particular those located at growth cones and along neurite branches (Fig. 8f and Supplementary Fig. S9E, F). In addition, we found that NGF treatment boosts the mitochondrial potential, as determined by higher MitoTracker red (MTR) staining (Fig. 8g and Supplementary Fig. S9D), in agreement with the data regarding mitochondrial bioenergetics (Fig. 7). All together, these data provide new evidence that NGF-mediated differentiation involves extensive modulation of

mitochondrial dynamics and biogenesis to increase their efficiency and meet higher energy requirements.

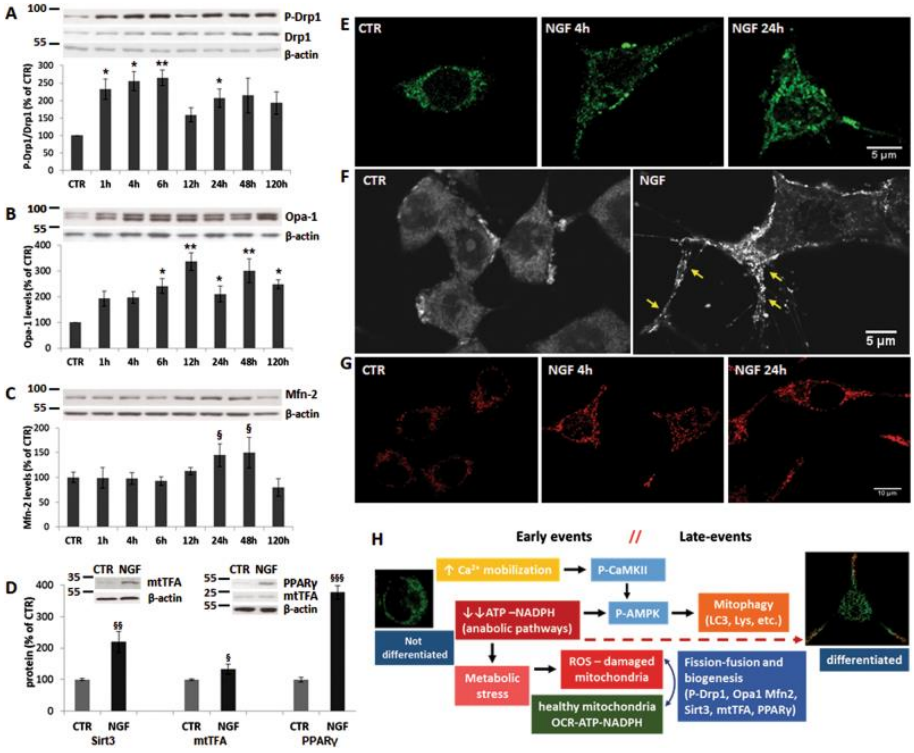

Fig. 8 Mitochondrial fission–fusion and biogenesis correlate with higher mitochondrial potential. **a–d** Densitometric analysis and representative immunoblot blot of P(616)-Drp1 and total Drp1 (**a**), Opa1 (**b**), Mfn2 (**c**) after treatment with NGF (10 ng/ml) for the indicated times; **d** levels of Sirt3, mtTFA, and PPARγ after NGF treatment for 24 h. Representative immunoblots are shown above. Protein levels were normalized by the β-actin content. Data, expressed as percent of CTR, are the mean ± SEM of three independent experiments in duplicate. *$p \leq 0.05$, **$p \leq 0.01$ vs. CTR (ANOVA and Dunnett's multiple comparisons test); § $p \leq 0.05$, §§ $p \leq 0.01$; §§§ $p \leq 0.001$ vs. CTR (*t*-test). **e** Representative images of PC12-615 cells treated with NGF (10 ng/ml) for 4 or 24 h followed by immunostaining for Mfn2. Scale bar = 5 μm. **f** Representative images of mitochondria stained by ethydium bromide after NGF treatment for 24 h. Arrows indicate mitochondria located at growth cones and along neurites. Scale bar = 5 μm. g Representative images of MTR staining in PC12-615 treated with NGF for 4 or 24 h. Scale bar = 10 μm. **h** Schematic representation of biochemical and molecular events during NGF-induced differentiation

Discussion

Unraveling molecular events involved in neuronal differentiation is crucial for a deeper understanding of brain function. Here, we newly report that NGF-induced differentiation requires the activation of mitophagy through mechanisms that are dependent upon altered energy homeostasis and requirement of mitochondrial remodeling. We show that NGF-dependent neurite outgrowth is strictly correlated with the induction of the autophagic flux (Figs. 1 and 2), as being blocked by its pharmacological inhibition and by siRNA knockdown of autophagyrelated genes (Figs. 3 and 4).

In search for mechanistic insights into this process, we considered that neuronal development requires a large amount of energy and building blocks, thereby suggesting that NGF-induced differentiation might influence the bioenergetic status. This working hypothesis was supported by our data of metabolic energy changes, including reduced levels of ATP and NADPH at early stages of NGF differentiation, regardless of increased OCR and related bioenergetic parameters (including ATP-linked respiration) that are indicative of boosted energy metabolism (Fig. 7). Moreover, the enhanced non-mitochondrial respiration may reflect an increase of NADPH oxidase activity and of anabolic reactions to produce amino acids, cholesterol, and fatty acids required for axonal growth. The increase of ECAR during NGF differentiation is also in agreement with previous findings of enhanced glucose metabolism in differentiated PC12 cells and in other neuronal models[12,41].

The impact of energy metabolism is substantiated by evidence that NGF-induced differentiation causes an early induction of P-AMPK and is fully prevented by CC (Fig. 6). AMPK is activated also in HeLa cells in response to NGF-mediated viability during glucose deprivation[42]. AMPK acts in concert with ULK1 to regulate phosphorylation and localization of ATG9[43]. In line with this finding, NGF-induced differentiation is disrupted in Atg9b-siRNA-transfected cells (Fig. 3). Our data are in accordance with other studies showing the relevance of AMPK signaling in regulating autophagy during neuronal development[18,22,25,44]. AMPK-β1 knockout was found to cause atrophy of dentate gyrus and suppress the differentiation of cultured hippocampal neurons[45,46].

In addition to metabolic stress, NGF-induced differentiation also correlates with P-CaMKII activation and is significantly prevented by Ca^{2+}/CaMKII blockers (Fig. 6), in line with evidence of NGF-dependent Ca^{2+}-release from ER[6]. Both AMPK and Ca^{2+}/CaMKII inhibition reduce or prevent the induction of the neuronal marker GAP-43 in response to NGF stimulation (Supplementary Fig. S6A). Our data are in agreement with previous reports showing the complex regulation of GAP-43 transcription by Ca^{2+}-CaMK, Akt, MAPK-ERK, PKA and PKC, which are activated downstream of NGF signaling[5,47,48]. Both AMPK and Ca^{2+}/CaMKII inhibition prevent autophagy[26,27], supporting the relevance of this process in NGF-induced differentiation. NGF-mediated mobilization of Ca^{2+} [6], as well its buffering by mitochondria (Supplementary Fig. S7) might activate

mitochondrial dehydrogenases and enhance oxidative phosphorylation[38]. However, the intense mitochondria activity makes them more prone to produce ROS, which accumulate in nondividing cells. Hence, the need to foster the turnover of overworked ROS-producing mitochondria by mitophagy, as determined by enhanced p62-CoxIV and LYS-MTG colocalization (Fig. 5)[49]. In addition, ROS levels further increase in siRNA-transfected cells, as well as in cells treated with autophagy inhibitors (Fig. 7).

The transient increase of ROS produced by NGF (Fig. 5) is similar to that observed in other models of neuronal differentiation[12,40,50]. It has been proposed that ROS might act as second messenger, since differentiation is prevented by antioxidant molecules[12,40,51]. It is conceivable that ROS increase following enhanced energy metabolism might serve to induce mitophagy for mitochondria quality control and remodeling in post-mitotic neurons[13,29,52,53]. We can speculate that this function might be achieved through Atg9 downstream of AMPK signaling, since Atg9L2(Atg9b) harbors a putative mitochondrial localization signal, although not experimentally characterized[53,54].

The increase of mitophagy is accompanied by higher P-Drp-1 levels (Fig. 8), based on the role of mitochondrial fission in the fragmentation of damaged overused mitochondria that must be cleared by mitophagy[53–55]. On the other hand, enhanced fragmentation facilitates translocation of mitochondria along growing neurites, in agreement with its role in axonal branching[2],

and is paralleled by early-upregulation of Opa1 and later induction of Mfn2 (Fig. 8). The increase of mitochondrial fusion, together with upregulation of mitochondrial biogenesis, might reflect the net increase of mitochondrial mass and the appearance of elongated networked mitochondria (Fig. 5), as well as the increase of mitochondrial potential and bioenergetics (Figs. 7 and 8).

Overall, we here provide the first evidence of a functional link between boosted energy metabolism and molecular events modulating mitophagy, and mitochondrial biogenesis and remodeling during NGF-induced differentiation. Our data are in agreement with a previous study showing metabolic reprogramming and mitochondrial biogenesis during maturation of cortical neurons[12] and might represent an extension of those findings to a specific NGF model. As depicted in Fig. 8h, we can schematically identify two major sets of events at early and late stages that flow into one another during NGF differentiation. From a dynamic perspective, we can speculate that the first set of changes might be caused by Ca^{2+}-CaMKII signaling, since Ca^{2+} mobilization occurs in milliseconds (Supplementary Fig. S7) and P-CaMKII is induced after 30 min of NGF treatment. Mitochondrial Ca^{2+} buffering might increase proton-leak and ROS generation, thus activating mitochondrial fragmentation and mitophagy. A second set of events might be more specifically linked to metabolic perturbations due to decreased ATP/NADPH used up in anabolic pathways and converging on P-AMPK to keep energy metabolism, mitophagy, and mitochondrial

dynamics active throughout the entire process of differentiation. Enhanced metabolism, together with mitochondrial fission–fusion and biogenesis, ensure a constant remodeling of mitochondria to fit morphological and functional changes of postmitotic neurons.

In conclusion, we show that NGF-dependent differentiation occurs through a complex signaling network timely and functionally related to the control of energy and redox homeostasis in response to higher energy demand to meet the morphological remodeling of post-mitotic neurons. The functional relevance of these interactions is fascinating, and further studies will be needed to better dissect this process in more details and obtain a metabolomic profile. NGF is essential in neuroprotection in the central and peripheral nervous system, through its anti-gliosis activity[56–58]. Moreover, NGF can regulate different stages of neuronal precursor maturation during neurogenesis in the subventricular zone[59], which might explain why NGF differentiation involves Ambra1-mediated autophagy[24]. Therefore, uncovering mechanisms underlying NGF-mediated modulation of mitochondrial function might be relevant to both neurogenesis and mechanism of regeneration following brain injury.

Materials and methods

Cell cultures and treatments

PC12 cells (clone 615) overexpressing the TrkA receptor32 were kindly provided by MV Chao (Skirball Institute, New York University School of Medicine, NY). PC12wt and PC12-615 cells were maintained in Dulbecco's modified Eagle medium (DMEM) supplemented with 10% fetal bovine serum, 5% heat-inactivated horse serum, 2 mM L-glutamine, 100 µg/ml streptomycin, 100 U/ml penicillin, 200 µg/ml G418, in a humidified atmosphere of 95% air 5% CO2 at 37 °C, as previously described[10]. All cell culture reagents were purchased from EuroClone (Milano, Italy). PC12 differentiation was achieved by using murine 2.5 S NGF (mNGF, Promega Inc., Madison WI, USA) purified from male mouse submaxillary glands. Differentiation was measured also following treatments with BAPTA/AM (Invitrogen, ThermoFisher Scientific) or Thapsigargin (Invitrogen, ThermoFisher Scientific). Wortmannin, 3-MA, rapamycin, bafilomycin A1, pepstatin, leupeptin, colchicine, nocodazole, dantrolene, compound C, STO609 were all purchased from SigmaAldrich.

Mitochondrial function and morphology

Mitochondrial mass and potential were assessed by using MitoTracker Red/Green (Molecular Probes Inc., Eugene OR, USA) staining, indicators of mitochondrial potential and mass/morphology, respectively. Briefly, cells (2×10^4 /well) were grown onto poly-L-lysine-coated coverslips and exposed to the

specific treatments. Cells were loaded with 20 and 200 nM MitoTracker Red and Green, respectively, or 1 μM rhodamine-123, or 1 μM ethydium bromide during the last 30 min of treatment and then rinsed twice with PBS. Coverslips were mounted with Dako Fluorescent Mounting Medium (Dako Agilent Technologies, Santa Clara CA, USA) and analyzed by fluorescence microscopy. Images were captured at 360 magnification (Plan Apo objective; 360 oil) using a motorized Nikon Eclipse 90i (Nikon, Tokyo, Japan) fluorescence microscope equipped with a CCD camera (Hamamatsu-CoolSnap, Hamamatsu Corporation, Tokyo, Japan), or by confocal microscopy using a Nikon Eclipse Ti inverted microscope and Nikon A1 confocal microscope with a 60 × Plan Apo oil immersion objective. NIH ImageJ and NIS-Element AR analysis software were used for image analysis and processing. Images were taken with the same parameters and fluorescence intensity of cells was measured and then averaged to obtain the mean fluorescence intensity (MFI). On average, about 100–150cells for each condition were analyzed in about ten randomly picked fields. Data, expressed as percent of CTR, are the mean ± SEM of three separate experiments, each performed in duplicate.

Immunofluorescent staining

PC12 cells were grown onto 12 mm poly-L-lysine-coated coverslips (2 × 10^4 cells/well). After treatments, cells were washed with PBS, fixed with 4% paraformaldehyde,

permeabilized with 0.5% Triton X100 in PBS and incubated with the blocking solution (10% normal goat serum) followed by overnight incubation with the following primary antibodies: rabbit SQSTM1/p62 (1:100, Cell Signaling Technologies), mouse CoxIV (1:200, Cell Signaling Technologies), rabbit Mfn2 (1:100, Cell Signaling Technologies), or mouse β-III tubulin (1:1000, Abcam, Cambridge, UK). After washing with PBS, coverslips were incubated for 2 h at room temperature with the goat antirabbit Alexa 488 or goat anti-mouse Alexa 546 conjugated antibodies (1:500; Molecular Probes, Invitrogen, Carlsbad, CA). After washes, nuclei were counterstained for 1 min with DAPI (100ng/ml) or Hoechst 33342 10 µg/ml for 15 min. Coverslips were mounted with Dako Fluorescent Mounting Medium (Dako Agilent Technologies) and analyzed by fluorescence microscopy, as described above.

Autophagy detection

Autophagic activity was detected by using the Cyto-ID™ Autophagy Detection Kit (ENZO Life Sciences). Briefly, PC12-615 cells (2.5×10^5 /well) were trypsinized, pelleted by centrifugation and washed in assay buffer. Cells were resuspended in 250 µl of freshly diluted Cyto-ID reagent and incubated at 37 °C for 30 min, followed by two washes and resuspension in 500 µl of assay buffer. The Cyto-ID fluorescence was immediately measured at excitation/ emission wavelengths of 480 nm/530 nm, respectively, using a Cary Eclipse Fluorescence Spectrophotometer (Agilent Technologies). The

autophagic flux was measured by Lysotracker-red staining (Molecular Probes) by adding Lysotracker-red (1 μM) during the last 30 min of treatment. Coverslips were mounted with Dako Fluorescent Mounting Medium (Dako Agilent Technologies) and analyzed by fluorescence microscopy, as described above.

Plasmid DNA and transfection

Plasmid DNA encoding mRFP-GFP tandem fluorescence-tagged LC3 (ptf-LC3 plasmid, ID 21074)[60] was obtained from Addgene (Cambridge, MA). The GFPRFP-LC3 protein allows for discrimination between autophagosomes and autolysosome based on GFP sensitivity to the acidic pH of lysosomes. To monitor for LC3 cleavage by lysosome proteases, PC12 cells (2×10^4 cells/ well) were plated onto 12 mm poly-L-lysine-coated coverslips and treated with the transfection mix containing 500 ng of plasmid DNA and Lipofectamine 2000 (Life Technologies) for 6 h. After transfection, cells were washed three times with culture medium and grown for 24 h before exposure to the specific treatments. After treatments, cells were washed with PBS and coverslips were mounted with Dako Fluorescent Mounting Medium (Dako Agilent Technologies) and analyzed for the number of vesicles/cell by fluorescence microscopy. Transfection of siRNAs was performed using Metafectene Pro (Biontex, Martinsried, Germany) using the siRNAs sequences for Ambra1, Atg9b, and Atg12 reported in Supplementary materials. A scrambled sequence was used as a control.

Bioenergetics by Seahorse technology

Mitochondrial OCR was determined by using a Seahorse XF24 Extracellular Flux Analyzer (Seahorse Bioscience, Copenhagen, Denmark). PC12-615 cells were seeded in XF plates 48 h prior to the assay. Cells were treated with NGF for 6–24 h and then analyzed by using the Seahorse XF Cell Mito Stress Test Kit (Seahorse Bioscience) according to manufacturer instructions. Three measurements of OCR and ECAR were taken for the baseline and after sequential injection of mitochondrial inhibitors. The ATP synthase inhibitor Oligomycin A (1 mM), the ATP synthesis uncoupler carbonyl cyanide4-trifluoromethoxyphenylhydrazone FCCP (0.8 µM), the complex I inhibitor rotenone (0.5 µM) and complex III inhibitor antimycin A (2 µM) were used to determine OCR parameters. OCR and ECAR from each well were normalized by the protein content by using the Bradford assay (Bio-Rad, Hemel Hempstead, UK).

NADP/NADPH assay

NADP and NADPH levels were detected using NADP/ NADPH Quantitation Colorimetric Kit (BioVision Inc., Milpitas CA, USA) according to the manufacturer's protocol. Briefly, cells (1.5×10^6/well) were lysed by sonication (two cycles: 5 s for five pulses at 70% power) in 800 µl of extraction buffer. Samples (125 µl) were then directly used to detect total NADP/NADPH. To detect NADPH only, samples were heated at 60 °C for 30 min to clear out all $NADP^+$ species. Colorimetric measurements were

performed at OD 450 nm using a Cary 60 ultraviolet–visible spectrophotometer (Agilent Technologies).

ATP determination

PC12-615 cells were plated into 6-well plates (7×10^4 cells) and treated with NGF (10 ng/ml) for 1–72 h. Cells were subsequently lysed by using lysis buffer and ATP activity was analyzed by using the adenosine 5′-triphosphate (ATP) Bioluminescent Assay Kit (Sigma-Aldrich) according to manufacturer instructions. The light intensity was measured with a luminometer (Lumat LB9507, Berthold) in a 5 s time period and expressed as relative light units/μg of protein.

ROS analysis by flow cytometry

Determination of intracellular levels of total ROS was carried out by flow cytometry using 2′,7′-dichlorodihydrofluorescein-diacetate (H_2DCFDA, Molecular Probes), as previously described[61]. Cells (2×10^5 cells/well) were plated in 6-well plates (EuroClone) precoated with poly-L-lysine (0.1 mg/ml). DCFH-DA was added during the last 30 min of treatments. Cells were harvested with 0.08% Trypsin and analyzed by FACS (FACScan Becton-Dickinson, San Jose, CA) using the Cell Quest Software (BD Bioscience). Fluorescence was measured on 1×10^4 cells and data were analyzed by using the Flowing Software 2.5.1 (Turku Center for Biotechnology, University of Turku, Finland).

Western blot analysis

Total cell extracts and western blotting were performed as previously described[10,61]. Cell lysates were prepared in lysis buffer containing proteases inhibitors (Mini EDTAfree Protease Inhibitor Cocktail, Roche Applied Science, Sussex, UK) and phosphatases inhibitor cocktail (PhosSTOP, Roche Applied Science). Protein concentration was determined by using the Bradford assay (Bio-Rad, Hemel Hempstead, UK). Total proteins (25 μg) were separated on 10–12% sodium dodecyl sulfate polyacrylamide gel electrophoresis gels and transferred to nitrocellulose Protran™ (PerkinElmer, Waltham MA, USA). After blocking, blots were probed overnight at 4 °C with the primary antibody in Tris-buffered saline 0.1% Tween-20 (TBST), followed by incubation for 1 h at room temperature with HRPconjugated donkey anti-rabbit or anti-mouse IgG (1:5000; GE Healthcare Life Sciences, Buckinghamshire, UK) for 1 h at room temperature. The following antibodies were used for western blots: rabbit phospho (Thr172)-AMPKα (1:1000), total AMPKα (1:1000), rabbit phospho(Thr286)-CaMKII (1:1000), total CaMKII (1:1000), rabbit phospho(Ser2448)-mTOR (1:1000), total mTOR (1:1000), rabbit LC3B (1:1000), rabbit Beclin-1 (1:1000), rabbit SQSTM1/p62 (1:1000), Phospho(Ser616)- Drp1 (1:1000), total Drp1 (1:1000), rabbit mitofusin-2 (1:100), rabbit Sirt3 (1:1000), mouse β-actin (1:1000), rabbit phospho(Ser473)-Akt (1:1000), total Akt (1:1000) were all purchased from Cell Signaling Technologies (Beverly MA, USA). Mouse Opa1 (1:1000) was from BD Biosciences (Franklin Lakes NJ, USA). Rabbit mtTFA

(1:1000), rabbit PPARγ (1:1000), rabbit Ambra1 (1:1000), rabbit Atg9b (1:1000), and rabbit Atg12 (1:1000) were from Santa Cruz Biotechnology, Dallas TX, USA). Mouse anti-GAP-43 (1:1000) was from Sigma. HRP-conjugated donkey anti-rabbit (1:5000) and anti-mouse IgGs (1:5000) were purchased from GE Healthcare Life Sciences (Little Chalfont, Buckinghamshire, UK). All immunoblots were probed for β-actin, to normalize for protein content. Detection was carried out by using the enhanced chemiluminescence system (ECL, GE Healthcare Life Sciences). Quantification of bands was performed by densitometry using NIH ImageJ software.

Statistical analysis

All data are presented as the mean ± SEM of the number of independent samples in separate experiments, as indicated in the figure legends. Statistical analysis was performed by using GraphPad Prism 6.0 (GraphPad Software, La Jolla, CA, USA). All quantitative data were analyzed by one-way ANOVA and Dunnett's multiple comparisons test for multiple treatments or by Student's t-test for single comparisons (*$p \leq 0.05$, **$p \leq 0.01$, ***$p \leq 0.001$ vs. CTR), as indicated in the figure legends. For morphology analyses, individual images of CTR and treated cells were assembled and the same adjustments were made for brightness, contrast, and sharpness using Adobe Photoshop (Adobe Systems, San Jose, CA).

Acknowledgements

This work was supported by grants from the Italian Ministry of University and Research (MIUR) (PRIN2007 to A.M.C. and M.P.; SYSBIONET-Italian ROADMAP ESFRI Infrastructures to L.A., A.M.C., and M.P.; IVASCOMAR-National Cluster to AMC); Blueprint Pharma srl; PRIMM srl; Regione Lomdardia (Dote Ricerca Applicata); Associazione Levi-Montalcini (fellowships to F.A.). We thank Dr. Miluscia Berbenni and Dr. Anna Maria Villa for technical contributions and support with confocal microscopy

Conflict of interest

The authors declare that they have no conflict of interest.

Publisher's note

Springer Nature remains neutral with regard to jurisdictional claims in published maps and institutional affiliations.

Supplementary Information accompanies this paper at https://doi.org/ 10.1038/s41419-018-0429-9.

References

1. Gallo, G. The cytoskeletal and signaling mechanisms of axon collateral branching. Dev. Neurobiol. 71, 201–220 (2011).

2. Spillane, M., Ketschek, A., Merianda, T. T., Twiss, J. L. & Gallo, G. Mitochondria coordinate sites of axon branching through localized intra-axonal protein synthesis. Cell Rep. 5, 1564–1575 (2013).

3. Levi-Montalcini, R. The nerve growth factor 35 years later. Science 237, 1154–1162 (1987).

4. Alberghina, L. & Colangelo, A. M. The modular systems biology approach to investigate the control of apoptosis in Alzheimer's disease neurodegeneration. Bmc. Neurosci. 7, S2 (2006).
5. Chao, M. V. Neurotrophins and their receptors: a convergence point for many signalling pathways. Nat. Rev. Neurosci. 4, 299–309 (2003).
6. De Bernardi, M. A., Rabins, S. J., Colangelo, A. M., Brooker, G. & Mocchetti, I. TrkA mediates the nerve growth factor-induced intracellular calcium accumulation. J. Biol. Chem. 271, 6092–6098 (1996).
7. Lau, P. M., Zucker, R. S. & Bentley, D. Induction of filopodia by direct local elevation of intracellular calcium ion concentration. J. Cell Biol. 145, 1265–1275 (1999).
8. Chada, S. R. & Hollenbeck, P. J. Nerve growth factor signaling regulates motility and docking of axonal mitochondria. Curr. Biol. 14, 1272–1276 (2004).
9. Verburg, J. & Hollenbeck, P. J. Mitochondrial membrane potential in axons increases with local nerve growth factor or semaphorin signaling. J. Neurosci. 28, 8306–8315 (2008).
10. Bianco, M. R. et al. Cross-talk between cell cycle induction and mitochondrial dysfunction during oxidative stress and nerve growth factor withdrawal in differentiated PC12 cells. J. Neurosci. Res. 89, 1302–1315 (2011).
11. Mattson, M. P., Gleichmann, M. & Cheng, A. Mitochondria in neuroplasticity and neurological disorders. Neuron 60, 748–766 (2008).
12. Agostini, M. et al. Metabolic reprogramming during neuronal differentiation. Cell Death Differ. 23, 1502–1514 (2016).
13. Esteban-Martínez, L. et al. Programmed mitophagy is essential for the glycolytic switch during cell differentiation. Embo. J. 36, 1688–1706 (2017).
14. Herrero-Mendez, A. et al. The bioenergetic and antioxidant status of neurons is controlled by continuous degradation of a key glycolytic enzyme by APC/CCdh1. Nat. Cell Biol. 11, 747–752 (2009).
15. Zheng, X. et al. Metabolic reprogramming during neuronal differentiation from aerobic glycolysis to neuronal oxidative phosphorylation. eLife 5, e13374 (2016).

16. Mizushima, N. & Levine, B. Autophagy in mammalian development and differentiation. Nat. Cell Biol. 12, 823–830 (2010).
17. Vázquez, P. et al. Atg5 and Ambra1 differentially modulate neurogenesis in neural stem cells. Autophagy 8, 187–199 (2012).
18. Zogovic, N. et al. Coordinated activation of AMP-activated protein kinase, extracellular signal-regulated kinase, and autophagy regulates phorbol myristate acetate-induced differentiation of SH-SY5Y neuroblastoma cells. J. Neurochem. 133, 223–232 (2015).
19. Fortini, P. et al. The fine tuning of metabolism, autophagy and differentiation during in vitro myogenesis. Cell Death Dis. 7, e2168 (2016).
20. Sin, J. et al. Mitophagy is required for mitochondrial biogenesis and myogenic differentiation of C2C12 myoblasts. Autophagy 12, 369–80 (2016).
21. Xie, Z. & Klionsky, D. J. Autophagosome formation: core machinery and adaptations. Nat. Cell Biol. 9, 1102–1109 (2007).
22. Filomeni, G., De Zio, D. & Cecconi, F. Oxidative stress and autophagy: the clash between damage and metabolic needs. Cell Death Differ. 22, 377–388 (2015).
23. Fimia, G. M. et al. Ambra1 regulates autophagy and development of the nervous system. Nature 447, 1121–1125 (2007).
24. Yazdankhah, M., Farioli-Vecchioli, S., Tonchev, A. B., Stoykova, A. & Cecconi, F. The autophagy regulators Ambra1 and Beclin 1 are required for adult neurogenesis in the brain subventricular zone. Cell Death Dis. 5, e1403 (2014).
25. Cardaci, S., Filomeni, G. & Ciriolo, M. R. Redox implications of AMPKmediated signal transduction beyond energetic clues. J. Cell Sci. 125, 2115–2125 (2012).
26. Høyer-Hansen, M. et al. Control of macroautophagy by calcium, calmodulindependent kinase kinase-beta, and Bcl-2. Mol. Cell 25, 193–205 (2007).
27. Grotemeier, A. et al. AMPK-independent induction of autophagy by cytosolic Ca^{2+} increase. Cell Signal. 22, 914–925 (2010).
28. Westermann, B. Mitochondrial fusion and fission in cell life and death. Nat. Rev. Mol. Cell Biol. 11, 872–884 (2010).

29. Ashrafi, G. & Schwarz, T. L. The pathways of mitophagy for quality control and clearance of mitochondria. Cell Death Differ. 20, 31–42 (2013).
30. Han, X. J. et al. CaM kinase I alpha-induced phosphorylation of Drp1 regulates mitochondrial morphology. J. Cell Biol. 182, 573–585 (2008).
31. Chang, C. R. & Blackstone, C. Dynamic regulation of mitochondrial fission through modification of the dynamin-related protein Drp1. Ann. NY Acad. Sci. 1201, 34–39 (2010).
32. Hempstead, B. L. et al. Overexpression of the trk tyrosine kinase rapidly accelerates nerve growth factor-induced differentiation. Neuron 9, 883–896 (1992).
33. Secondo, A. et al. Involvement of the Na+/Ca2+exchanger isoform 1 (NCX1) in neuronal growth factor (NGF)-induced Neuronal Differentiation through Ca^{2+}-dependent Akt Phosphorylation. J. Biol. Chem. 290, 1319–1331 (2015).
34. Mizushima, N., Yoshimori, T. & Levine, B. Methods in mammalian autophagy research. Cell 140, 313–326 (2010).
35. Anderson, K. A. et al. Hypothalamic CaMKK2 contributes to the regulation of energy balance. Cell Metab. 7, 377–388 (2008).
36. Takadera, T. & Ohyashiki, T. Apoptotic cell death and CPP32-like activation induced by thapsigargin and their prevention by nerve growth factor in PC12 cells. Biochim. Biophys. Acta 1401, 63–71 (1998).
37. Mnich, K. et al. Nerve growth factor-mediated inhibition of apoptosis postcaspase activation is due to removal of active caspase-3 in a lysosomedependent manner. Cell Death Dis. 5, e1202 (2014).
38. Griffiths, E. J. & Rutter, G. A. Mitochondrial calcium as a key regulator of mitochondrial ATP production in mammalian cells. Biochim. Biophys. Acta 1787, 1324–1333 (2009).
39. Divakaruni, A. S., Paradyse, A., Ferrick, D. A., Murphy, A. N. & Jastroch, M. Analysis and interpretation of microplate-based oxygen consumption and pH data. Methods Enzymol. 547, 309–354 (2014).
40. Vieira, H. L., Alves, P. M. & Vercelli, A. Modulation of neuronal stem cell differentiation by hypoxia and reactive oxygen species. Prog. Neurobiol. 93, 444–455 (2011).

41. Waki, A. et al. Dynamic changes in glucose metabolism accompanying the expression of the neural phenotype after differentiation in PC12 cells. Brain Res. 894, 88–94 (2001).
42. Ting, L. et al. AMP-activated protein kinase supports the NGF-induced viability of human HeLa cells to glucose starvation. Mol. Biol. Rep. 37, 2593–2598 (2010).
43. Mack, H. I., Zheng, B., Asaram, J. M. & Thomas, S. M. AMPK-dependent phosphorylation of ULK1 regulates ATG9 localization. Autophagy 8, 1197–1214 (2012).
44. Poels, J., Spasić, M. R., Callaerts, P. & Norga, K. K. Expanding roles for AMPactivated protein kinase in neuronal survival and autophagy. Bioessays 31, 944–952 (2009).
45. Dasgupta, B. & Milbrandt, J. AMP-activated protein kinase phosphorylates retinoblastoma protein to control mammalian brain development. Dev. Cell 16, 256–270 (2009).
46. Amato, S. et al. AMP-activated protein kinase regulates neuronal polarization by interfering with PI3-kinase localization. Science 332, 247–251 (2011).
47. Costello, B., Meymandi, A. & Freeman, J. A. Factors influencing GAP-43 gene expression in PC12 pheochromocytoma cells. J. Neurosci. 10, 1398–1406 (1990).
48. Das, K. P., Freudenrich, T. M. & Mundy, W. R. Assessment of PC12 cell differentiation and neurite growth: a comparison of morphological and neurochemical measures. Neurotoxicol. Teratol. 26, 397–406 (2004).
49. Dolman, N. J., Chambers, K. M., Mandavilli, B., Batchelor, R. H. & Janes, M. S. Tools and techniques to measure mitophagy using fluorescence microscopy. Autophagy 9, 1653–1662 (2013).
50. Olguín-Albuerne, M. & Morán, J. ROS produced by NOX2 control in vitro development of cerebellar granule neurons development. ASN Neuro 7, 1759091415578712 (2015).
51. Suzukawa, K. et al. Nerve growth factor-induced neuronal differentiation requires generation of Rac1-regulated reactive oxygen species. J. Biol. Chem. 275, 13175–13178 (2000).

52. Levine, B. & Klionsky, D. J. Development by self-digestion: molecular mechanisms and biological functions of autophagy. Dev. Cell 6, 463–477 (2004).
53. Scherz-Shouval, R. & Elazar, Z. ROS, mitochondria and the regulation of autophagy. Trends Cell Biol. 17, 422–427 (2007).
54. Toyama, E. Q. et al. AMP-activated protein kinase mediates mitochondrial fission in response to energy stress. Science 351, 275–281 (2016).
55. Westermann, B. Bioenergetic role of mitochondrial fusion and fission. Biochim. Biophys. Acta 1817, 1833–1838 (2012).
56. Tuszynski, M. H. et al. A phase I clinical trial of nerve growth factor gene therapy for Alzheimer disease. Nat. Med. 11, 551–555 (2005).
57. Marcello, L. et al. Remodelling of supraspinal neuroglial network in neuropathic pain is featured by a reactive gliosis of the nociceptive amygdala. Eur. J. Pain 17, 799–810 (2013).
58. De Luca, C. et al. Astrocytes and microglia-mediated immune response in maladaptive plasticity is differently modulated by NGF in the ventral horn of the spinal cord following peripheral nerve injury. Cell. Mol. Neurobiol. 36, 37–46 (2016).
59. Scardigli, R. et al. Neutralization of nerve growth factor impairs proliferation and differentiation of adult neural progenitors in the subventricular zone. Stem Cells 32, 2516–2528 (2014).
60. Kimura, S., Noda, T. & Yoshimori, T. Dissection of the autophagosome maturation process by a novel reporter protein, tandem fluorescent-tagged LC3. Autophagy 3, 452–460 (2007).
61. Cirillo, G. et al. Purinergic modulation of spinal neuroglial maladaptive plasticity following peripheral nerve injury. Mol. Neurobiol. 52, 1440–1457 (2015).

SUPPLEMENTARY MATERIALS

Differentiation by Nerve Growth Factor (NGF) involves mechanisms of crosstalk between energy homeostasis and mitochondrial remodeling
by F Martorana, D Gaglio*, MR Bianco*, F Aprea, A Virtuoso, M Bonanomi, L Alberghina, M Papa, AM Colangelo

Supplementary Figure S-1

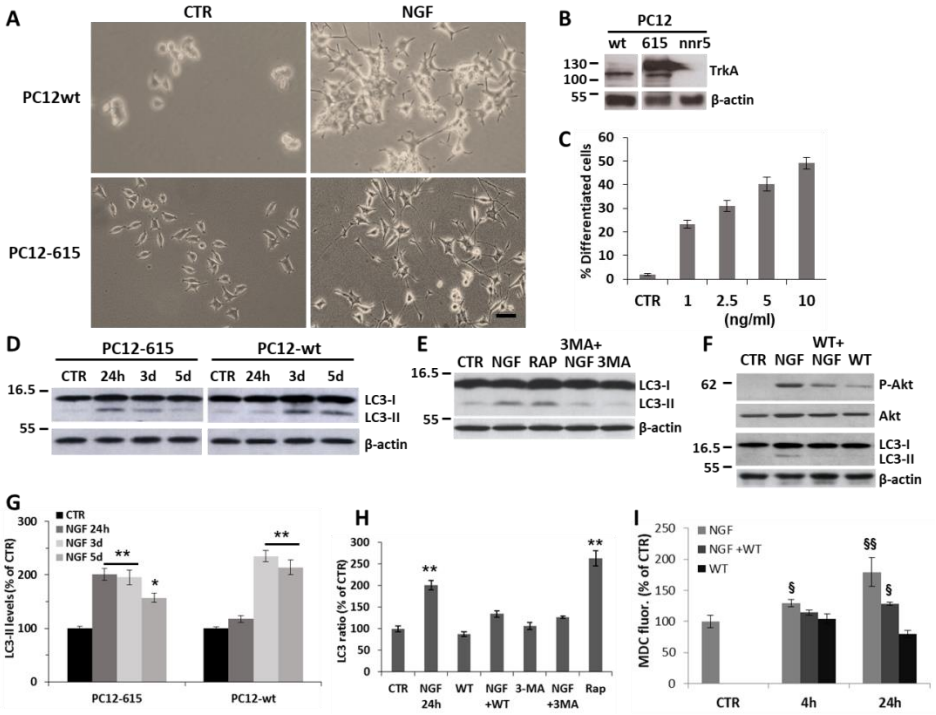

Figure S1. Comparison of autophagy in PC12wt and PC12-615. A) Representative images of PC12-wt and PC12-615 cells exposed to NGF (50 or 10ng/ml, respectively) for 72h. Scale bar = 25 µm. **B**) Expression levels of TrkA in PC12 wt, 615 and nnr5. **C**) Dose-response of PC12-615 differentiation with NGF (1, 2.5, 5 or 10 ng/ml) for 24h. Data are the mean ±SEM of three experiments with duplicate samples. **D**) Representative western blot for comparative analysis of LC3-II content in PC12-615 and PC12wt cells treated with NGF (10 or 50 ng/ml, respectively) for 24h or 3-5 days. LC3-II levels are comparable, but delayed in PC12wt. **E**) Representative immunoblots of LC3-II in PC12-615 treated for 24h with NGF (10ng/ml), alone or in combination with 3-methyladenine (3-MA, 10 mM). The effect of NGF is similar to that induced by Rapamycin (Rap, 200 nM). **F**) Representative immunoblots of LC3-II and P-Akt and total Akt in PC12-615 treated with NGF (10ng/ml), alone or in the presence of wortmannin (WT, 200 nM). **G-H**) Densitometric analysis of LC3-II normalized by the β-actin content in PC12-615 and PC12wt cells treated with NGF (10 or 50 ng/ml, respectively) for 24h or 3-5 days (**G**), and

the effect of 3-MA and WT inhibition (**H**). Data in G-H are the mean ±SEM of three independent experiments in duplicate. **I**) Fluorimetric analysis of monodansylcadaverine (MDC) staining in PC12-615 treated with NGF (10 ng/ml) for 4 or 24h. A partial reduction of acidic vacuoles is found when cells are preincubated for 10 min with WT. $*$ $p \leq 0.05$, $**$ $p \leq 0.01$ versus CTR (ANOVA and Dunnett's multiple comparisons test). § $p \leq 0.05$, §§ $p \leq 0.01$ versus CTR (*t*-test).

Supplementary Figure S-2

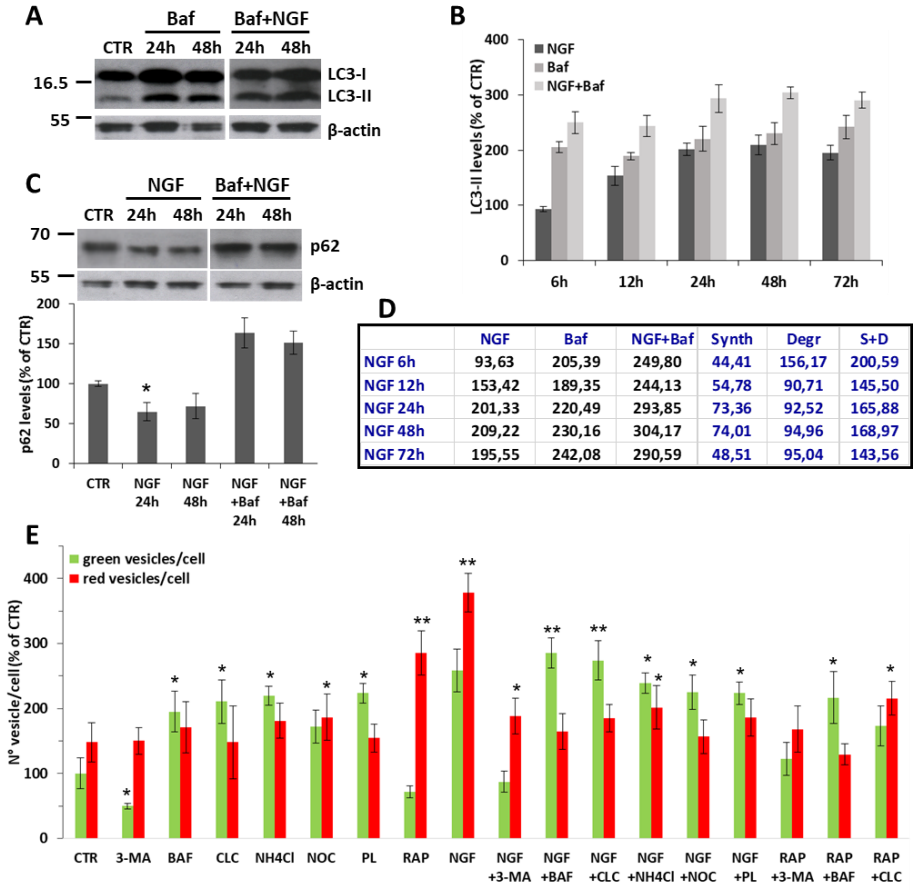

	NGF	Baf	NGF+Baf	Synth	Degr	S+D
NGF 6h	93,63	205,39	249,80	44,41	156,17	200,59
NGF 12h	153,42	189,35	244,13	54,78	90,71	145,50
NGF 24h	201,33	220,49	293,85	73,36	92,52	165,88
NGF 48h	209,22	230,16	304,17	74,01	94,96	168,97
NGF 72h	195,55	242,08	290,59	48,51	95,04	143,56

Figure S2. Analysis of the autophagic flux in NGF-treated PC12 cells. A) Representative western blot of LC3-II levels in PC12-615 cells treated for 24-48h with NGF (10 ng/ml) alone or in the presence of Baf (100 nM). **B**) Quantitation of LC3-II/β-actin ratio during the entire time-course 6-72h. Data, expressed as percent of CTR, are the mean ±SEM of three independent experiments in duplicate. **C**) Representative immunoblot and quantitation of p62 in PC12 cells treated for 24-48h with NGF (10 ng/ml) alone or in the presence of Baf (100 nM). Data are the mean ±SEM of two independent

experiments in duplicate. **D**) The box shows the mean data and the corresponding rates of LC3-II synthesis and degradation at 6-12-24-48-72h of NGF treatment. **E**) Quantitation of green and red vesicles in GFP-RFP-LC3-transfected PC12 cells treated with NGF (10 ng/ml) or Rap (200 nM) alone or in combination with 3-MA (10mM), or Baf (100 nM), or CLC (1 µM) (Figure 2E), or Nocodazole (NOC, 1µM), or NH_4Cl (12.5mM) or a mix of the lysosomal inhibitors pepstatin/leupeptin (PL, 10 µM). Data, expressed as percent of CTR, are the mean ±SEM of vesicles normalized by the total number of cells (about 100 cells for each condition) in 10 randomly picked fields from three independent experiments. $*$ $p \leq 0.05$, $**$ $p \leq 0.01$ versus CTR (*t*-test).

Supplementary Figure S-3

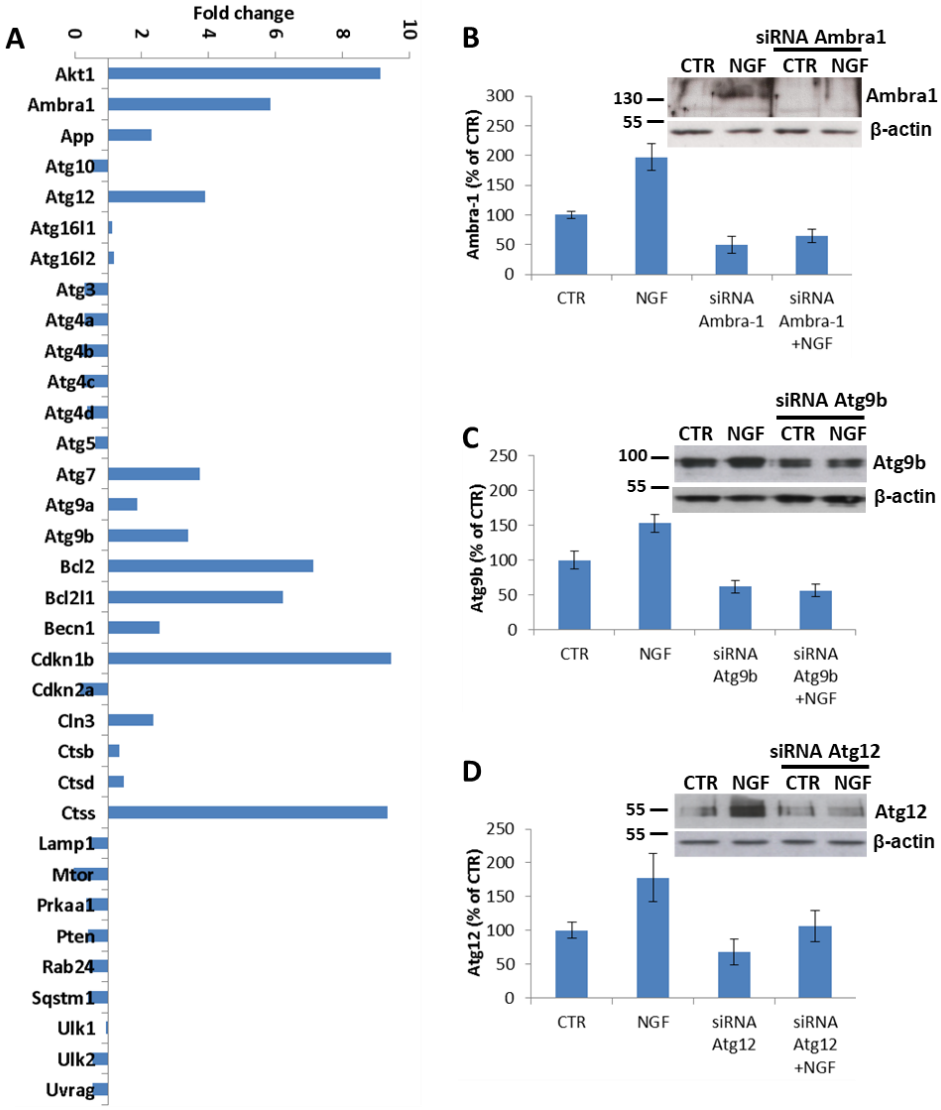

Figure S3. Expression of autophagy genes in response to NGF. A) RT-PCR array for autophagy genes on PC12-615 treated with NGF for 6h. Data, expressed as fold of induction (ΔΔCt), are the mean of two independent experiments. In addition to induction of Akt1 and Bcl-2, NGF increases Ambra1, as well as of Atg7, Atg9b and Atg12, which are involved in autophagosome biogenesis and elongation. Moreover, NGF increases Cyclin-dependent kinase inhibitor 1B (Cdkn1b, p27Kip1), a cell cycle inhibitor during NGF differentiation (Bianco et al., 2011), and cathepsin S (Ctss), a lysosomal cysteine protease. **B-D**) Expression levels and representative immunoblot of Ambra-1, Atg9b and Atg12 after NGF treatment for 24h. Blots were probed for

β-actin to normalize for protein content. siRNA knockdown, which reduces protein content by about 30-50% (si-Ambra1, 50.3%; si-Atg9b, 38.4%; si-Atg12, 31.6%), abolishes the NGF-mediated induction of protein content.

Supplementary Figure S-4

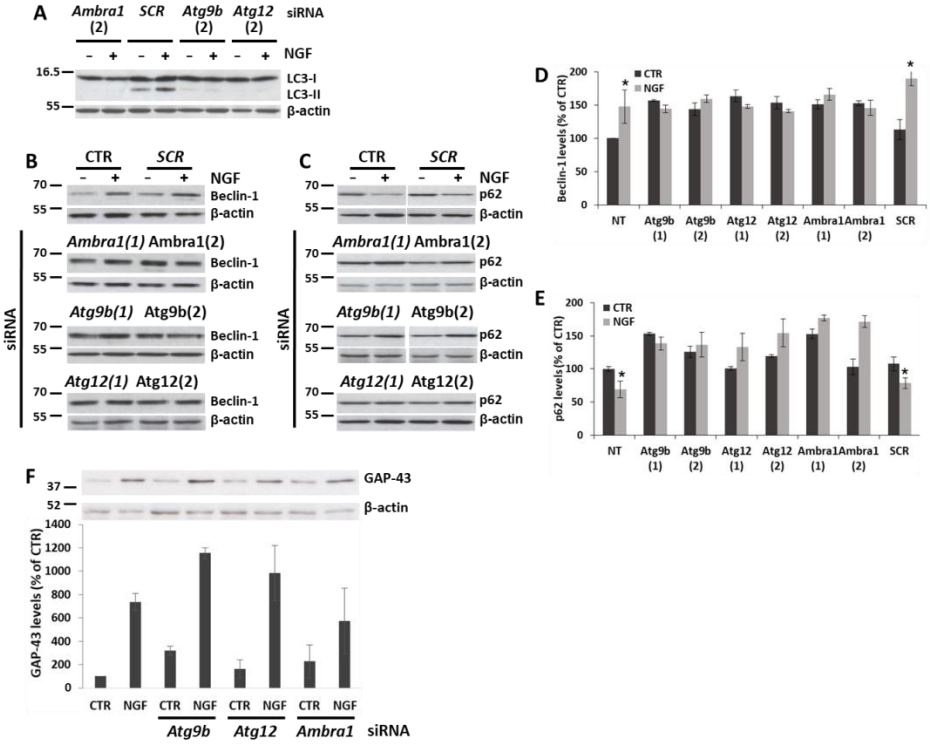

Figure S4. Inhibition of NGF-mediated autophagy by siRNA knockout of autophagy genes. **A**) Representative western blot of LC3-II in PC12-615 cells transfected with siRNA-*Ambra1*(2), siRNA-*Atg9b*(2), or siRNA-*Atg12*(2), followed by NGF (10 ng/ml) treatment for 24h. **B-C**) Representative immunoblots of beclin-1 (B) and p62 (C) in PC12-615 cells transfected with siRNA-*Ambra1* (1-2), or siRNA-*Atg9b* (1-2), or siRNA-*Atg12* (1-2) or SCR, followed by NGF treatment for 24h, as compared to non-transfected (CTR) cells. Blots were probed for β-actin to normalize for protein content. All siRNA were run on parallel gels. **D-E**) Densitometric analysis of beclin-1 (D) and p62 (E) in PC12-615 not-transfected (NT) or siRNA transfected cells followed by NGF treatment for 24h. NGF fails to regulate LC3-II (A), beclin-1 (B and D) and p62 (C and E) in siRNA transfected cells, but not in NT or scrambled siRNA (siSCR) used to control for non-specific effects of siRNA transfection. Data, expressed as percent of CTR, are the mean ±SEM of three independent samples. $*p \leq 0.05$ versus CTR (*t*-test). **F**) Expression levels and representative immunoblot of GAP-43 in PC12-615 treated with NGF for 24h. NGF-mediated induction of GAP-43 levels is not changed by siRNA

knockdown of *Ambra-1*, or *Atg9b* or *Atg12*, as compared to not transfected cells. A slight increase of GAP-43 is seen in the CTR of transfected cells, most likely due to the transfection procedure, as observed in siRNA-SCR transfected cells (data not shown). Data are the mean of four independent samples.

Supplementary Figure S-5

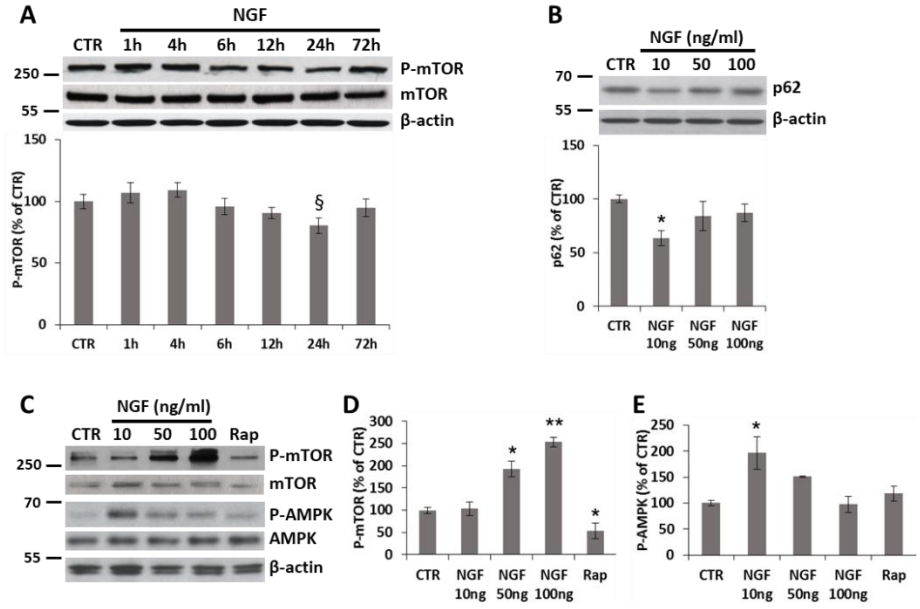

Figure S5. The effect of NGF on P-mTOR and P-AMPK is dose-dependent. A) Densitometric analysis and representative immunoblot blot of P(Ser2448)-mTOR and total mTOR after treatment with NGF (10 ng/ml) for the indicated times. Data are the mean ±SEM of three experiments in duplicate. § p≤ 0.05 versus CTR (t-test). **B**) Dose-response and representative immunoblot for p62 content in PC12-615 cells treated with NGF 10-50-100 ng/ml for 4h. High NGF concentrations (50 or 100 ng/ml) do not change p62 levels. **C**) Representative blots of P-mTOR, total mTOR, P-AMPK and total AMPK in PC12-615 cells treated with NGF 10-50-100 ng/ml for 4h. Blots were probed for β-actin to normalize for protein content. High concentrations of NGF (50 or 100 ng/ml) cause a dose-dependent increase in P-mTOR, inversely correlated with the decrease of P-AMPK levels. Rap (200 nM) is used as a control. **D-E**) Dose-response of P-mTOR (D) and P-AMPK (E) in PC12-615 cells treated with NGF 10-50-100 ng/ml for 4h. Data in B and D-E represent the mean ±SEM of three independent samples. * p≤ 0.05, ** p≤ 0.01 versus CTR (ANOVA and Dunnett's multiple comparisons test). § $p \leq 0.05$ versus CTR (*t*-test).

Supplementary Figure S-6

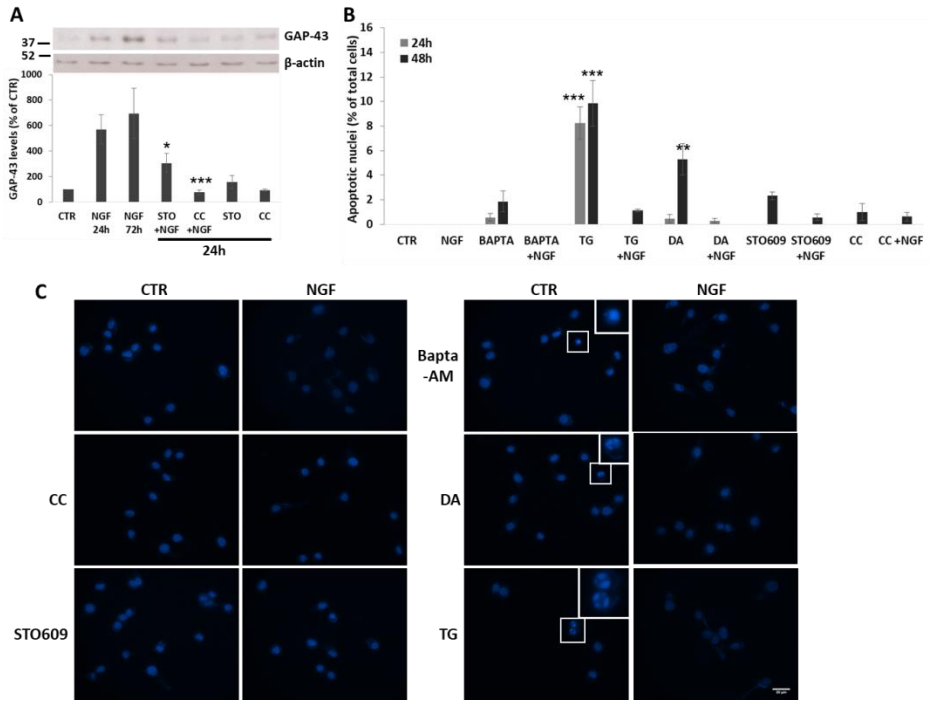

Figure S6. Effect of kinases inhibitors and Ca^{2+} blockers on cell survival during NGF-induced differentiation. **A**) Expression levels and representative immunoblot of GAP-43 in PC12-615 treated with NGF for 24-72h. Blots were probed for β-actin to normalize for protein content. NGF-mediated induction of GAP-43 is partially decreased by Ca^{2+}/CaMKII inhibitor STO609 (25 μM) and fully prevented by CC (10 μM), as compared to NGF at 24h. Data are the mean of three separate experiments with duplicate samples. **B**) Quantitation of apoptotic nuclei during NGF differentiation (24-48h) in the presence of kinases inhibitors or Ca^{2+} blockers. Data, expressed as percent of total cells in 10 random fields for each sample, are the mean ±SEM of three independent experiments with duplicate samples. **C**) Representative images of Hoechst-33342 staining of apoptotic nuclei in PC12-615 cells treated for 24h with NGF (10ng/ml) alone or in combination with CC (10 μM), STO609 (25 μM) Bapta-AM (1 μM), DA (20 μM) or TG (100 nM). Scale bar = 20 μm. $*$ $p \leq 0.05$, $**$ $p \leq 0.01$, $***$ $p \leq 0.001$ versus CTR (ANOVA and Dunnett's multiple comparisons test).

Supplementary Figure S-7

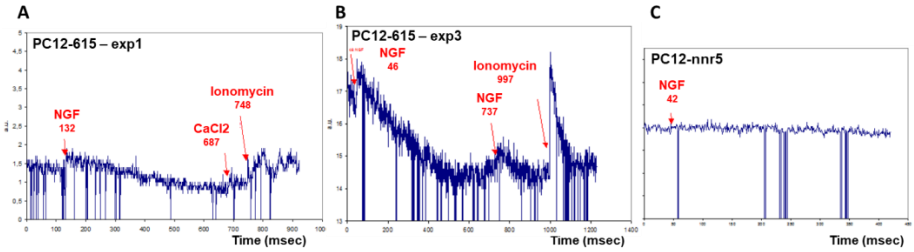

Figure S7. NGF promotes mitochondrial Calcium entry. A-C) Representative profiles of mitochondrial Ca^{2+} entry after NGF treatment in PC12-615 (**A-B**), as compared to PC12 nnr5 (**C**) used as negative control (PC12nnr5 do not express TrkA, but only the p75 receptor). Arrows indicate the time of addition of NGF at 132 msec, after baseline stabilization (**A**), or 46 msec and 737 msec (**B**), or 42 msec (**C**), as well as times of addition of CaCl2 (687 msec in A) or ionomycin (748 msec in A, 997 msec in B).

Supplementary Figure S-8

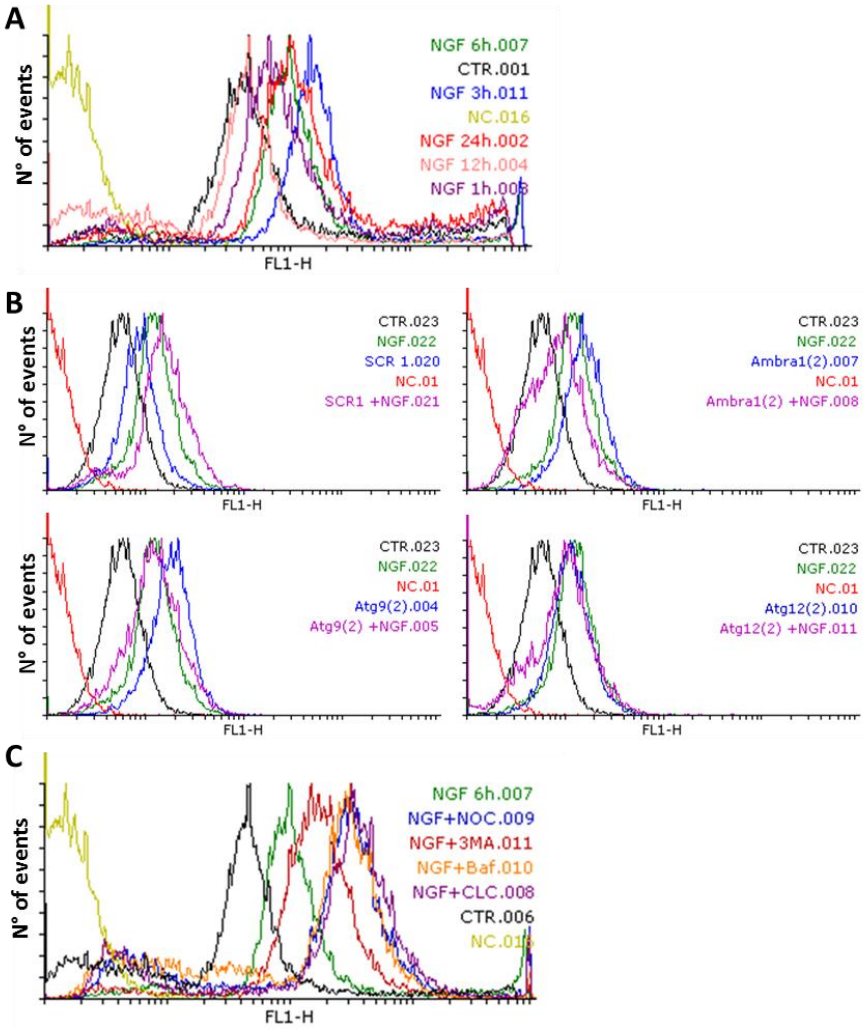

Figure S8. ROS levels in PC12 treated with NGF. A-B-C) Representative FACS profiles of DCFH-DA staining in: **A**) PC12 treated with NGF (10 ng/ml) for the indicated times; **B**) PC12 transfected with *Ambra-1*, *Atg9b* or *Atg12* siRNA and treated with NGF (10 ng/ml) for 6h; **C**) PC12 treated with NGF (10 ng/ml) alone or in combination with the indicated autophagy inhibitors for 6h.

Supplementary Figure S-9

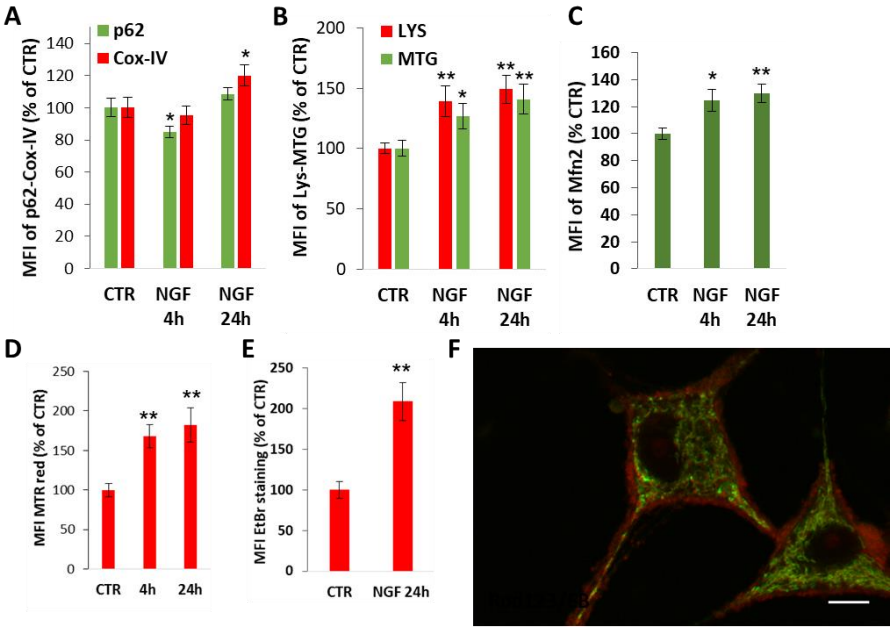

Figure S9. Quantitation of mitophagy and mitochondrial dynamics. A-B-C) Quantitation of p62/CoxIV (**A**), LYS/MTG (**B**) and Mfn2 (**C**) fluorescence expressed as mean fluorescence intensity (MFI) normalized by the total number of cells. **D**) Mitotracker red (MTR) fluorescence measured as MFI normalized by the total number of cells. On average, about 100 cells for each condition were counted in about 10 randomly picked fields for all fluorescence imaging studies. Data, expressed as percent of CTR, are the mean ±SEM of three experiments with duplicate samples. * p≤ 0.05, ** p≤ 0.01 versus CTR (*t*-test). **E**) Quantitation of Ethydium bromide fluorescence expressed as MFI/cell. **F**) Representative image of mitochondria morphology, by differential labeling with Rhodamine 123 (a cationic, green fluorescent dye that is sequestered by active mitochondria) and Ethydium Bromide (red). In NGF-treated cells most of central mitochondria appear tubular, while peripheral mitochondria are mostly fragmented and labeled by EB. Scale bar = 5 µm.

Supplementary Materials and Methods

Cell viability

Cell survival was assessed by MTT assay (Sigma). The reduction of the yellow tetrazolium salt (MTT) to the purple formazan is dependent on the activity of mitochondrial dehydrogenases by intact mitochondria and can also be taken as an index of mitochondrial activity. Briefly, PC12-615 cells (8000 cells/well) were plated in 96-well plates (Euroclone) pre-coated with poly-L-lysine (0.1 mg/ml). Following treatments, tetrazolium salts (0.5 mg/ml) were added directly to the culture medium for 2h at 37°C in a humidified atmosphere. After incubation, dimethyl sulfoxide (DMSO) was added into the wells, and plates were agitated for 15 minutes. The absorbance of samples was measured at wavelength 570 nm (630 nm background wavelength) with a Microplate Reader (Bio-Rad, Hercules, CA). MTT conversion levels were expressed as a percentage of control.

Hoechst 33342 staining assay

Apoptotic cell death was detected by monitoring morphological changes of nuclei using Hoechst 33342 staining. Briefly, PC12 cells were grown onto 12mm poly-L-lysine-coated coverslips ($2x10^4$ cells/well). After treatments, cells were washed with PBS three times and stained with Hoechst 33342 (10 µg/ml) for 10 min at room temperature in the dark. Coverslips were mounted with Dako Fluorescent Mounting Medium (Dako Agilent Technologies). Images were acquired at 60X magnification using a fluorescence microscope (Nikon Eclipse 90i) equipped with a CCD camera. NIH ImageJ software was used for image analysis and processing. Apoptotic cells were counted in 10 random fields for each sample, and expressed as percent of the total cells.

RNA Extraction and RT-PCR array for autophagy genes

To assess the expression of autophagy-related genes, the rat Autophagy RT² Profiler™ PCR Array kit (Qiagen SABiosciences, Frederick, MD) was used, which allows to study the expression of 84 key genes involved in autophagy. The assay was performed according to the specifications of the manufacturer. PC12-615 cells ($8x10^5$ cells/60-mm dishes) were treated with NGF (10ng/ml) for 6h. After treatments, total RNA was extracted by using the RNeasy Mini Kit (Qiagen, Dusseldorf, Germany) and then incubated with RNase-free DNase (Qiagen) for 5 min at 42°C to eliminate genomic DNA contaminants. After measuring RNA concentration and purity, RNA (0.5 ng) was converted to cDNA using RT2 First Strand Kit for 20 min (15 min at 42°C; 5 min at 95°C). Real time PCR was performed with RT² SYBR Green ROX qPCR Mastermix using the Real-Time PCR System 7500 Fast (Applied Biosystem, Life Technologies) according to the manufacturer's instructions. Quantification of RNA was accomplished by using the $\Delta\Delta C_t$ method (fold changes in Ct values of all genes). Relative amounts of mRNA for genes of interest were normalized to the housekeeping gene GAPDH.

siRNAs sequences for Ambra1, Atg9b and Atg12

siRNAs for Ambra1, Atg9b and Atg12 were synthesized by PRIMM s.r.l. (Milano, Italy) using the following sequences:

A9b 1-1 5'-UCACCAAGAUCUACAGCUAUU-3'
A9b 1-2 5'-UAGCUGUAGAUCUUGGUGAUU-3'
A9b 2-1 5'-CCAAAGGAUUUCCAGGAGAUU-3'
A9b 2-2 5'-UCUCCUGGAAAUCCUUUGGUU-3'
A12 1-1 5'-CGGAGCAGUUGUUUAUUUAUU-3'
A12 1-2 5'-UAAAUAAACAACUGCUCCGUU-3'
A12 2-1 5'-AGACACUCCCAUAAUGAAAUU-3'
A12 2-2 5'-UUUCAUUAUGGGAGUGUCUUU-3'
A1 1-1 5'-AGGAAAUGCUCAACAAUAAUU-3'
A1 1-2 5'-UUAUUGUUGAGCAUUUCCUUU-3'
A1 2-1 5'-GGAUAAGACUCGAUGGAUGUU-3'
A1 2-2 5'-CAUCCAUCGAGUCUUAUCCUU-3'
SCR1 5'-GUCGAGAUAGGUGACAUAGUU-3'
SCR2 5'-CTATGTCACCTATCTCGACUU-3'

MDC staining for detection of acidic vacuoles

Cells ($7x10^4$ cells/well) were plated in 6-well plates (EuroClone) precoated with poly-L-lysine (0.1 mg/ml). After specific treatments, acidic vacuoles were assessed by adding 50 µM of MDC (Sigma) during the last 10 min of incubation. Cells were then washed with PBS, detached in PBS containing 0.1% TritonX-100, 10mM Tris HCl pH 8.00 and immediately analyzed using the Varian Cary Eclipse Fluorescence Spectrophotometer (Agilent Technologies). Excitation wavelength = 380 nm; emission wavelength = 460 nm.

CHAPTER 4

1. Summary

For a long time, it was believed that astrocytes were inactive elements just providing a scaffold function in the CNS. Now, it is known that astrocytes play important roles in maintaining brain homeostasis and it has become clear that astrocytic dysfunction plays a relevant role in neurodegenerative processes. Neurodegenerative disorders are characterized by dysfunction and loss of specific neuronal populations in response to age-related or toxic events that involve metabolic dysfunction, oxidative stress, loss of trophic support and neuroinflammation [1,2].

Biochemical and structural changes of astrocytes during neuroinflammation represent a physiological response to CNS injury to minimize and repair the initial damage. Nevertheless, prolonged brain insults provide detrimental signals that can compromise astrocytic and neuronal functions and lead to chronic neuroinflammation [1].

In fact, during injury or disease, microglia can sense endogenous “danger signals” that are released by damaged cells followed by activation of astrocytes [3]. Activated astrocytes appear to exert beneficial effects in the CNS by producing several mediators of neuroprotection, growth and differentiation, anti-inflammatory cytokines, chemokines, and angiogenic factors [4]. However, proinflammatory cytokines can also produce an auto-toxic self-

substained inflammatory loop, that affects neuroglial homeostasis by activating signalling pathways that are deleterious to neuronal function. Therefore, it can be assumed that inflammation in CNS disease is an ambivalent process that may have both protective and destructive effects. For instance, activated glial cells produce ROS accumulation that can cause mitochondrial dysfunction.

On the other hand, recently, it is becoming clear that cells also use autophagy as a physiological process for recycling damaged molecules and organelles [5]. This mechanism, that is important for mitochondrial quality control [6], may play an essential role in acute and chronic inflammation and the impairment of autophagic machinery in neurons may contribute to neurodegeneration [7,8]. This hypothesis is based on the observation that inhibition of autophagy results in the accumulation of dysfunctional mitochondria that leads to a harmful impact on the bioenergetic status of the cell [7].

Mitochondria are very dynamic organelles. In particular, mitochondrial dynamic processes (involving alternation of fission/fusion cycles and their axonal transport) and biogenesis are crucial for neuronal homeostasis and synaptic function. Alteration of the balance between fission and fusion can determine the fate of neuronal cells. In fact, dysfunctional mitochondria are supposed to play a cardinal role in the pathogenesis of various neurological disorders such as multiple sclerosis, AD, PD and stroke.

In this study, we have focused our research activity on the

molecular mechanisms underlying the potential cross-talk between neuroinflammatory processes and mitochondrial dysfunction. To this end, we have analyzed the activity of antioxidant molecules on astrocytes and neurons in models of astroglia-mediated inflammation, to investigate their capability to reduce inflammatory and oxidative damage. Moreover, we have investigated mechanisms of mitochondrial remodelling and metabolic function in neuronal NGF-induced differentiation, which is important to better understand the role of NGF in both neurogenesis and mechanisms of regeneration following brain injury.

2. Discussion

2.1 Differential Modulation of NF-κB in Neurons and Astrocytes Underlies Neuroprotection and Antigliosis Activity of Natural Antioxidant Molecules

This study shows a promising anti-gliosis and neuroprotective activity exerted by a cocktail of natural antioxidants. We show that these molecules are able to reduce astrocytic activation and to protect neurons exposed to astroglia-mediated inflammation by modulating in different manner the NF-kB pathway. A previous study of the lab showed that antioxidant cocktails promoted neuroprotection on NGF-deprived neuronal cells by depleting ROS levels and improving mitochondrial function [9]. This study shows for the first time the synergic protection by low-dose of

antioxidant cocktails on primary cultures of neurons and astrocytes, thus supporting the idea that a balanced intake of antioxidant dietary factors is able to act on both components of neuroglial networks and exert both neuroprotection and anti-gliosis activity through differential activation of NF-kB pathway converging on modulation of mitochondrial function. In agreement with the emerging evidence about the many beneficial activities of nutraceuticals, these data candidate dietary antioxidant molecules as a supportive therapeutic strategy to reduce inflammatory and oxidative damage in neurodegenerative disorders, and the relevance of healthy diets in maintaining brain function.

2.2 Differentiation by nerve growth factor (NGF) involves mechanisms of crosstalk between energy homeostasis and mitochondrial remodeling

In this study, we evaluated the relevance of autophagy during NGF-induced differentiation and the molecular mechanisms implicated in this process. We have observed that NGF-induced differentiation requires specific activation of autophagy mediated by Atg9 and Ambra1. Indeed, genetic or pharmacological inhibition of autophagy causes defective differentiation in the presence of NGF.

We also performed a detailed study of mitochondrial trafficking involved in axonal growth in response to NGF. We demonstrated that NGF-induced differentiation involves a modulation of mitochondrial dynamics to increase their efficiency and meet

higher energy requirement.

Our data provide the first evidence that NGF-dependent differentiation occurs through a complex signaling network related to the control of energy homeostasis in response to higher energy demand. Moreover, we have identified two sets of events that occur during NGF differentiation. One set of events is due to calcium signaling, followed by an increase of proton-leak and ROS production thus activating mitochondrial fragmentation and mitophagy. A second set of events is linked to metabolic perturbations due to decreased ATP/NADPH used up in anabolic pathways and converging on P-AMPK to keep energy metabolism, mitophagy and mitochondrial dynamics active for the entire process of differentiation.

This study offers new insights into mechanisms of NGF activity during differentiation and a deeper understanding its role in modulating mitochondrial function, which is relevant to both neuronal homeostasis and neurogenesis following brain injury.

3. Future perspectives

The results obtained in these years represent a small part of a larger project that has the expectation to elucidate mechanisms underlying pathological progression of neurodegeneration in PD. PD is a very common neurodegenerative disorder, characterized by a slow and progressive degeneration of dopaminergic neurons in the *substantia nigra*. Several molecular and cellular changes involved in neuronal degeneration have been identified,

including oxidative stress, mitochondrial dysfunction and excitotoxicity, which may lead to apoptotic processes. Furthermore, neuroinflammatory mechanisms might contribute to the cascade of events leading to neuronal degeneration. Indeed, imaging studies *in-vivo* and in PD patients show neuroinflammatory events in several cerebral areas and microglial activation [10,11].

Moreover, several studies reported the relevance of mitochondrial dysfunction in development of PD. Genes, such as PTEN-induced kinase-1 (PINK1) and Parkin that are directly related to some cases of familial PD, are involved in mitochondrial quality control and regulation of mitochondrial morphology, respectively [12,13].

All together, our results are the starting point to investigate the role of NGF and antioxidant molecules in models of PD, and also the implication of mitochondrial dynamics and mitophagy in this pathology.

To this end, we are currently performing experiments by using an *in-vivo* pharmacological model of PD, in which the neurotoxin 6-hydroxydopamine (6-OHDA) is injected in the striatum area by stereotaxic surgery. This model will give us information about the crosstalk between reactive gliosis and alteration of mitochondrial dynamics in determining neuronal dysfunction. In addition, we will investigate whether a rescue of dopaminergic function can be achieved by administration of NGF or antioxidant molecules, based on their neuroprotective and antigliosis activity [14,15].

References

[1] Colangelo AM, Alberghina L, Papa M. Astrogliosis as a therapeutic target for neurodegenerative diseases. Neurosci Lett 2014;565:59–64. https://doi.org/10.1016/j.neulet.2014.01.014.

[2] Verkhratsky A, Parpura V, Pekna M, Pekny M, Sofroniew M. Glia in the pathogenesis of neurodegenerative diseases. Biochem Soc Trans 2014;42:1291–301. https://doi.org/10.1042/BST20140107.

[3] Burda JE, Sofroniew MV. Seducing astrocytes to the dark side. Cell Res 2017;27:726–7. https://doi.org/10.1038/cr.2017.37.

[4] Liberto CM, Albrecht PJ, Herx LM, Yong VW, Levison SW. Pro-regenerative properties of cytokine-activated astrocytes. J Neurochem 2004;89:1092–100. https://doi.org/10.1111/j.1471-4159.2004.02420.x.

[5] Yang Z, Klionsky DJ. An overview of the molecular mechanism of autophagy. Curr Top Microbiol Immunol 2009;335:1–32. https://doi.org/10.1007/978-3-642-00302-8_1.

[6] Ashrafi G, Schwarz TL. The pathways of mitophagy for quality control and clearance of mitochondria. Cell Death Differ 2013;20:31–42. https://doi.org/10.1038/cdd.2012.81.

[7] Hara T, Nakamura K, Matsui M, Yamamoto A, Nakahara Y, Suzuki-Migishima R, et al. Suppression of basal autophagy in neural cells causes neurodegenerative disease in mice. Nature 2006;441:885–9. https://doi.org/10.1038/nature04724.

[8] Mizushima N, Hara T. Intracellular quality control by autophagy: how does autophagy prevent neurodegeneration? Autophagy 2006;2:302–4. https://doi.org/10.4161/auto.2945.

[9] Amara F, Berbenni M, Fragni M, Leoni G, Viggiani S, Ippolito VM, et al. Neuroprotection by Cocktails of Dietary Antioxidants under Conditions of Nerve Growth Factor Deprivation. Oxid Med Cell Longev 2015;2015:217258. https://doi.org/10.1155/2015/217258.

[10] Gerhard A, Pavese N, Hotton G, Turkheimer F, Es M, Hammers A, et al. In vivo imaging of microglial activation with [11C](R)-PK11195 PET in

idiopathic Parkinson's disease. Neurobiol Dis 2006;21:404–12. https://doi.org/10.1016/j.nbd.2005.08.002.

[11] Hirsch EC, Hunot S. Neuroinflammation in Parkinson's disease: a target for neuroprotection? Lancet Neurol 2009;8:382–97. https://doi.org/10.1016/S1474-4422(09)70062-6.

[12] Grünewald A, Voges L, Rakovic A, Kasten M, Vandebona H, Hemmelmann C, et al. Mutant Parkin impairs mitochondrial function and morphology in human fibroblasts. PloS One 2010;5:e12962. https://doi.org/10.1371/journal.pone.0012962.

[13] Liu M, Bing G. Lipopolysaccharide animal models for Parkinson's disease. Park Dis 2011;2011:327089. https://doi.org/10.4061/2011/327089.

[14] Colangelo AM, Bianco MR, Vitagliano L, Cavaliere C, Cirillo G, De Gioia L, et al. A new nerve growth factor-mimetic peptide active on neuropathic pain in rats. J Neurosci Off J Soc Neurosci 2008;28:2698–709. https://doi.org/10.1523/JNEUROSCI.5201-07.2008.

[15] Cirillo G, Colangelo AM, Bianco MR, Cavaliere C, Zaccaro L, Sarmientos P, et al. BB14, a Nerve Growth Factor (NGF)-like peptide shown to be effective in reducing reactive astrogliosis and restoring synaptic homeostasis in a rat model of peripheral nerve injury. Biotechnol Adv 2012;30:223–32. https://doi.org/10.1016/j.biotechadv.2011.05.008.

List of publications

1) Norante R. P., Peggion C., Rossi D., **Martorana F.**, De Mario A., Lia A., Massimino M. L., Bertoli A. “ALS-Associated SOD1(G93A) Decreases SERCA Pump Levels and Increases Store-Operated $Ca2^{+}$ Entry in Primary Spinal Cord Astrocytes from a Transgenic Mouse Model.”

Int. J. Mol. Sci. 2019 Oct 17, 20(20), 5151

2) **Martorana F**, Foti M, Virtuoso A, Gaglio D, Aprea F, Latronico T, Rossano R, Riccio P, Papa M, Alberghina L, Colangelo AM. “Differential Modulation of NF-κB in Neurons and Astrocytes Underlies Neuroprotection and Antigliosis Activity of Natural Antioxidant Molecules”.

Oxid Med Cell Longev. 2019 Aug 14;2019:8056904

3) Brambilla L, **Martorana F**, Guidotti G, Rossi D. “Dysregulation of Astrocytic HMGB1 Signaling in Amyotrophic Lateral Sclerosis”.

Front Neurosci. 2018 Aug 29;12:622.

4) **Martorana F**, Gaglio D, Bianco MR, Aprea F, Virtuoso A, Bonanomi M, Alberghina L, Papa M, Colangelo AM. “Differentiation by nerve growth factor (NGF) involves mechanisms of crosstalk between energy homeostasis and mitochondrial remodelling”.

Cell Death Dis. 2018 Mar 9;9(3):391.

Submitted

- Kolodkin A., Sharma R. P., Colangelo A.M., Ignatenko A., **Martorana F.**, Jennen D., Briede J.J., Brady N., Barberis M., Mondeel T.D.G.A., Papa M., Kumar V., Peters B., Skupin A., Alberghina L., Balling R., Westerhoff H. “ROS networks: design principles, elixirs, and precision therapies of aging and Parkinson's disease”.

Quando si arriva alla fine di un percorso è inevitabile tirarne le somme. Tornano in mente tutti i momenti vissuti, tutti gli eventi accaduti e tutte le persone che ne hanno fatto parte. Alcune di queste persone sono state presenze preziose e fondamentali per arrivare a questo giorno e che non posso non ringraziare.

Sono grata alla professoressa Granucci che mi ha permesso di svolgere il dottorato.

Ringrazio Anna Maria per il suo sostegno in quest'avventura e il tempo che mi ha dedicato.

Un grazie speciale va ai colleghi del corso che hanno reso questi tre anni indimenticabili. Forse ci perderemo, forse con alcuni rimarremo in contatto, ma sicuramente nella mia memoria rimarranno i messaggi, le paturnie dei giorni prima della consegna e le giornate passate insieme.

Momenti di sconforto ovviamente ce ne sono stati, la paura di non riuscire a gestire tutto, di non arrivare al termine ed è stato in questi momenti che ho avuto accanto delle persone meravigliose che mi hanno sostenuta e incoraggiata. C'è stata Roberta con le sue iniezioni di ottimismo; Francesca con le sue sedute di psicoterapia a qualunque ora del giorno, amica preziosa come poche che anche dopo una giornata no, trova sempre il tempo per uno sfogo e la parola giusta per consolare.

E poi c'è lei, la mia Fede…. Non potevo desiderare di lavorare con una persona migliore di lei… Non solo collega, ma amica preziosa che mi mancherà… cavolo se mi mancherà!

Infine, grazie alla mia famiglia, ai miei "uomini" che hanno creduto in me e sostenuto sempre: "san" Simone che mi sopporta da anni e che ha fatto ricorso a tutta la sua pazienza nei giorni in cui sono stata intrattabile, e il mio Chicchi: spero che un giorno, quando te lo racconterò, tu sia orgoglioso della tua mamma tornata studentessa per raggiungere questo traguardo.